PREDICTION OF ROTOR POSITION FROM ROTOR SLOT HARMONICS EXISTING IN MOTOR STATOR CURRENT

A THESIS SUBMITTED TO
THE GRADUATE SCHOOL OF NATURAL AND APPLIED SCIENCES
OF
MIDDLE EAST TECHNICAL UNIVERSITY

BY

TAYFUN FİLCİ

IN PARTIAL FULFILLMENT OF THE REQUIREMENTS
FOR
THE DEGREE OF MASTER OF SCIENCE
IN
ELECTRICAL AND ELECTRONICS ENGINEERING

FEBRUARY 2016

Approval of the thesis:

IMPLEMENTATION OF SENSORLESS VECTOR CONTROL DRIVE WITH CURRENT POSITION ESTIMATION

submitted by **TAYFUN FİLCİ** in partial fulfillment of the requirements for the degree of **Master of Science in Electrical and Electronics Engineering Department, Middle East Technical University** by,

Prof. Dr. Gülbin Dural Ünver
Dean, Graduate School of **Natural and Applied Sciences** _____

Prof. Dr. Gönül Turhan Sayan
Head of Department, **Electrical and Electronics Eng.** _____

Prof. Dr. Hulusi Bülent Ertan
Supervisor, **Electrical and Electronics Eng. Dept., METU** _____

Examining Committee Members:

Prof. Dr. Muammer Ermiş
Electrical and Electronics Eng. Dept., METU _____

Prof. Dr. Hulusi Bülent Ertan
Electrical and Electronics Eng. Dept., METU _____

Prof. Dr. Gözde Bozdağı Akar
Electrical and Electronics Eng. Dept., METU _____

Assist. Prof. Dr. Ozan Keysan
Electrical and Electronics Eng. Dept., METU _____

Assoc. Prof. Dr. M. Timur Aydemir
Electrical and Electronics Eng. Dept., GaziUnv. _____

Date: 02/02/2016

I hereby declare that all information in this document has been obtained and presented in accordance with academic rules and ethical conduct. I also declare that, as required by these rules and conduct, I have fully cited and referenced all material and results that are not original to this work.

Name, Last name : Tayfun FİLCİ

Signature :

ABSTRACT

IMPLEMENTATION OF SENSORLESS VECTOR CONTROL DRIVE WITH CURRENT POSITION ESTIMATION

Filci, Tayfun

M. S., Department of Electrical and Electronics Engineering

Supervisor: Prof. Dr. H. Bülent Ertan

February 2016, 124 pages

In this thesis, an algorithm will be developed and implemented online for the estimation of rotor position from the rotor slot harmonics in stator currents. Experiments will be done on an inverter driven induction motor hardware, and the performance of the position detection algorithm will be evaluated in comparison with commercial encoder outputs.

Keywords: Sensorless Drive, Rotor Slot Harmonics, Rotor Position Estimation, Rotor Speed Estimation

ÖZ

AKIM BİLGİSİNDEN KONUM HESAPLAYARAK SENSÖRSÜZ OLARAK VEKTÖR MOTOR KONTROLÜNÜN UYGULANMASI

Filci, Tayfun

Yüksek Lisans, Elektrik ve Elektronik Mühendisliği Bölümü

Tez Yöneticisi: Prof. Dr. H. Bülent Ertan

Şubat 2016, 124 sayfa

Bu tezde, rotor pozisyonun stator akımlarının içindeki rotor oluğu harmoniklerinden hesaplanmasını içeren bir algoritma geliştirilecek ve uygulanacaktır. Deneyler evirici ile sürülen indüksiyon motor üzerinde yapılacak ve rotor pozisyonu kestirim algoritmasının performansı ticari sensorlarla kıyaslanarak değerlendirilecektir.

Anahtar Kelimeler: Sensorsuz Motor Sürme, Rotor Oluğu Harrmonikleri, Rotor Pozisyonu Kestirimi, Rotor Hızı Kestirimi

To my family,

and

to my love,

Filiz Ece Filci

ACKNOWLEDGEMENTS

I cannot express enough thanks to my advisor, Prof. Dr. H. Bülent Ertan for his excellent guiding, caring, patience and encouragement throughout the thesis. I had an outstanding research activity under his supervision.

I am grateful to ASELSAN Electronic Industries for giving me opportunity to improve my engineering capabilities and for providing me every kind of hardware, software and financial support.

I would like to extend my special appreciation to my love Filiz Ece Filci for his support, patience, and kindness throughout my graduate study.

TABLE OF CONTENTS

LIST OF TABLES

TABLES

LIST OF FIGURES

FIGURES

LIST OF ABBREVIATIONS

AC	: Alternative Current
ADC	: Analog to Digital Converter
DAC	: Digital to Analog Converter
dB	: Decibel
DC	: Direct Current
DSP	: Digital Signal Processor
emf	: Electro-Motive Force
FFT	: Fast Fourier Transform
FIR	: Finite Impulse Response
FPGA	: Field Programmable Gate Array
Hz	: Hertz
IGBT	: Insulated Gate Bipolar Transistor
IIR	: Infinite Impulse Response
I/O	: Input/Output
IPM	: Intelligent Power Module
kW	: Kilowatts
min	: Minute
MMF	: Magneto-Motive Force
mV	: Milivolts

PWM : Pulse Width Modulation

RPM : Revolution per Minute

RSH : Rotor Slot Harmonics

sec : Second

CHAPTER 1

INTRODUCTION

The use of induction machines increased with the help of the field oriented control techniques as these techniques increased the dynamic performance of the induction motor drives. There are two ways to achieve field orientation control; direct flux orientation and indirect flux orientation. While direct field orientation is achieved by measuring the flux **[1]** with a sensor like Hall probe, indirect field orientation does not require this kind of a sensor. Instead of measuring flux, stator current magnitude and rotor speed are used to calculate the slip **[2]**. However a speed sensor is needed to measure the rotor speed at indirect field orientation.

Direct field orientation with the voltage model is the preferred way as it eliminates the use of a speed sensor. However, it has some drawbacks at low speeds. The stator flux linkage is calculated as given in **[3]** as **(1)** where $\hat{u}_s$ is the stator voltage vector, $\hat{\imath}_s$ is the stator current vector and r_s is stator resistance and u_{off} models all errors.

$$\hat{\Psi}_s = \int (\hat{u}_s - r_s \hat{\imath}_s + u_{off})\, d\tau \qquad \textbf{(1)}$$

The most important error source in direct field orientation with voltage model is mismatch in modeling r_s. It is difficult to estimate the flux at low speeds as the voltage magnitude decreases at low speeds and stator resistance voltage drop becomes dominant. Due to this fact flux estimation is difficult and contains cumulative error as stated also in **[3]**. Implementing the current model is better for low speeds as a position sensor is used to sense rotor position; on the other hand, adding a speed sensor or encoder brings about extra effort like additional electronic

and mechanical mounting which decreases the robustness of the drive **[5]**. Last but not least, for low power applications, the cost of the system increases drastically as the cost of the sensor reaches to a comparable level to the cost of the motor itself **[2]**.

In application of sensorless vector control, there are different ways to estimate the rotor position without using a sensor. In **[6]**, **[7]** and **[8]**, the rotor position and velocity is estimated by injecting a high frequency signal. Some harmonics are generated in stator currents and the air gap flux due to the injected signal and the frequency of these harmonics are used to estimate the rotor speed. However, in order to have observable harmonic signals, the injected signal becomes large which causes torque ripples and loss increase.

Using the saliencies to estimate the rotor speed is another known method **[9]**. Saliencies exist due to the time varying air gap permeance, or due to presence of slots, or may be deliberately introduced and contain information about the rotor position **[9]**. Saliencies can be detected in different ways like measuring the phase current, voltage or neutral point voltage. Rotor slot harmonics (RSH) are one of the popular saliencies used to detect, motor faults, rotor speed etc. **[9]**.

1.1 High Frequency Signal Injection

In the high frequency signal injection method, a signal is superimposed on the fundamental supply excitation **[8]**. Some saliencies are produced due to the injected signal and they contain information about the rotor speed. In order to understand this phenomenon, let's look at the stator and rotor voltage equations **[10]**;

$$v^s_{qds} = r_s.i^s_{qds} + p\lambda^s_{qds} \text{ Stator voltage equation} \quad \textbf{(2)}$$

$$0 = r_r.i^s_{qdr} + (p - jw_r).\lambda^s_{qdr} \text{ Rotor voltage equation} \quad \textbf{(3)}$$

as;

$$\lambda^s_{qds} = L_s.i^s_{qds} + L_m.i^s_{qdr} \text{ Stator flux linkage} \quad \textbf{(4)}$$

$$\lambda^s_{qdr} = L_m.i^s_{qds} + L_r.i^s_{qdr} \text{ Rotor flux linkage} \quad \textbf{(5)}$$

where;

v_{qds}^{s} is stator d-q axis voltage in stationary reference frame,

r_s is stator resistance,

i_{qds}^{s} is stator d-q axis current in stationary reference frame,

p is derivative operator,

r_r is rotor resistance,

i_{qdr}^{s} is rotor d-q axis current in stationary reference frame,

w_r is angular velocity,

L_m is mutual inductance,

L_r is rotor inductance,

L_s is stator inductance.

As proposed in **[8]**, the stator and rotor resistances can be neglected at high frequencies, and the rotor voltage equation becomes as given in **(6)**

$$0 \cong (p - jw_r).\lambda_{qdr}^{s} \quad \textbf{(6)}$$

The derivative operator can be replaced by $jw_c$where the excitation carrier frequency w_c is constant. In order to relate the rotor and stator currents the following manipulation is used.

$$0 \cong j(w_c - w_r).\lambda_{qdr}^{s} \cong j(w_c - w_r).\left(L_m.i_{qds}^{s} + L_r.i_{qdr}^{s}\right) \quad \textbf{(7)}$$

$$i_{qdr}^{s} = -\left(\frac{L_m}{L_r}\right).i_{qds}^{s} \quad \textbf{(8)}$$

Using equations **(2)** and **(8)**;

$$v_{qds\_c}^{s} \cong j.w_c.L_{\sigma s}.i_{qds\_c}^{s} \quad \textbf{(9)}$$

Where stator transient inductance;

$$L_{\sigma s} = \left(L_s - \frac{{L_m}^2}{L_r}\right) \quad \textbf{(10)}$$

The stator transient inductance is not constant on a machine where the rotor slot openings vary, but it becomes a function of rotor position as in **[11] (11)**;

$$L_{\sigma s} = \begin{bmatrix} \Sigma L_{\sigma s} + \Delta L_{\sigma s}\cos(h\theta_r) & -\Delta L_{\sigma s}\sin(h\theta_r) \\ -\Delta L_{\sigma s}\sin(h\theta_r) & \Sigma L_{\sigma s} - \Delta L_{\sigma s}\cos(h\theta_r) \end{bmatrix} \quad \textbf{(11)}$$

where;

$\Sigma L_{\sigma s} = \frac{1}{2}.\left(L_{\sigma qs} + L_{\sigma ds}\right)$is the average stator transient inductance,

$\Delta L_{\sigma s} = \frac{1}{2}.\left(L_{\sigma qs} - L_{\sigma ds}\right)$ is the differential stator transient inductance caused by saliency,

$L_{\sigma qs}, L_{\sigma ds}$ are the q and d stator transient inductances caused by saliency,

h is the harmonic number of saliency,

θ_r is the rotor position in electrical degree.

If the carrier voltage is a balanced three phase voltage, the result contains the rotor speed information as follows **[11]**;

$$i^s_{qds_c} = \begin{bmatrix} i^s_{qs_c} \\ i^s_{ds_c} \end{bmatrix} = I_{cp}\begin{bmatrix} \sin(w_c t) \\ \cos(w_c t) \end{bmatrix} - I_{cn}\begin{bmatrix} \sin(h\theta_r - w_c t) \\ \cos(h\theta_r - w_c t) \end{bmatrix}$$

$$= -j.I_{cp}.e^{jw_c t} + j.I_{cn}.e^{j(h\theta_r - w_c t)} \quad \textbf{(12)}$$

$$I_{cp} = \frac{V_{sc}}{w_c.(\Sigma L_{\sigma s}{}^2 - \Delta L_{\sigma s}{}^2)}.\Sigma L_{\sigma s} \quad \textbf{(13)}$$

$$I_{cn} = \frac{V_{sc}}{w_c.(\Sigma L_{\sigma s}{}^2 - \Delta L_{\sigma s}{}^2)}.\Delta L_{\sigma s} \quad \textbf{(14)}$$

I_{cp} and $I_{cn}$are the positive and negative sequence components. The positive sequence component contains no information about the rotor position and is related to the average stator transient inductance; however, negative sequence contains rotor speed information, as given in **(12)**.

An example of signal injection method is given in **[12]**. Short durational test vectors are applied by inverter drive in between the fundamental driving waveform, and a transient is created on the phase currents of the machine. As the applied vectors are

equal and opposite pairs, the sum of all becomes zero and have no effect on the fundamental excitation. By measuring the zero sequence current of a delta connected machine, a signal which is position dependent is obtained. Figure 1 illustrates the applied test vectors in balance, in a vector controlled algorithm and Figure 2 shows the results of position prediction using this method **[12]**.

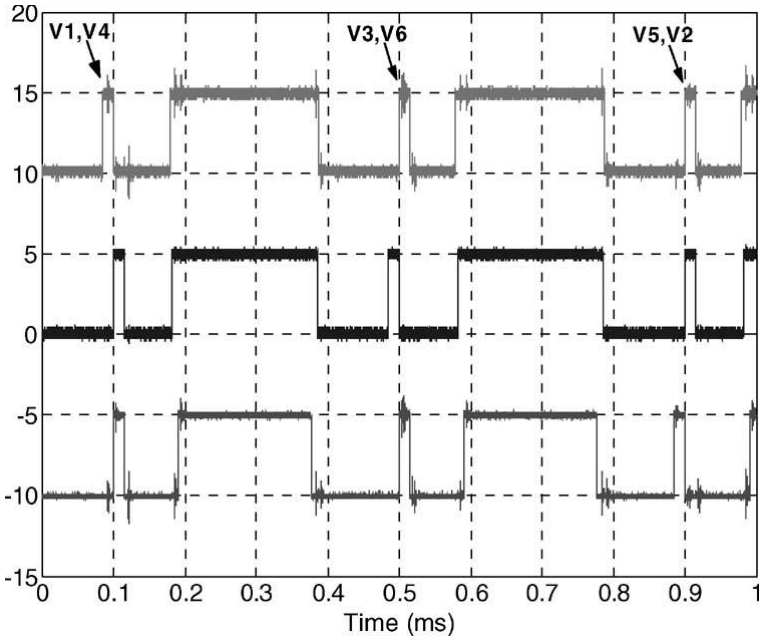

Figure 1 Test vectors [12]

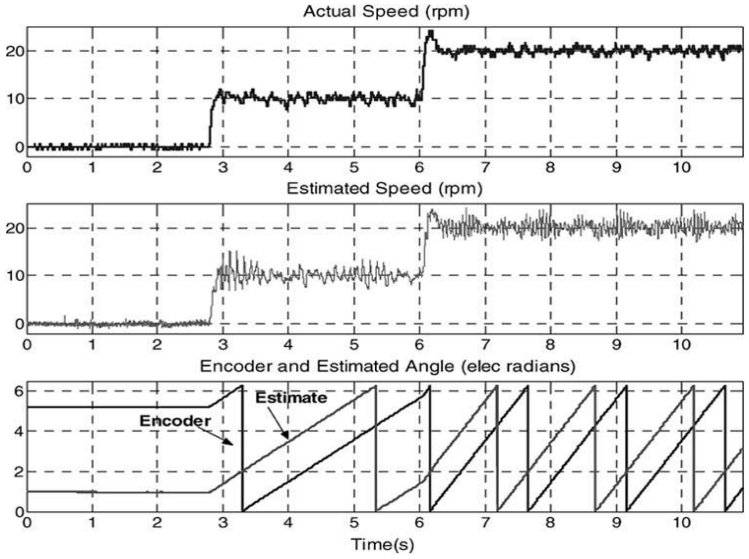

Figure 2 Position estimation and speed estimation for 0 to 10 to 20 r/min at no load [12]

As seen from Figure 2, injecting test signals by using the driver hardware and detecting them from the zero sequence current, rotor speed and position can be estimated.

Other than measuring zero sequence current and using the algorithm proposed in **[12],** rotor speed and position can be estimated by measuring the line current and line voltage and trying to detect the harmonics created due to the injected signal. The challenging part of this method is to obtain the information in between the many other harmonics.

In **[13],** injection based sensorless control methods are compared. Three different methods are utilized; negative sequence carrier signal current, zero sequence carrier signal voltage and pulse width modulation zero sequence voltage. At the end of the performance evaluation and comparison of three different method of signal injection **[13]** concludes that all methods can be used for rotor position estimation and field orientation.

In **[13],** the information of the injected signal which carries information about the rotor position is extracted by using filtering methods in one of the methods discussed. The motor drive signal is rotated with the rotating reference frame, resulting in a relative dc component to be filtered. A single low pass filter, called synchronous frame filtering is then used to filter out the spatial information. Figure 3 gives the block diagram of the discussed algorithm. The synchronous frame filtering method to estimate rotor position is claimed to be suitable for vector control algorithms, however, signal injection is needed and also the drive signals shall be modified to implement the filtering.

Another method proposed in **[13]** for extracting the information about the rotor position from the injected signal is using observers. The proposed observer flow chart is given in Figure 3 and is used to estimate rotor speed from the negative sequence component **[11]**, **[13]** without using spectral estimation methods like FFT. The error signal, which is the vector cross product of measured negative sequence carrier signal current vector and the saliency model negative sequence carrier signal

vector, closes the phase lock loop of the speed estimator, and the estimated position tracks the actual rotor position.

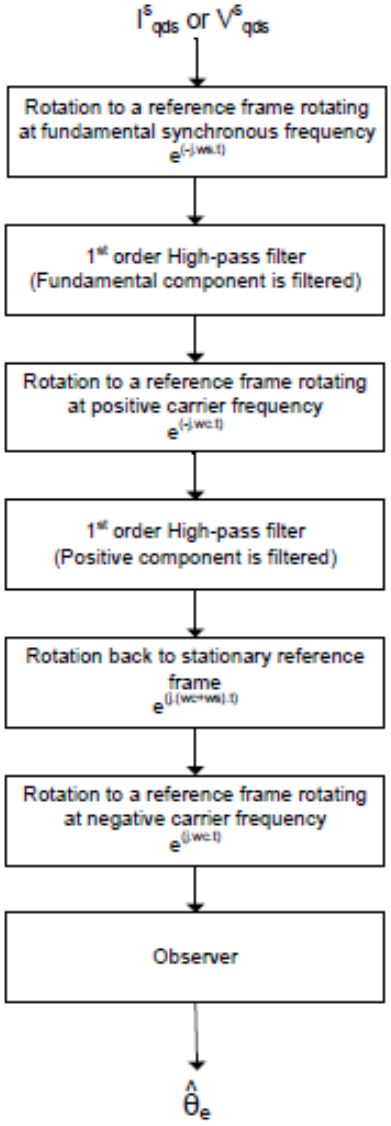

Figure 3 Signal processing used to extract spatial information from voltage or current carrier signal injection [13]

The estimation accuracy of saliency based models depends on the used saliency model **[15]**. A single saliency estimation model can result in high error when multiple saliencies exist and this problem can be solved by using a narrow bandwidth

observer or multiple saliency observers **[15**]. In **[15**], Degner and Lorentz works on a signal injection method and aims to increase the resolution and bandwidth of saliency based tracking techniques. They propose modeling machines with multiple saliencies to increase estimator accuracy.

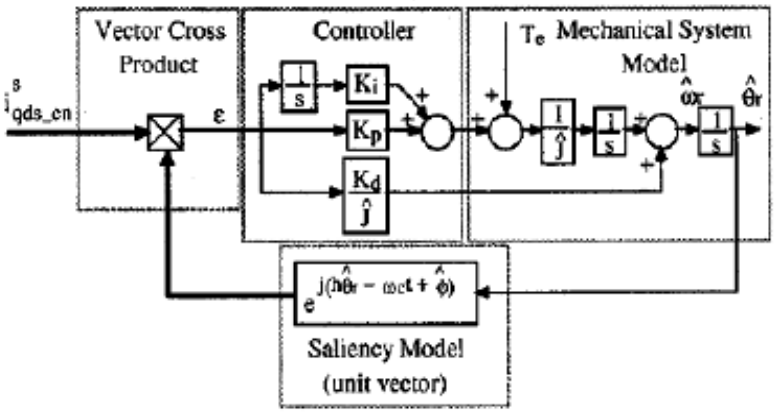

Figure 4 Tracking observer for the estimation of rotor position in a machine with a harmonic saliency [13]

In **[14],** the full load and full flux condition of a signal injected sensorless position control is investigated and it is shown that using modulating effect of rotor slots to estimate rotor position brings about good accuracy. The paper focuses on high-load and full-flux condition of a symmetric cage induction motor and the deteriorating effect of saturation harmonics at full flux condition at high load is solved by a harmonic compensation scheme. It is also claimed in **[14]** that saturation harmonic suppression technique can be used to track rotor position.

Injecting a test carrier is advantageous as it is able to work at low speeds down to zero. Another advantage of the method is that it is not dependent on the motor parameters. However, the main disadvantage is that the applied PWM driving signal is modified. Because of the relatively high magnitude injected signal, torque and speed fluctuations occur **[17]**.

1.2 Speed Estimation by Using the Rotor Slot Harmonics

Using RSHs to estimate the rotor position and speed is widely used method. The harmonics caused by the permeance variation due to the machine slots contains

information about the rotor speed and no signal injection is needed **[18]**. In this work, Ishida, Hayashi and Ueda places search coils on the stator 120 degrees apart and fundamental slot harmonics are induced to these coils. By series connection of the coils the fundamental voltage cancels out and implementing analog filtering to the induced voltage results in RSH detection **[18]**. This method needs modification of the machine as placing search coils on the stator is needed.

To be able to use the RSHs for estimation, the nature of the harmonics shall be understood firstly. In their study **[20]**, Ishida and Iwata proved that RSHs exist in air-gap flux due to stator and rotor iron cores to install wirings (or bars). The RSHs are induced on the stator windings when the rotor rotates. Moreover, the claim that the frequency of RSHs is not dependent on electrical parameters of the induction motor other than the stator frequency. More importantly, as the RSHs exist due to the mechanical structure, the rotor speed or the slip can be detected from the stator phase voltages. They formulated the air gap flux as follows;

$$B(\theta,t) = B_0 \cos(\omega t - \theta)\left[1 + k_H cos\left(\frac{Z}{P}\omega_r t - \theta\right)\right] \quad \textbf{(15)}$$

where;

θ : angular position on the stator surface,

ω_r : angular velocity (both θ and ω_r are in electrical angle scale),

ω : angular frequency of the power supply,

Z: number of slots,

P: number of pole pairs,

B_0: magnitude of fundamental component of flux density,

k_H: ratio of amplitude of the variation to the fundamental component.

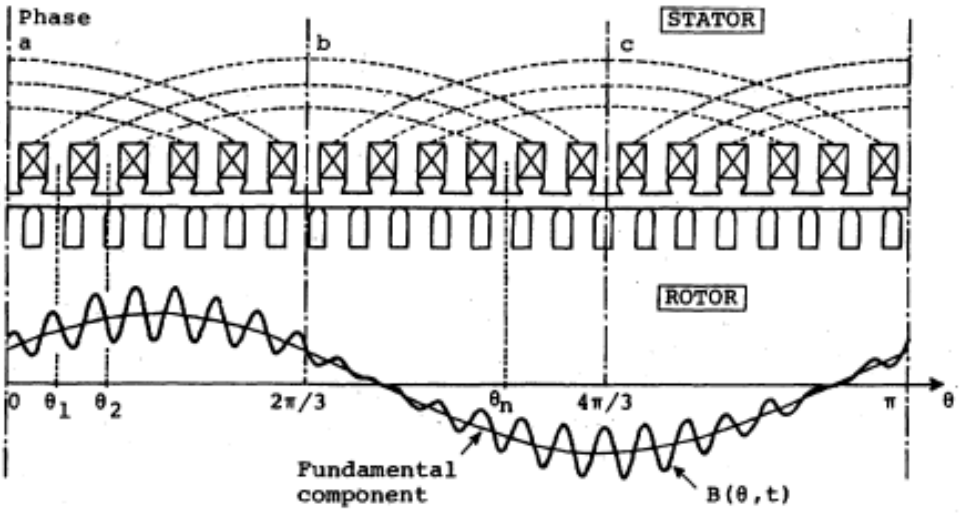

Figure 5 Air-gap structure and flux distribution of an induction motor [20]

By assuming that there exist a search coil exist on a stator tooth whose position is θ_n, its induced voltage can be expressed as;

$$v_c(t) = -N\frac{d\phi}{dt} \tag{16}$$

$$v_c(t) = -k.B_0\sin(w_s t - \theta_n) - k_f.B_0 k_H(N_r w_r w_s)\sin[(N_r w_r + w_s)t - (N_r + 1)\theta_n] - k_r.B_0 k_H(N_r w_r - w_s)\sin[(N_r w_r - w_s)t - (N_r - 1)\theta_n] \tag{17}$$

Equation **(17)** can be used to express the RSHs in an electrical machine. The RSHs are expressed as two pair components; which are actually the output of a modulation process, the rotor slot velocity($N_r w_r$) is modulated with the angular velocity of the supply (w_s) **[21]**.

According to **[20]**, the expression given in **[19]** can also be expressed as follows;

$$B(\theta,t) = B_1\cos(w_s t) + B_f\cos\left[\left(\frac{Z}{P}w_r + w_s\right)t - (P+Z)\theta + \Psi_f\right] + B_r\cos\left[\left(\frac{Z}{P}w_r - w_s\right)t - (P-Z)\theta + \Psi_r\right] \tag{18}$$

where;

θ: is mechanical angle,

t: is time,

w_s: is the supply angular frequency,

P: is the number of pole pairs,

w_r: is the rotor angular frequency,

Ψ: is phase angle.

Equation **(19)** gives the forward (positive sign) and backward (negative sign) slot harmonics **[19]**.

$$w_{rsh} = (Z/P)w_r \mp w_s \quad \textbf{(19)}$$

Equation **(19)** clearly describes that the RSHs frequency is a linear function of the rotor speed, w_r. The rotor speed can be calculated by the RSHs frequency if the rotor slot number and the pole number are known. Equation **(18)**can also be written in the form of **(19)**.

$$f_r = (P/Z)(f_{rsh} \mp f_s) \quad \textbf{(20)}$$

The rotor speed, N_r(rpm) can be calculated from the RSHs frequency f_r.

$$N_r = \frac{60 f_r}{P} \quad \textbf{(21)}$$

Rearranging equation **(20)**and **(21)** gives the following direct relation between the RSHs frequency and the rotor speed.

$$N_r = (60/Z)(f_{rsh} \mp f_s) \quad \textbf{(22)}$$

Equation **(22)** shows that by knowing the supply frequency and the rotor slot number, the rotor speed can be calculated from the RSHs frequency. As the supply frequency is the control variable, it is known by the driver. Moreover, Keysan **[21]** proposes methods to calculate the number of the rotor slots if it is not supplied by the manufacturer. As a result, the rotor speed can be calculated if the frequency of the RSHs is known.

An example of speed estimation from RSHs is given in **[23]**. The stator current is used to extract the RSHs by examining its frequency content with spectral

transformation. The stator current is sampled for 4 seconds with a sampling rate of 1kHz, resulting in 4096 samples. Then, a spectrum analyzing method, FFT, is used to detect the RSHs **[22]**. The most significant disadvantage of analyzing the frequency spectrum method is the need long data record time and computational time of transformation. To decrease the elapsed time between two estimations, the transformation is conducted at every 100ms, so only 2.5% of the total input data is refreshed; the others are the previously recorded samples **[22]**. Although this modification improves the estimation frequency, the FFT computational time (about 50ms) is still high and makes the method inapplicable for online implementation of a position feedback vector control drive. It must be noted that online implementation requires obtaining the rotor position information within some hundreds of micro seconds.

FFT analysis method results in high position prediction error when the shaft speed change is a fast as shown in Figure 6-a.It can be observed that the time lag between the rotor speed estimation and actual speed is in the order of 2 seconds. For slow transients the delay is in the order of hundred millisecond sas seen in Figure 6-b. Therefore it can be concluded that FFT method for position estimation cannot be used at a vector control drive which works and needs actual position in about hundreds of microseconds.

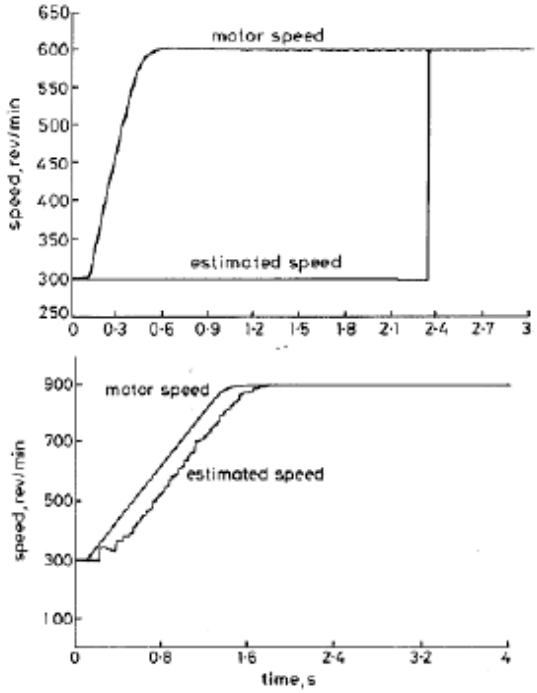

Figure 6 Actual and estimated speed for fast and slower rate transients [23]

In **[21]**, Keysan proposes a method to estimate the rotor speed without spectral analysis. Keysan captures the flux information as voltage coupled to a search coil wound around the motor shaft, then demodulates the captured data, finally filters out the RSH and measures its frequency by counting the zero crossings. The flowchart of the proposed algorithm is as in Figure 7.

By demodulation, the modulated pair of RSHs is reconstructed at the actual RSHs frequency. Band-pass filtering separates the RSHs from the other signals existing in the captured data, and the zero crossing detection gives the result of the frequency of the RSH. As the frequency of the RSH is directly related to the rotor speed, the zero crossings of the signal can be expressed as the passing of a rotor slot with respect to the reference frame. This implies that each zero crossing can be expressed in terms of rotor position **[21]**. The speed information can also be calculated by the position information by looking at position change rate. Even though the proposal seems to be applicable within a vector control algorithm, it is not implemented on a running machine and real time estimation is not experimented. Moreover, modification on the machine is needed as placing a search coil is needed.

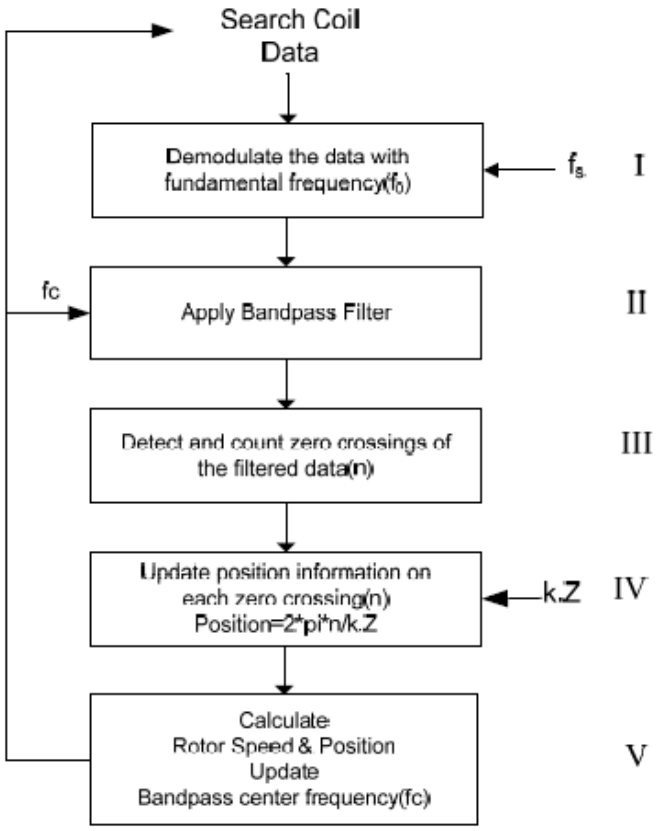

Figure 7 Block diagram rotor speed and position detection algorithm [21]

The method proposed by Keysan in **[21]** needs rotor slot number for the predictions. This parameter may not be supplied by the manufacturer. In **[22]** Keysan proposed a method to calculate the rotor slot number of a machine from the induced emf in an external search coil. The search coil voltage is recorded and its frequency spectrum is analyzed via FFT. The RSHs and the rotor saliency harmonics are analyzed as shown in Figure 8and the number of rotor slots is calculated **[22]**.

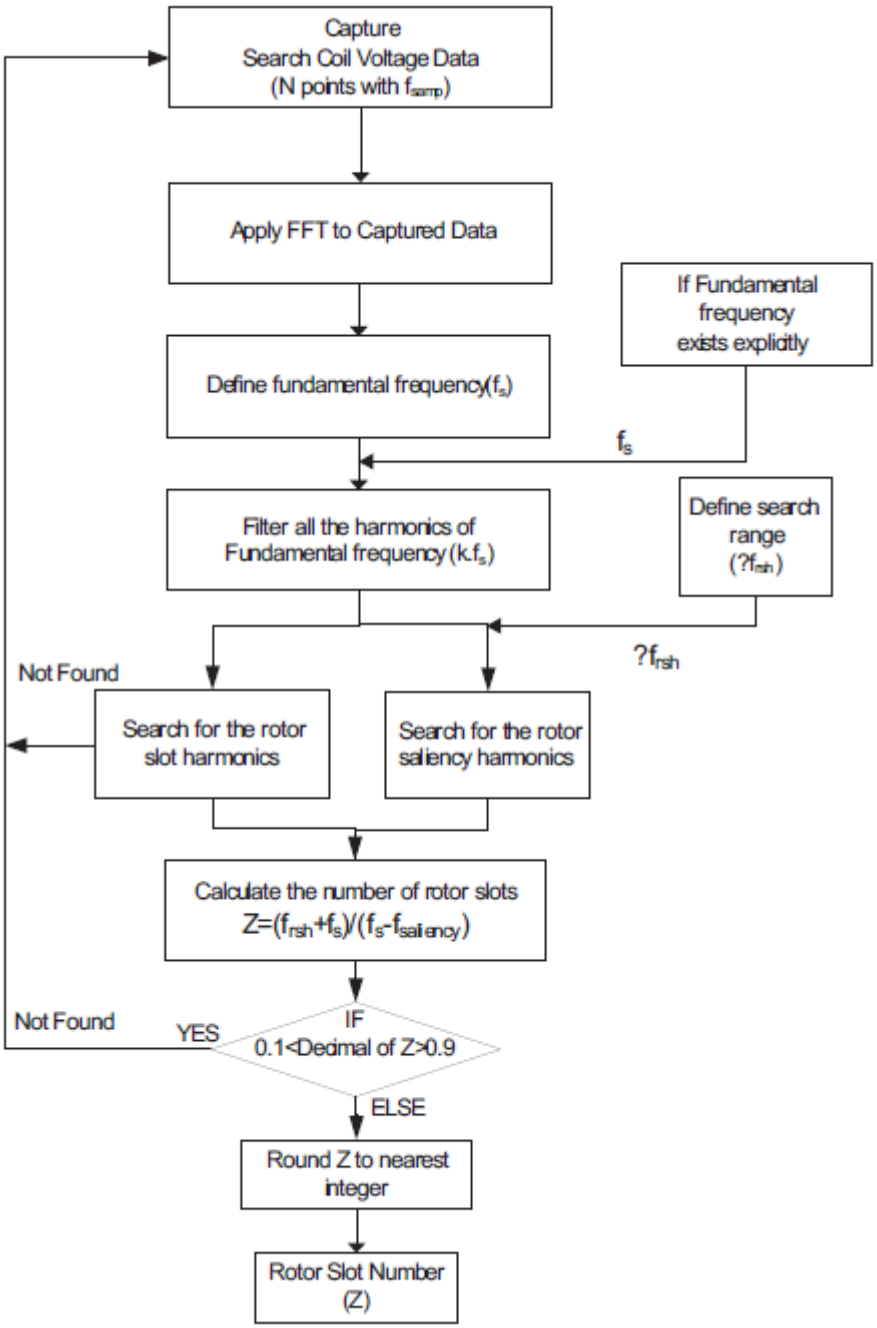

Figure 8 Determination of rotor slot numbers of an induction motor [22]

1.3 Aim and Content of the Thesis

In this thesis, the aim is to find out whether the algorithm proposed by Keysan in **[21]** can be implemented using the motor current for predicting the rotor position while the motor is running. Also it is desired to find out the speed range and also

accuracy of the rotor position predictions. Since the stator current is always available in a vector controlled drive, the implementation of this approach does not need any sensors. The information on rotor position may be used within a sensorless vector controlled drive as the sole source of position information. Alternatively this information may be used for correcting the drift in the calculation of the rotor flux. In any case the accuracy of the position information is expected to increase and therefore torque response of the drive is expected to be better over a wider frequency range. It may be postulated that if the position information is accurate an open loop sensorless drive performance may approach the response of a drive with position sensor. Note that since there is no need for an external sensor, this approach may be also applied to existing drive applications, simply be updating the drive software.

In order to determine whether stator current data is suitable for the algorithm, first the stator current data will be investigated to find out the nature of the harmonics in the stator current. For this purpose the stator current will be recorded under various operating conditions and the harmonics contained in the recorded. This recorded information will be analyzed offline and identifying the rotor position. In this manner the range of supply frequencies where this algorithm may be used for position control will be identified. Afterwards, the algorithm will be implemented on a test set-up and the position estimation results will be compared with a commercial encoder data providing rotor position information. While implementing the algorithm, the filter implementation during online system will be explained. The limiting factors of the algorithm and the online implementation will be analyzed.

In Chapter 1, the need of speed and position sensing in motor control is expressed. Different position sensing methods in the literature are examined and their advantages and disadvantages are listed. The proposed algorithm by Keysan in **[21]**is also summarized as it is the algorithm that needed to be implemented for detecting rotor position from the motor current.

In Chapter 2, the stator current frequency content is studied offline to show that the RSHs exist and are observable in stator phase current. The speed limit of the algorithm is specified by investigating the amplitude of the harmonics. The data is

recorded firstly from variac driven machines, then inverter drivers are used to record current data and it is shown that the algorithm can be used in inverter driven systems. Lastly, the proposed algorithm is implemented offline and the results prove that the algorithm can be implemented with stator current input.

In Chapter 3, detailed analysis of the proposed algorithm by Keysan in **[21]** is given. The hardware and the software used in the online algorithm are explained. The analysis is done to select the proper filtering implementation.

In Chapter 4, the results of the online implementation are given to show that the algorithm can be implemented in online systems. Some improvements that are implemented to correct the estimation result are stated and their effects are analyzed. Lastly, the weaknesses and the disadvantages of the algorithm and the reasons for them are listed.

In Chapter 5, the study done on rotor position estimation is concluded and the suggested future work is listed.

CHAPTER 2

ANALYSIS OF ROTOR SLOT HARMONICS DETECTION FROM STATOR CURRENT AND OFFLINE IMPLEMENTATION OF THE ALGORITHM

It is shown in **[23]** that RSHs can be detected from the stator current data. In this chapter, it will be analyzed whether the stator current data is suitable to be used in the proposed algorithm. To do this, the frequency spectrum of the stator current data will be investigated. Trials will be made by using different inverter drivers and at different sample rates to show that the algorithm can be implemented with inverter drivers and to specify the sample rate requirements. After expressing that the RSHs exists and detectable in the stator current data, some experiments will be conducted on the recorded data to show that the stator current information can be used as an input to the position algorithm. As a result of the studies in this chapter, it will be shown that the stator current can be used as input to the proposed algorithm and the use of search coils can be eliminated.

2.1 Offline Investigation of Rotor Slot Harmonics in the Stator Current

In order to analyze the frequency content of the stator current data for RSHs; current data is recorded and that data is processed. As implementation of frequency spectrum analysis is easy via MATLAB's FFT function, this method is preferred to get the frequency spectrum. In order to be able to use the tool, it is important to record data long enough to have the desired resolution and with appropriate time step. The data record length corresponds to the resolution in the frequency domain and the data record time step corresponds to the maximum frequency to be analyzed. The

maximum frequency to be analyzed will be determined by choosing the RSH couple to use in the algorithm. It will be chosen by comparing the amplitudes of the harmonics. The laboratory set-up used is specified in Section 2.2 and the needed data record characteristics are analyzed in Section 2.4**.**

2.2 The Laboratory Setup Used in the Test

The stator current data is recorded using an induction machine. The motor's rated power is 1.1kW, it has 6-poles and it is a wye-connected induction motor. It has 36 stator and 26 rotor slots. The tests are conducted at no load conditions. In order to have less noise in the frequency spectrum, this motor is firstly supplied from the mains through a variac. It is apparent that the motor is driven at constant 50 Hz mains frequency as variac is not able to change the frequency. If the system works well at less noisy 50Hz mains supply, two inverter drivers will be used to see the effect of the type of drive. Inverter drivers are also used to change the drive frequency to see the effect of drive frequency change and as a result change of rotor speed. As motor drives, two inverter drivers are used, one is a commercial driver, produced by Siemens Inc, whose characteristic is given in **[24]**; the other one is a specially designed inverter driver by Kayhan, whose characteristic is given in **[25]**.

In this part of the work, the stator current is recorded for 1 seconds with 5000 data points and 10000 data points in order to have 5kHz and 10kHz sampling rate with a current probe (fluke 80I-110S) of 100mV/A and an oscilloscope (Agilent Infinivision MSO-X-3024A) The characteristics of LEM current sensors used for online implementation are given in **[25]** and the current probe is similar, the current probe results can be used to record data for offline tests. The recorded data is taken as a .csv file from the oscilloscope and the trials are conducted offline at Matlab program. As offline trials are easier for implementation and conduct trials for filtering, the filter for online implementation will be firstly tried at offline algorithm.

The amplitude axis in frequency spectrum figures in this work which are calculated by FFT transformation in Matlab are in fact in mV as the stator current is current recorded by the current probe. Keysan in **[21]** uses external search coil voltage which

is in the order of 0.2mV-0.6mV to detect the rotor position. In this work, the current data is received as mV also, either from a current probe of an oscilloscope 1mV-6mV or from a LEM current sensor. As the search coil voltage is analyzed in **[21]** by Keysan, the Amplitude axis unit is also mV in his analysis. As both units are mV, their amplitudes can be compared.

2.3 The Loaded Test Set-up

While implementing the loaded tests, another 1kW induction motor is coupled to the test motor shaft in order to load the test motor mechanically as shown in Figure 9.

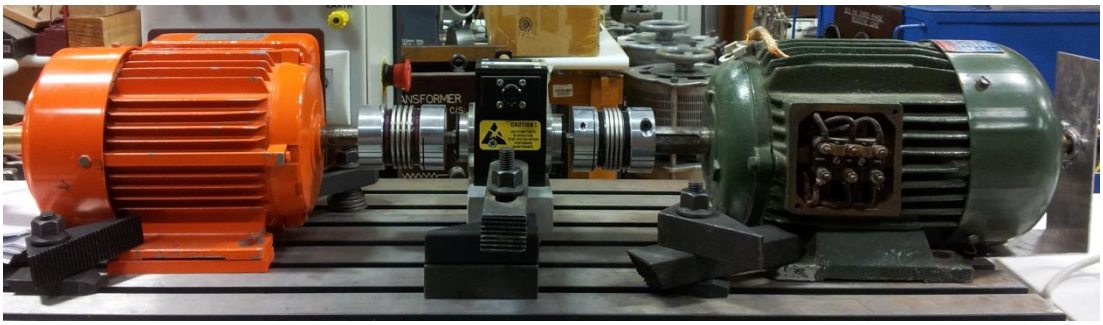

Figure 9 The loaded test motor set-up

While the test motor is driven at V/f control, the load motor is controlled at constant torque mode via the commercial inverter whose details are given in Chapter 2. Both motors are electrically connected in such a way that the tendency to turn the shaft of the motor of both drivers was the same way. The constant torque mode driven load motor is then over-driven by the test motor to the generation mode, so the test motor becomes loaded. A resistor is placed on the DC bus of the commercial inverter so that the generated energy can be dissipated and over-voltage condition for the inverter DC bus is prevented.

2.4 Data Recording

There exist some important factors while recording the motor current data. These factors directly affect the results of the analysis. The recorded data will be processed with the FFT function of MATLAB program.

The frequency range that should be analyzed can be calculated as **(23)** in **[21]**;

$$\text{RSHs Frequency} = n \times \frac{Z}{P} \times fr \pm k \times fs \quad \textbf{(23)}$$

$$\text{Rotor Speed} = \frac{60 \times \text{fr}}{P} \quad \textbf{(24)}$$

where;

fs is the supply frequency,

P is the number of poles.

Rated specified mechanical rotor speed is 1000 rpm, and the expected RSHs frequencies at rated speed is calculated and tabulated at Table 1.

Table 1 Expected rotor slot harmonics frequency

1st couple(Hz)	2nd couple(Hz)	3rd couple(Hz)	4th couple(Hz)	5th couple(Hz)
433±50	866±50	1299±50	1732±50	2165±50

As the maximum frequency that is desired to exist in the analysis is 2215Hz, the data shall be sampled at least 2 times higher rate than this frequency range (Nyquist rate). For this reason the data should be recorded such that the result of FFT analysis reaches up to 5kHz.

Another factor that should be kept in mind is the resolution of the frequency domain analysis. Previous work conducted on this issue **[21]** suggests 1Hz resolution is enough and that resolution will also be used in this research.

In the light of this information, the data recording is conducted as follows;

$$f = \frac{1}{T_{max}} \gg T_{max} = 1s = \text{the data record length} \quad \textbf{(25)}$$

$$f_{max} = \frac{T_{max}}{time\ step} = \frac{T_{max}}{{}^{1}/_{\#of\ data\ points}} = 5000 \gg \#\text{of data points} = 5000 \quad \textbf{(26)}$$

In this chapter, the test results of spectral analysis of stator current will be investigated in terms of RSHs. The tests are conducted at different drive frequencies to see the effect of rotor speed on the spectrum. Similarly, data obtained from

inverter drivers are analyzed to see the effect of driver hardware. Last but not least, data is recorded at different sample rates and their results are analyzed to see the effect of sample rate. The results of spectral analysis of stator current are compared with the results of Keysan in **[21]** to be able to show that the stator current data is also suitable for the position estimation.

2.5 Frequency Spectrum Analysis of Stator Current of Variac Driven Machine at 50 Hz

To identify the RSHs in the stator current, the frequency content of it is analyzed. The expected RSH frequencies are tabulated at Table 2when the machine rotor speed is 996rpm.The motor is driven through the mains via a variac, so the fundamental stator drive frequency is 50 Hz. The data is recorded at no load condition.

Table 2 50 Hz 996 rpm expected rotor slot harmonics

Supply freq. (Hz)	Rotor speed (rpm)	Middle freq. (Hz)	1st couple (Hz)		2nd couple (Hz)		3st couple (Hz)		4th couple (Hz)		5th couple (Hz)	
49,96	996	431	381	481	813	913	1244	1344	1676	1776	2108	2207

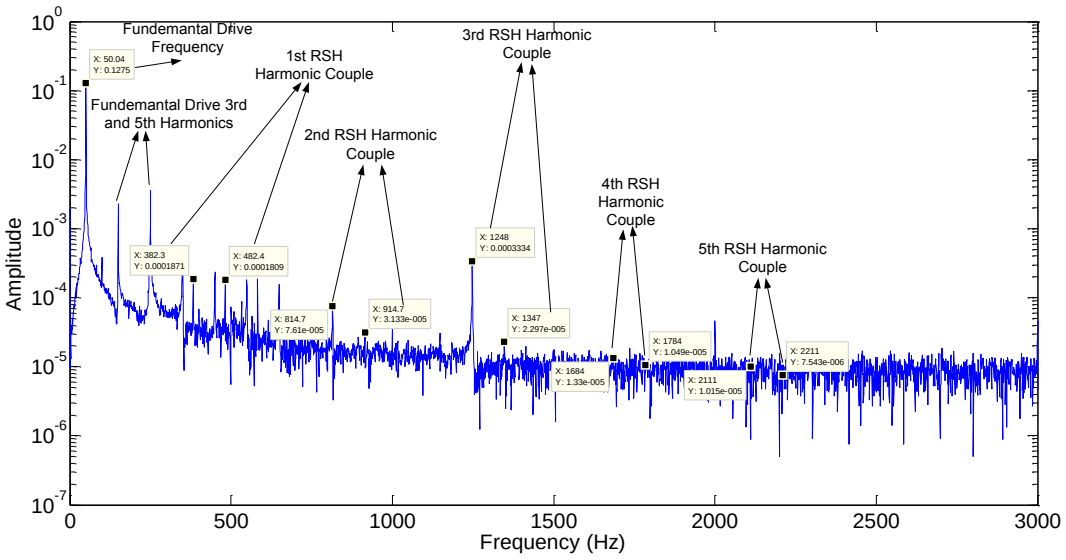

Figure 10 RSHs analysis of frequency content of stator current where the machine is driven with variac at 50Hz fundamental frequency

The test result given in Figure 10 where the motor is supplied through a variac at 50Hz fundamental frequency at no load shows that the RSHs exist as couples in the stator current data. It is also seen from Figure 10, the 3rd RSH has the highest magnitude compared to the noise level in its vicinity. The result given in Figure 10 is similar to the search coil frequency content analyzed in **[21]** as given in Figure 11. The RSHs spectral analysis conducted by Keysan in **[21]** by recording search coil voltage at 50Hz drive frequency is given in Figure 11. His results show that RSHs exist and are observable while the motor is driven at 50Hz at no load.

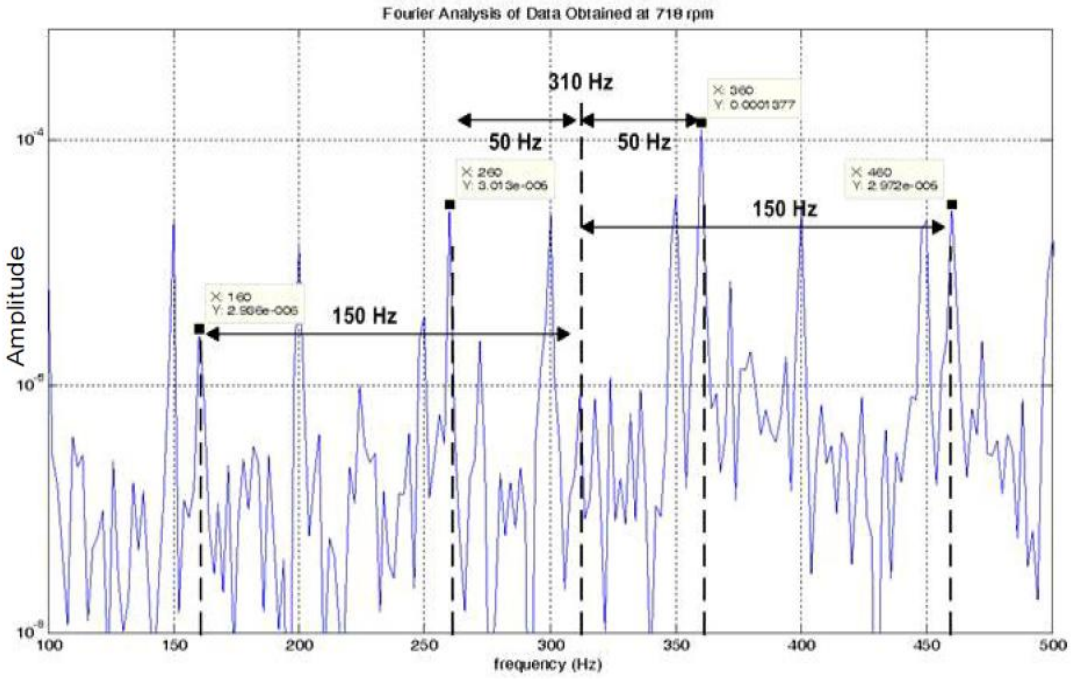

Figure 11 Frequency content analysis of search coil voltage for investigation of RSHs at 50Hz inverter driven machine [21]

The RSH couples amplitude is tabulated with respect to harmonic number in Table 3.

Table 3 RSH amplitude with respect to harmonic number at 50 Hz (sinus supply at no-load)

	Harmonic #1	Harmonic #2	Harmonic #3	Harmonic #4	Harmonic #5
Amplitude(mV)	1,8	0,76	3,3	0,14	0,099

It can be inferred from Table 3that the 3rd RSH has the highest amplitude in average, and it's the most suitable harmonic to be used in the estimation.

2.6 Frequency Spectrum Analysis of Stator Current of Inverter Driven Machine for Investigation of Rotor Slot Harmonics

In this section, it is aimed to see whether RSHs are observable at frequency content of stator current of inverter driven machines. Two inverters are used to drive the motor at no load, and stator current of the motor is recorded and analyzed offline. One of the inverter is a commercial driver, produced by Siemens Inc, whose characteristic is given in **[24]** (will be called as commercial inverter), other is a specially designed inverter driver by Kayhan, and whose characteristic is given in **[25]** (will be called as homemade). The frequency content of stator current (50Hz - No load) of inverter driven machines are given in Figure 12 and Figure 13.

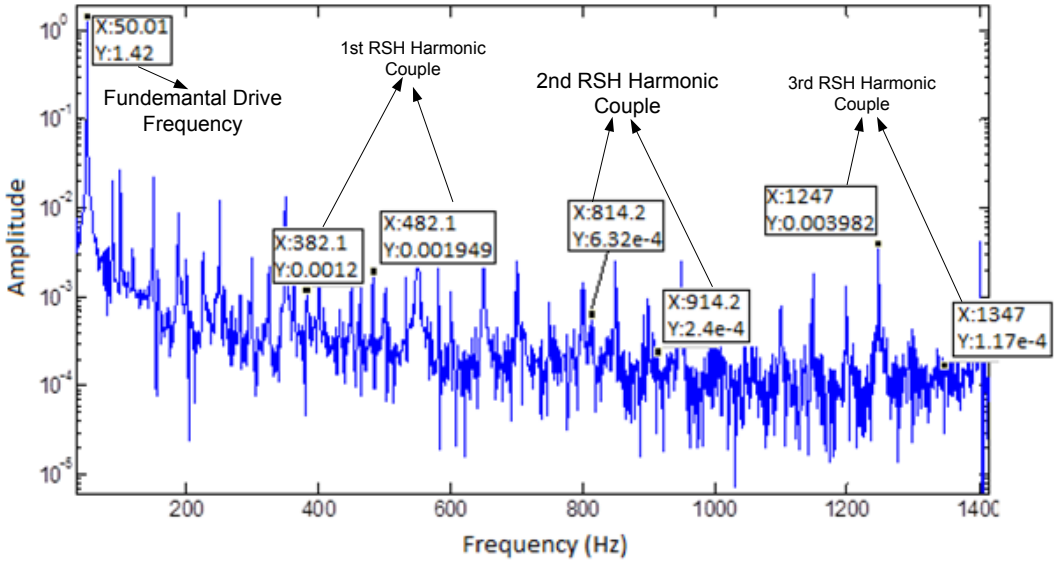

Figure 12 Frequency content of stator current of inverter driven machine using homemade driver in [25]at 50 Hz fundamental frequency

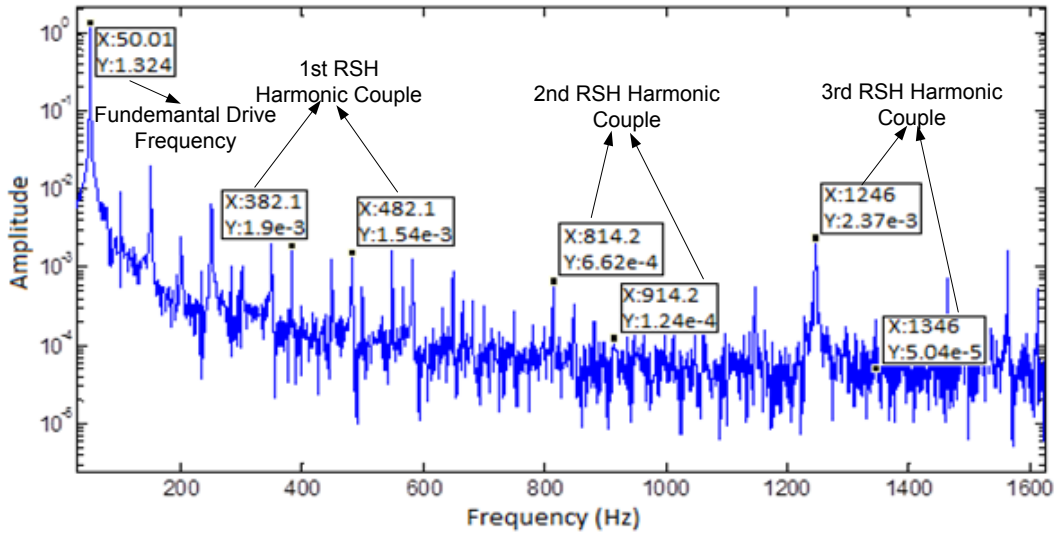

Figure 13 Frequency content of stator current of inverter driven machine using commercial driver in [24] at 50 Hz fundamental frequency

The comparison of RSH magnitude variation with 3 drivers given in Table 4 show that the algorithm can be applied to inverter driven systems as the RSHs, especially the 3rd couple, is observable at all three drivers. It can also be inferred from Table 4 that even though the RSHs magnitude changes with the used driver at different harmonic numbers, the amplitudes are in the same order and all the harmonics are detectable.

Table 4 RSH Magnitude Change with Varying Drivers When the motor is driven at 50Hz at No-load at 998rpm

	Harmonic #1 Amplitude (mV)	Harmonic #2 Amplitude (mV)	Harmonic #3 Amplitude (mV)
Siemens Inverter Driven	1,9	0,66	2,37
Homemade Inverter Driven	1,94	0,63	3,98
Variac (Sinus) Driven	1,8	0,76	3,3

Moreover it can be inferred from Figure 10, Figure 12 and Figure 13 that even though the frequency spectrum of stator current of inverter driven tests are noisier than variac driven machine stator current frequency spectrum, the noise level around the 3rd RSH couple is lower compared to other harmonic couples and the algorithm can be implemented using 3rd harmonic couple.

2.7 Frequency Spectrum Analysis of Stator Current with Increased Sample Rate

In this section, frequency content of stator current is analyzed (50Hz - no load) offline at higher data record rate. While stator current was recorded for 1sec with 5000 samples per second in the previous analysis, the data is recorded for 1sec with 10000 samples in this section.

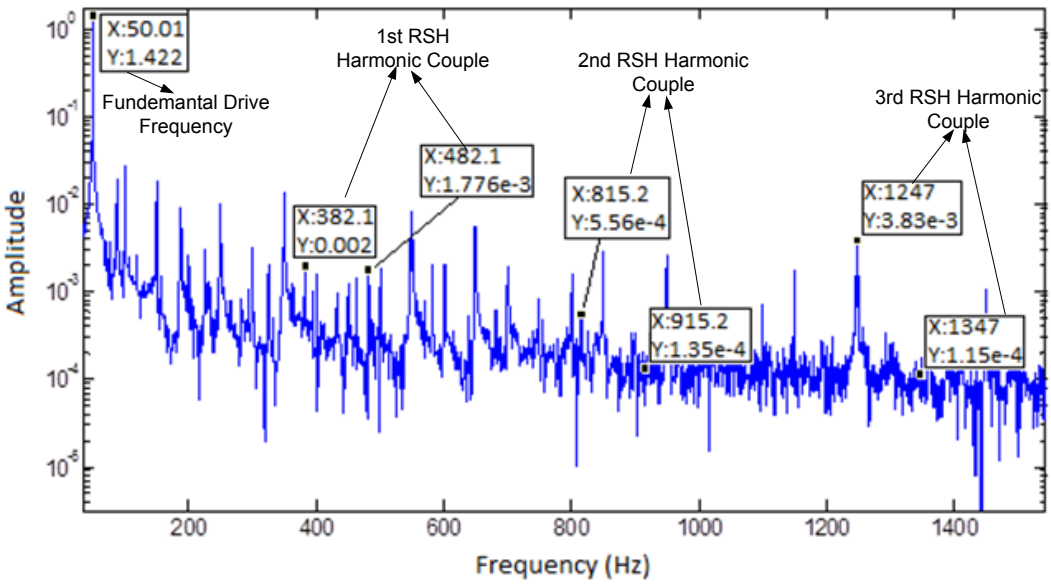

Figure 14 Frequency content of stator current driven with homemade inverter in [25] at 50 Hz fundamental frequency with recorded 10000 data points per second

The frequency content of stator current using driver in **[25]** at 50 Hz fundamental frequency with 10000 data points per second sampling rate is given in Figure 14. The

amplitude comparison of the same the data sample rate in RSHs is given in Table 5. It is seen from the table that the RSHs magnitude does not change significantly with data sample rate. So, increasing the data sample rate does not affect the algorithm results in the amplitude of the RSH.

Table 5 Amplitude comparison of RSH magnitude with increased sample rate with 50 Hz homemade inverter in [25] driven machine at no-load

	Harmonic #1 Amplitude (mA)	Harmonic #2 Amplitude (mA)	Harmonic #3 Amplitude (mA)
5000 data/s Sample Rate	1,94	0,63	3,98
10000 data/s Sample Rate	2	0,56	3,83

Table 5 shows that the RSHs are also observable at recorded stator current data of inverter driven machines at higher sampling rates. It can also be inferred from Figure 14 that increasing data record points does not result in less noisy frequency spectrum.

2.8 Frequency Spectrum Analysis of Stator Current at Inverter Driven Machine at Constant Speed with Different Drive Frequencies

In this section, the drive frequency, as a result the rotor speed is changed and the frequency spectrum of stator current is analyzed to see the effect of rotor speed on RSHs.

2.8.1 Stator Current Frequency Spectrum at 40 Hz Fundamental Drive Frequency

The expected RSHs frequencies in stator current of the machineat40 Hz drive frequency at 795rpm rotor speed are tabulated at Table 6. The machine is driven at 40Hz fundamental frequency at no load.

Table 6 Expected RSH frequency in stator current when the rotor speed is 795 rpm

Supply freq (Hz)	Rotor speed (rpm)	Middle freq. (Hz)	1st couple (Hz)		2nd couple (Hz)		3rd couple (Hz)		4th couple (Hz)		5th couple (Hz)	
39,8	795	344	304	384	649	729	993	1073	1338	1418	1682	1762

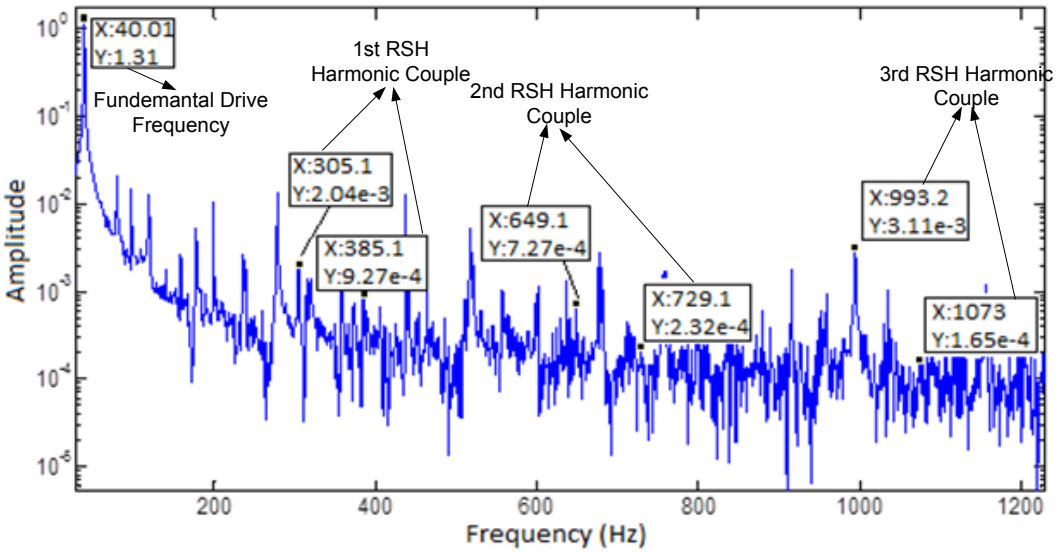

Figure 15 Frequency content analysis of stator current of inverter driven machine using homemade driver in [25] at 40 Hz (795rpm) fundamental supply frequency for investigation of RSHs

Table 4 shows that the algorithm can also be applied at 40 Hz drive frequency at 795rpm rotor speed as the RSHs magnitude is 10 times higher than the amplitude of search coil RSH magnitude.

Table 7 RSH amplitude comparison in search coil voltage and stator current at 40Hz drive frequency

	Harmonic #1 Amplitude	Drive Frequency(Hz)	Rotor Speed (rpm)
Search Coil Voltage (mV)	0,314	40	686
Stator Current (mV)	2,04	40	795

The spectral analysis result of search coil voltage test conducted at 40Hz driven machine is given in Figure 16 and it is seen that the search coil frequency spectrum and stator current frequency spectrum are similar when analyzing the RSHs.

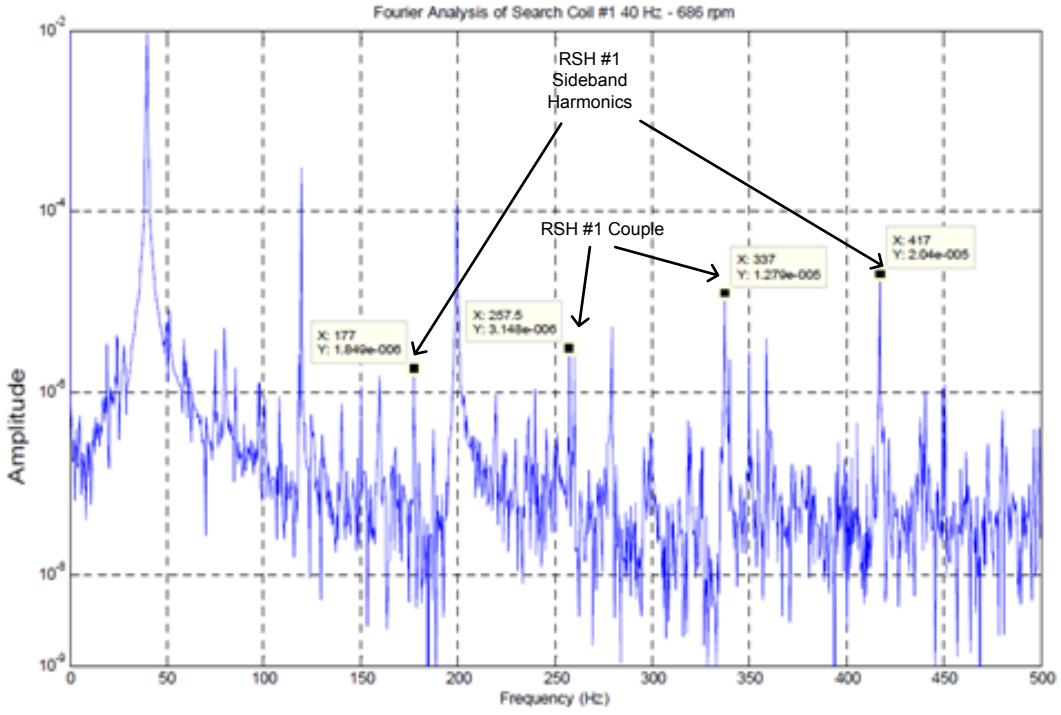

Figure 16 Frequency content analysis of search coil voltage with 40Hz inverter driven machine for investigation of RSHs [21]

2.8.2 Stator Current Frequency Spectrum 20 Hz Fundamental Drive Frequency

The expected RSHs frequencies in stator current when the rotor speed is 398rpm are tabulated at Table 8 for 20 Hz driven machine at no load.

Table 8 Expected RSHs frequency in stator current when the rotor speed is 398 rpm

Supply Freq. (Hz)	Rotor speed (rpm)	Middle freq. (Hz)	1st couple (Hz)		2nd couple (Hz)		3rd couple (Hz)		4th couple (Hz)		5th couple (Hz)	
20,00	398	172	152	192	324	364	497	537	669	709	842	882

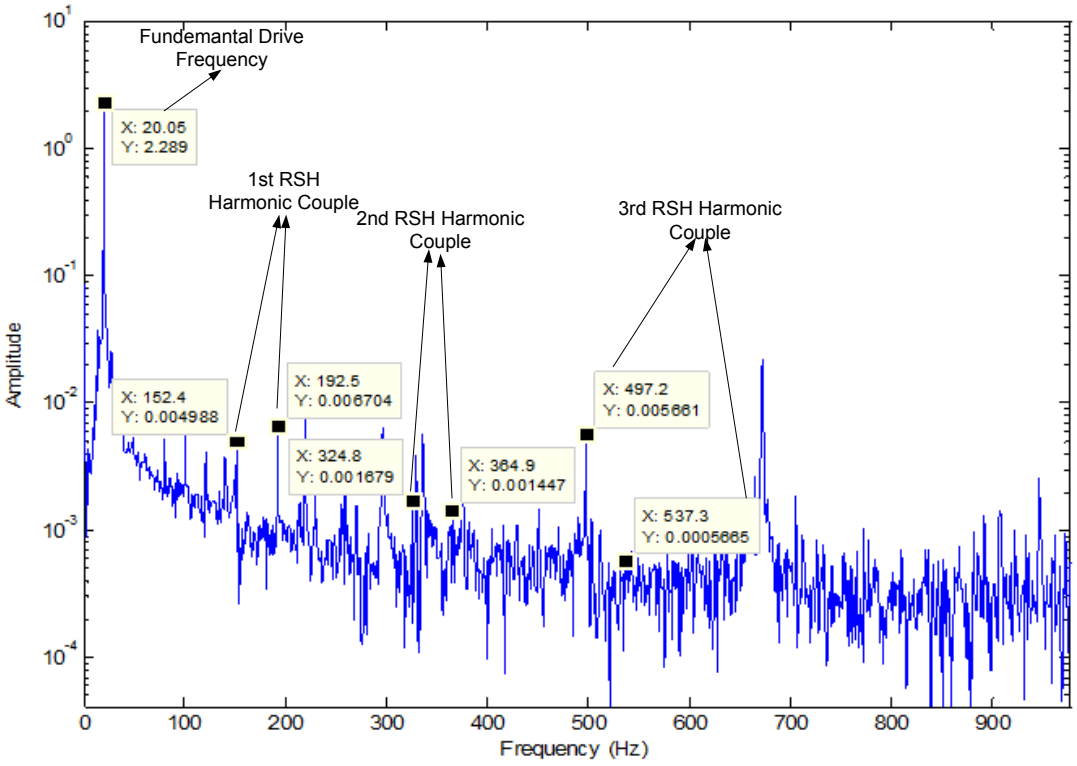

Figure 17 Frequency content of stator current of inverter driven machine using homemade driver in [25] at 20Hz (398rpm) fundamental drive frequency

The frequency spectrum of stator current when it is recordedusing driver in **[25]** at 20Hz fundamental drive frequency is given in Figure 17and it shows that the RSHs are still observable with stator current input. The RSHs spectral analysis conducted by Keysan in **[21]** by recording search coil voltage is given in Figure 18. The amplitudes of 20Hz drive frequency results are compared at Table 9 and it is seen that the RSH magnitude of stator current is higher in magnitude than the search coil RSH. So, it can be inferred that the RSH in stator current can be used to detect the rotor speed as the stator current frequency spectrum and search coil frequency spectrum are similar and the expected RSHs are observable as expected.

Table 9 RSH amplitude comparison in search coil voltage and stator current at 20Hz drive frequency

	Harmonic #1 Amplitude	Drive Frequency(Hz)	Rotor Speed (rpm)
Search Coil Voltage (mV)	0,99	20	236
Stator Current (mV)	6,7	20	398

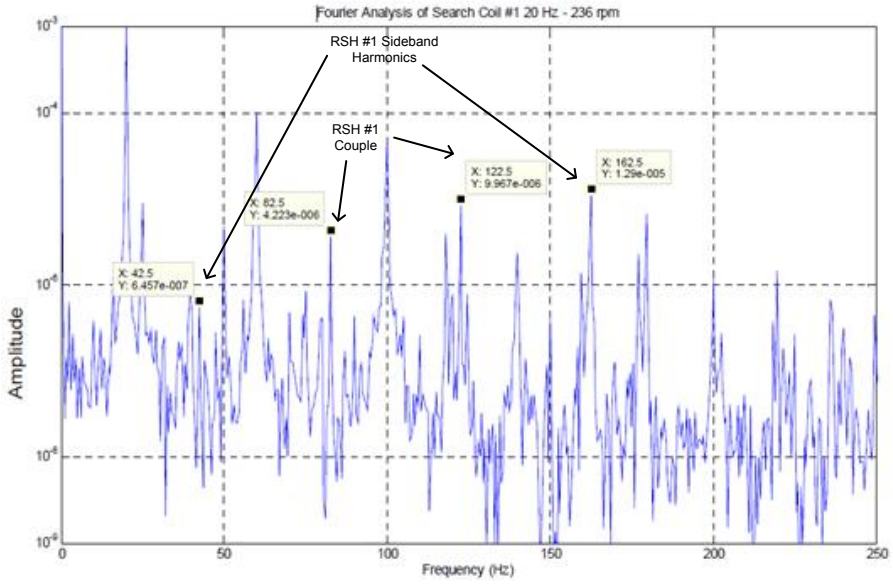

Figure 18 Frequency content analysis of search coil voltage with 20Hz inverter driven machine for investigation of RSHs [21]

2.9 Frequency Spectrum Analysis of Stator Current at Low Rotor Speeds

The frequency spectrum of RSHs are analyzed at low rotor speeds by driving the motor at low drive frequencies and the stator current data is recorded and analyzed offline. The frequency spectrum given in Figure 19 gives the frequency spectrum while the machine is driven at 10Hz fundamental drive frequency and running at about 200rpm and it is seen that the RSHs are still observable even though their magnitude are close to the noise floor.

The frequency spectrum given in Figure 20 gives the frequency spectrum while the machine is supplied at 5Hz fundamental drive frequency and running at about 100rpm rotor speed. It is seen that the RSHs are not observable in the frequency spectrum of the stator current. However, the online tests conducted in Section 4.3 shows that the position and speed can be estimated with some loss of zero crossing detection and position error.

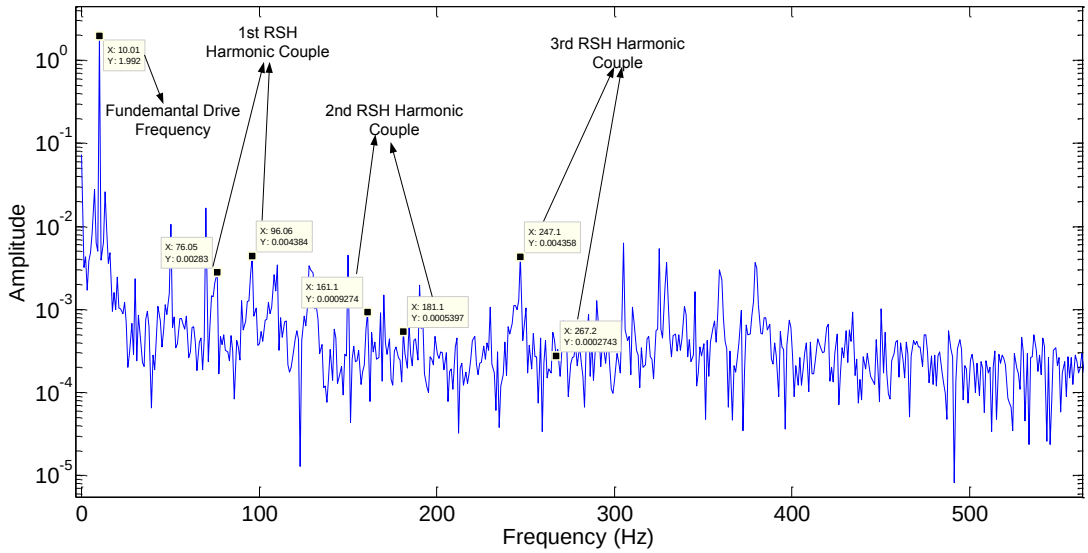

Figure 19 Frequency content analysis of stator current of inverter driven machine using homemade driver in [25] at 10 Hz fundamental drive frequency for investigation of RSHs

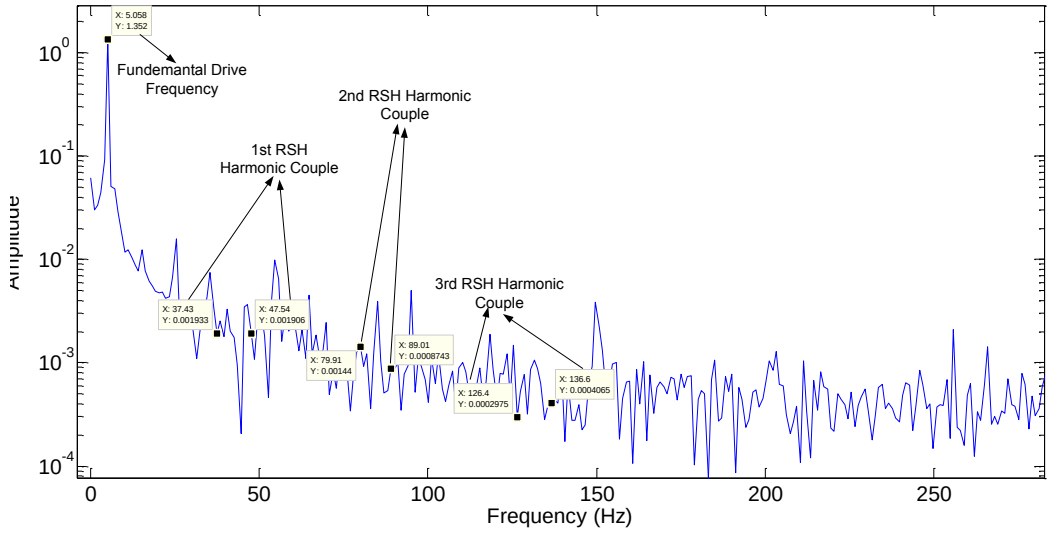

Figure 20 Frequency content analysis of stator current of inverter driven machine using homemade driver in [25] at 5 Hz fundamental drive frequency for investigation of RSHs

2.10 Frequency Spectrum Analysis of Stator Current at High Rotor Speeds

The frequency spectrum of RSHs are analyzed at high rotor speeds by driving the motor at high drive frequencies and the stator current data is recorded and analyzed offline. The frequency spectrum given in Figure 21gives the frequency spectrum while the machine is driven by 75Hz supply fundamental frequency and it is seen that the RSHs are still observable.

The frequency spectrum given in Figure 22 gives the frequency spectrum while the machine is driven by 90Hz supply fundamental frequency. The 3rd couple of RSHs frequency is at the edge of the Nyquist data record rate. It can be inferred from this result that the position estimation algorithm can be implemented to high speeds up to RSHs reach to Nyquist frequency limited by the data sampling rate.

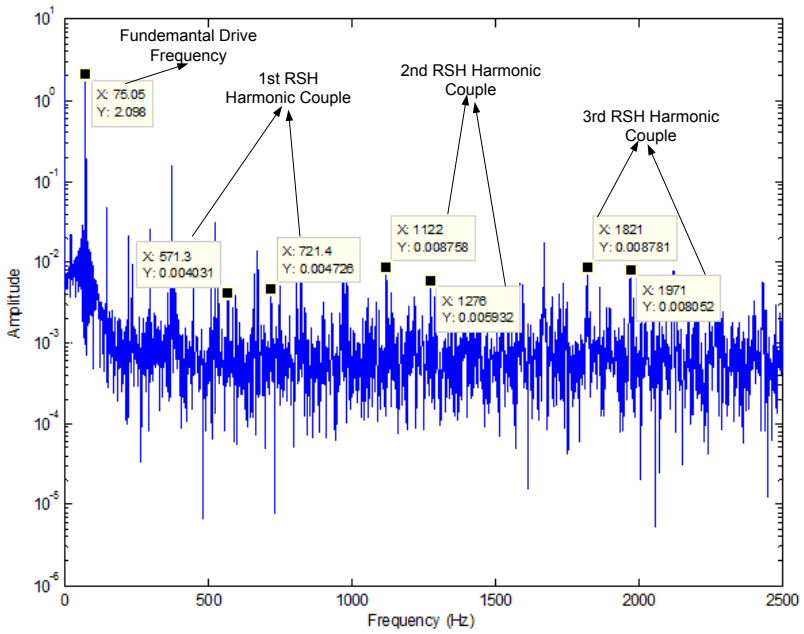

Figure 21 Frequency content analysis of stator current of inverter driven machine using homemade driver in [25] at 75Hz drive frequency for investigation of RSHs

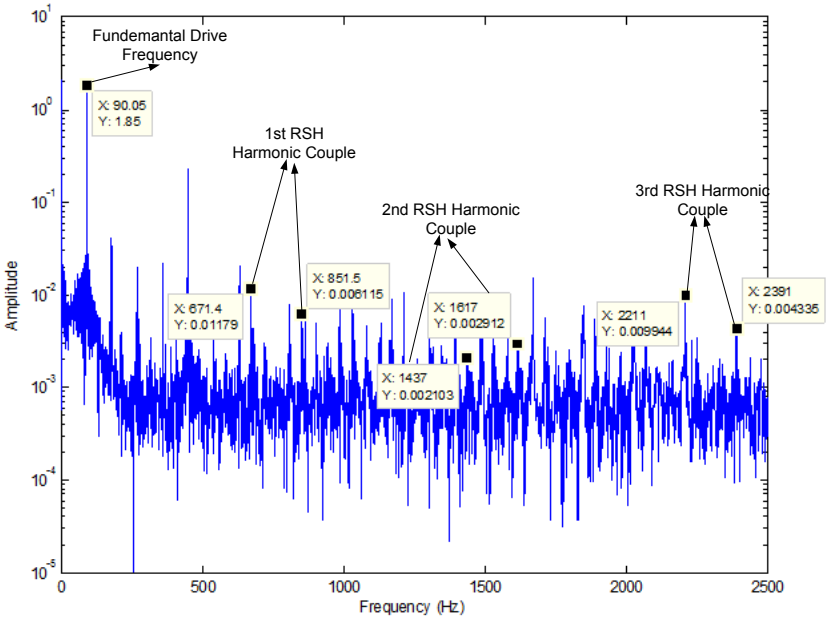

Figure 22 Frequency content analysis of stator current of inverter driven machine using homemade driver in [25] at 90Hz drive frequency for investigation of RSHs

2.11 Summary of Frequency Spectrum Analysis of the Stator Current

The tests of different sampling rate show that high sampling rate does not mean better frequency spectrum. If the RSHs are to be analyzed in frequency domain, increasing the sampling rate would not bring about better results in the analysis. As seen from frequency spectrum stator current of different drive frequencies driven form inverter drivers, the RSHs are detectable with both inverter drivers used and test results matches with the results in **[21]** (see Table 4**)**. The comparison of the results shows that the RSHs exist and they are observable at inverter driven motor stator current. However, it is seen that the noisy nature of the inverter drives sometimes adversely affect the frequency spectrum and adds some undesired harmonics to the intervals of interest.

The frequency spectrum of stator current at different rotor speed shows that the RSHs are observable at different rotor speeds. However, the frequency spectrum of stator current at 5Hz drive frequency shows that the RSHs magnitude decreases with decreasing frequency, implying decreasing RSH magnitude.

The magnitude of first and third RSHs existing in the stator currents change with respect to drive frequency at half load and full load conditions are experimented like no-load tests and the results are summarized with comparison of no-load RSH magnitudes as given in Figure 23 and Figure 24. It can be observed that the harmonic magnitudes increase with load as expected as the rotor MMF gets larger with increasing load. However, the shape of the change in RSH remains very similar under all operating conditions.

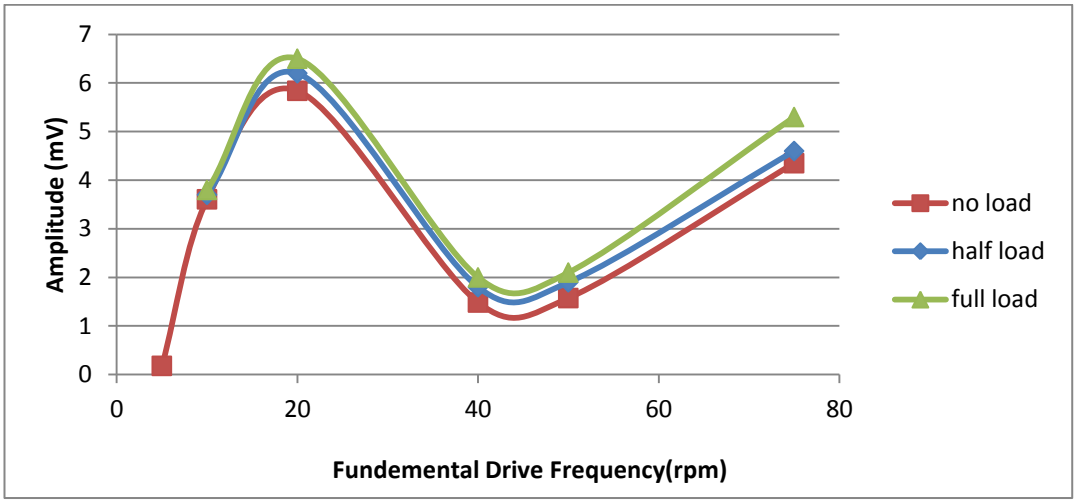

Figure 23 Amplitude change of 1st RSH in stator current with changing rotor speed

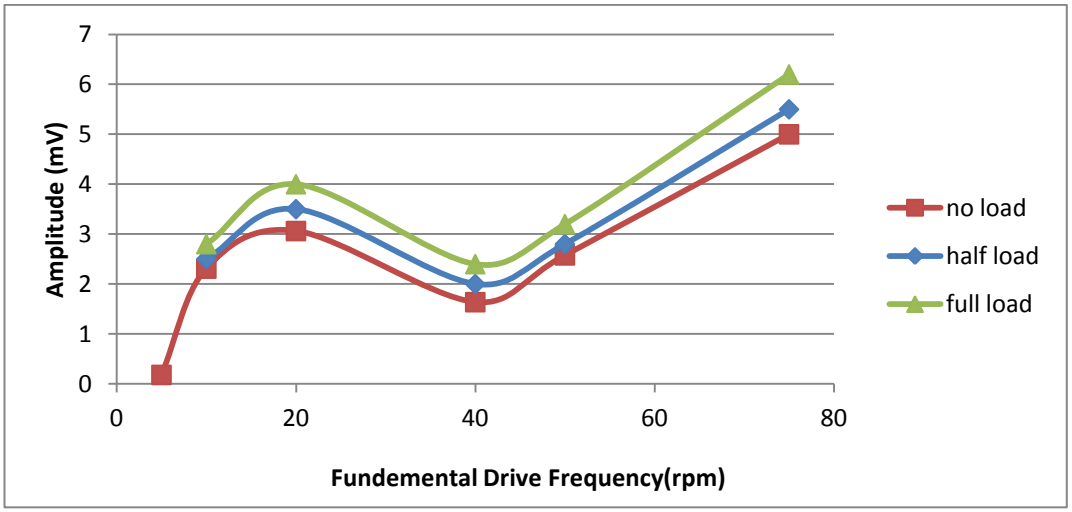

Figure 24 Amplitude change of 3rd RSH in stator current with changing rotor speed

It is seen that the RSHs magnitude decreases drastically at low speeds as like the harmonics existing in the search coil voltage as proposed in **[21]**. However, the magnitude also decreases with increasing frequency in contrast to the search coil results in **[21].** The search coil senses the air gap flux directly and the information of search coil voltage directly related to the air gap flux. However, the stator current does not directly reflect the air gap flux. The air gap flux information coupled to stator current in the stator windings are filtered by the leakage inductance and stator

resistance. The model of the filter is given in Figure 25 and its frequency response is given in Figure 26. It is seen that the filter has a nonlinear response and it attenuates some of the harmonic frequencies more than the others. As the attenuation remains nearly constant after 1kHz and the RSHs continue to increase as proposed in **[21]**, the lowest harmonic magnitude is at about 1kHz corresponding 40Hz drive frequency. Due to this effect, the harmonic magnitudes corresponding to 40Hz drive frequency are reduced more than other frequencies resulting in the shapes given in Figure 23 and Figure 24.

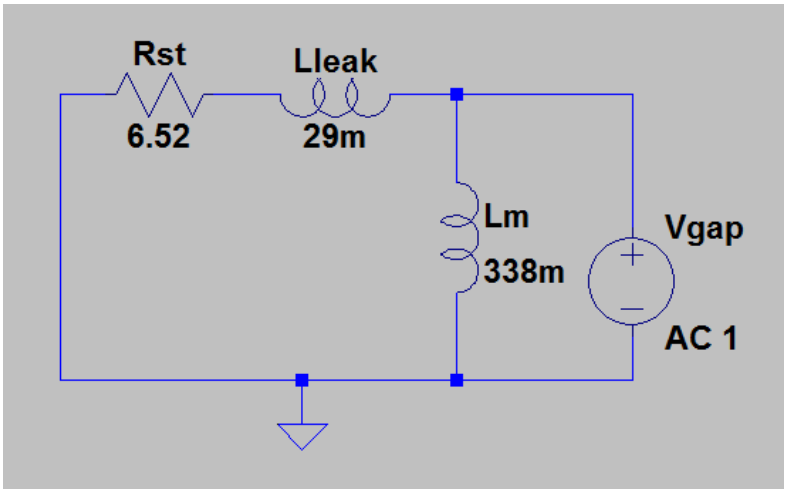

Figure 25 Stator side modeling of the motor for analyzing the stator current frequency spectrum and filtering effect of the machine parameters

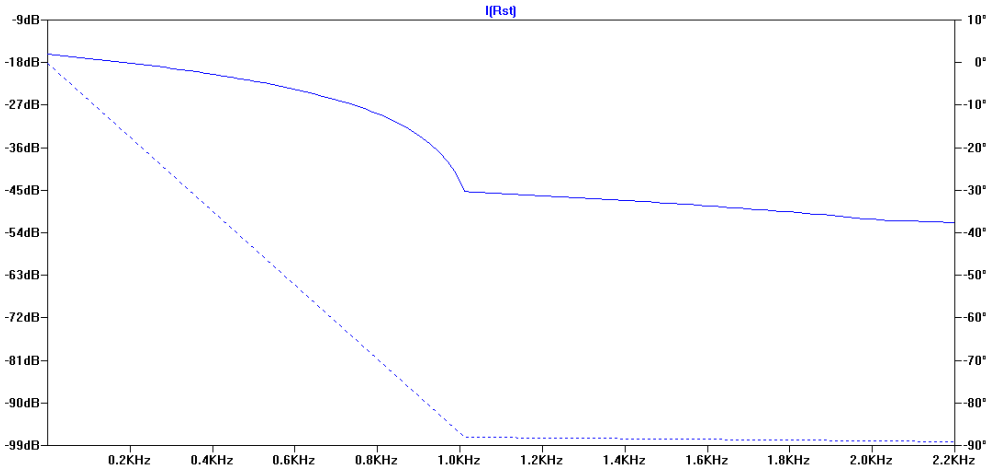

Figure 26 Simulation result of the circuit given in Figure 25 showing the filtering effect on the RSHs existing in the stator current

As seen from Figure 23 and Figure 24, the RSHs amplitude decreases and gets close to zero at low speeds. This decrease in magnitude adversely affects the RSH detection. As a result, it can be said that this algorithm may not work at low speeds **[21]**. The speed limit using driver given at **[25]** is decided as 100rpm by looking at Figure 24.

2.12 Need For Offline Implementation of the Algorithm

The proposed algorithm with search coil input works offline in **[21].** The algorithm takes search coil voltage as input, demodulates it. Then, the RSH is filtered out by a band-pass filter in order to separate the harmonic from other frequency content. Lastly, the filtered RSH is reconstructed at time domain and the frequency of the harmonic is detected to calculate the rotor speed and the zero-cross instants of the time domain signal is treated as one rotor slot turn of the motor shaft.

The offline investigation of the algorithm is conducted to see whether stator current input is suitable for the algorithm and to decide the filter specifications.

2.13 Broad Filter Specifications for the Algorithm

The filter specification is important because the filter center frequency needs to be changed with changing rotor speed at online implementation and moreover the filtering shall be conducted within a control period of 150μs for online implementation. The vector control algorithm occupies about 75μs and therefore it is decided to limit the time available for position and speed estimation to less than 50μs.

In this section, the filter needed for the algorithm will be specified, then the suitable filter choice will be given in detail. At the end of the filter discussion, the filter used in **[21]** will be compared with the proposed filter in this work.

The investigations will be conducted keeping into mind that the filter will be used within an online algorithm, however it will be first tested offline to assure that in fact it successfully performs the required function. The filter is used to separate the RSHs

from other signals and the result of the filter gives the time domain data of the RSH, due to this fact, the filter becomes the most important block of the algorithm.

2.14 Required Filter Specification

Filter is the most important block of the online implementation because it selects the desired RSH and filter out others. The required filter should be a digital band-pass filter. An ideal band pass filter passes a certain frequency range and attenuates frequencies outside that range. The characteristic of a typical band-pass filter can be given as in Figure 27, where f_L and f_H are the lower and higher frequencies of the bandpass filter respectively and f_C is the center frequency of the filter.

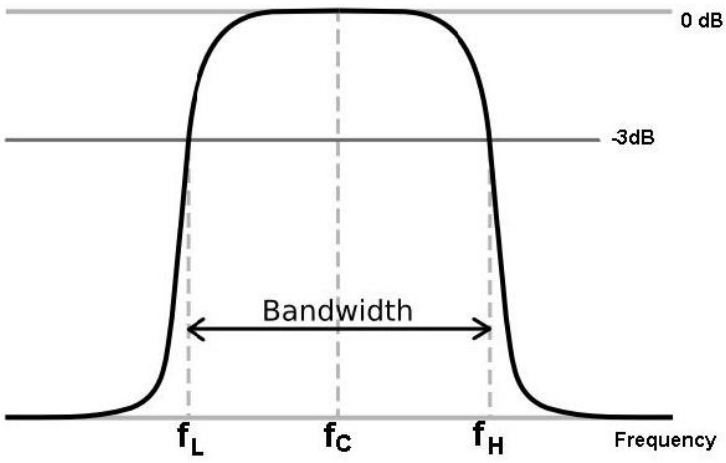

Figure 27 Typical band-pass filter characteristic

By band-pass filtering, the desired RSHs can be reconstructed as described in section 3.3. By this way the desired RSH can be analyzed without FFT. The most important property to be satisfied by the filter block is the cut-off frequency change over time. The filter's center frequency shall track the RSHs frequency and the bandwidth shall be modified at the same time with the changing drive frequency. The other important features of filter are the calculation time and filtering quality.

2.15 The Frequency Range Selection

The minimum and maximum frequencies where the filter works are one of the important parameters that should be decided. In order to decide these parameters, the

RSHs' maximum and minimum frequencies should be calculated first according to **(27)** and **(28)**.

$$\text{RSHs Frequency} = n\frac{Z}{P}f_r \pm kf_s \quad \textbf{(27)}$$

$$f_r = \frac{Rotor\ Speed(rpm)\times P}{60} \quad \textbf{(28)}$$

In **(27)**,Z is the number of rotor slots, P is the number of the pole pairs, f_r and f_s are the rotor and stator electrical frequencies respectively. For a 26 rotor slot 6 pole pair motor, the 3rd RSH 1st pair exists at;

$$RSH = 3\frac{26}{6}f_r \pm 1f_s = 13f_r \pm f_s \quad \textbf{(29)}$$

The maximum rotor speed is 1000rpm and the maximum supply frequency is 50Hz; so the maximum frequency to look for the RSHs becomes;

$$RSH_{max} = 13\frac{1000\times 6}{60} \pm 50 = 1300 \pm 50Hz \quad \textbf{(30)}$$

2.16 The Bandwidth of the Filter

The other factor that should be decided is the bandwidth of the filter. The bandwidth of the filter shall be less enough that it will be able to filter the sideband signals that are aside $n$fr $\pm$ 2fs. Moreover, it is an advantage of having small bandwidth as there are less noise on the recovered waveform. On the other hand, it is more difficult to track the desired signal in the bandwidth if the bandwidth is too small. Because of these reasons, the filter should be wide enough to recognize the RSH signal, and should be narrow enough not to have undesired other high magnitude noise and sideband harmonics.

Another factor that should be kept into mind while deciding the bandwidth is the mechanical time constant of the machine. The machine speed change shall be considered while choosing the filter bandwidth because the RSH frequency changes with the same ratio. The mechanical time constant of used motor is calculated as 39ms at 4τ from **[34]**. The execution time of the motor control algorithm is 150µs. So the speed change in 150µs is %0.38. In other words, the maximum speed change of

the motor 3.4rpm. 3.4 rpm speed change corresponds to 4.42Hz change in RSHs. In order to able to locate the filter at the next estimation cycle at online implementation, the bandwidth of the filter should be 2 times higher than this value (approximately 10Hz).

As a result of these discussions, the center frequency of filter should be at the previous 3rd RSH frequency, the bandwidth shall be less than 4fsand shall be higher than 10Hz in order to filter out the sideband harmonics. There should not be a gap between the two consecutive filter bandwidth's so that any signal appears in the desired frequency range can be recovered.

2.17 The Edge Sharpness of the Filter

Another important parameter that has a big impact on the number of filter parameters is the sharpness of the edges of the filter. The sharpness should be as low as possible to have least number of parameters. The sideband harmonics should be out of the filter and should be suppressed; so the edges of the filter shall end at the sideband frequencies. This implies that the slope of the edges becomes as in **(31)**.

$$Edge\ slope = \frac{suppression\ rate(dB)}{\frac{fs}{2}} \quad \textbf{(31)}$$

Another factor that changes the number of filter parameters is the suppression rate. If the suppression rate increases, then the number of filter parameters increases. So the suppression rate must be as low as possible to have simple, less time consuming and less memory allocating filter. From previous recordings, the amplitude level between the 3rd harmonics and the noise floor is about 10dB. Moreover, the other undesired noise levels that can be mistaken is also about 10dB above the noise floor. Then, a filter with 20dB suppression rate has a safety margin with 10dB is enough to filter the RSHs.

2.18 Determination of Filter Cut-Off Frequencies

Another factor of the filter is the cut-off frequencies. As previously discussed, the filter shall be able to filter sideband harmonics successfully and the frequency

difference between the stopping edges shall be less than $4f_s$. In order to have a safety margin, the difference between the stopping edges is decided as $3f_s$, meaning that the stop edges is placed ($f_{center} - 3f_s/2$) and ($f_{center} + 3f_s/2$).

Decision of the passing edges is more complicated. If the difference between the passing edges is too small, the number of the needed filter increases. However; if the bandwidth is small, then the filter will have less sharp edges and its order and the calculation time decreases. In addition to these calculation issues, another important factor is the algorithm itself. The filter bandwidth shall be decided such that the selected filter shall remain unchanged when the speed is kept constant. As a result, the lower pass-edge of the filter is placed ($0.98f_{center}$) and the higher edge is placed at ($1.02f_{center}$). By means of these requirements, the needed filters can be tabulated as in the Table 10.

Table 10 Required filter specifications

Filter Number (#)	Rotor Speed (rpm)	Drive Frequency (Hz)	Filter Center Frequency (f_c)	Filter Bandwidth (Hz)	Filter Lower Attenuation Edge (Hz)	Filter Lower Pass Edge (Hz)	Filter Higher Pass Edge (Hz)	Filter Higher Attenuation Edge (Hz)
1	1500	75	1950	52	1838	1924	1976	2063
2	1480	74	1924	52	1813	1898	1950	2035
3	1460	73	1898	52	1789	1872	1924	2008
4	1440	72	1872	52	1764	1846	1898	1980
5	1420	71	1846	52	1740	1820	1872	1953
6	1400	70	1820	52	1715	1794	1846	1925
7	1380	69	1794	52	1691	1768	1820	1898
8	1360	68	1768	52	1666	1742	1794	1870
9	1340	67	1742	52	1642	1716	1768	1843
10	1320	66	1716	52	1617	1690	1742	1815

Filter Number (#)	Rotor Speed (rpm)	Drive Frequency (Hz)	Filter Center Frequency (f_c)	Filter Bandwidth (Hz)	Filter Lower Attenuation Edge (Hz)	Filter Lower Pass Edge (Hz)	Filter Higher Pass Edge (Hz)	Filter Higher Attenuation Edge (Hz)
11	1300	65	1690	52	1593	1664	1716	1788
12	1280	64	1664	52	1568	1638	1690	1760
13	1260	63	1638	52	1544	1612	1664	1733
14	1240	62	1612	52	1519	1586	1638	1705
15	1220	61	1586	52	1495	1560	1612	1678
16	1200	60	1560	52	1470	1534	1586	1650
17	1180	59	1534	52	1446	1508	1560	1623
18	1160	58	1508	52	1421	1482	1534	1595
19	1140	57	1482	52	1397	1456	1508	1568
20	1120	56	1456	52	1372	1430	1482	1540
21	1100	55	1430	52	1348	1404	1456	1513
22	1080	54	1404	52	1323	1378	1430	1485
23	1060	53	1378	52	1299	1352	1404	1458
24	1040	52	1352	52	1274	1326	1378	1430
25	1020	51	1326	52	1250	1300	1352	1403
26	1000	50	1300	52	1225	1274	1326	1375
27	980	49	1274	52	1201	1248	1300	1348
28	960	48	1248	52	1176	1222	1274	1320
29	940	47	1222	52	1152	1196	1248	1293
30	920	46	1196	52	1127	1170	1222	1265
31	900	45	1170	52	1103	1144	1196	1238

Filter Number (#)	Rotor Speed (rpm)	Drive Frequency (Hz)	Filter Center Frequency (f_c)	Filter Bandwidth (Hz)	Filter Lower Attenuation Edge (Hz)	Filter Lower Pass Edge (Hz)	Filter Higher Pass Edge (Hz)	Filter Higher Attenuation Edge (Hz)
32	880	44	1144	52	1078	1118	1170	1210
33	860	43	1118	52	1054	1092	1144	1183
34	840	42	1092	52	1029	1066	1118	1155
35	820	41	1066	52	1005	1040	1092	1128
36	800	40	1040	52	980	1014	1066	1100
37	780	39	1014	52	956	988	1040	1073
38	760	38	988	52	931	962	1014	1045
39	740	37	962	52	907	936	988	1018
40	720	36	936	52	882	910	962	990
41	700	35	910	52	858	884	936	963
42	680	34	884	52	832	858	910	936
43	660	33	858	52	806	832	884	910
44	640	32	832	52	780	806	858	884
45	620	31	806	52	754	780	832	858
46	600	30	780	52	728	754	806	832
47	580	29	754	52	702	728	780	806
48	560	28	728	52	676	702	754	780
49	540	27	702	52	650	676	728	754
50	520	26	676	52	624	650	702	728
51	500	25	650	52	598	624	676	702
52	480	24	624	52	572	598	650	676

Filter Number (#)	Rotor Speed (rpm)	Drive Frequency (Hz)	Filter Center Frequency (f_c)	Filter Bandwidth (Hz)	Filter Lower Attenuation Edge (Hz)	Filter Lower Pass Edge (Hz)	Filter Higher Pass Edge (Hz)	Filter Higher Attenuation Edge (Hz)
53	460	23	598	52	546	572	624	650
54	440	22	572	52	520	546	598	624
55	420	21	546	52	494	520	572	598
56	400	20	520	52	468	494	546	572
57	380	19	494	52	442	468	520	546
58	360	18	468	52	416	442	494	520
59	340	17	442	51	391	417	468	493
60	320	16	416	48	368	392	440	464
61	300	15	390	45	345	368	413	435
62	280	14	364	42	322	343	385	406
63	260	13	338	39	299	319	358	377
64	240	12	312	36	276	294	330	348
65	220	11	286	33	253	270	303	319
66	200	10	260	13	245	254	267	275
67	190	9,5	247	13	233	241	254	261
68	180	9	234	13	221	228	241	248
69	170	8,5	221	13	208	215	228	234
70	160	8	208	13	195	202	215	221
71	150	7,5	195	13	182	189	202	208
72	140	7	182	13	169	176	189	195
73	130	6,5	169	13	156	163	176	182

Filter Number (#)	Rotor Speed (rpm)	Drive Frequency (Hz)	Filter Center Frequency (f_c)	Filter Bandwidth (Hz)	Filter Lower Attenuation Edge (Hz)	Filter Lower Pass Edge (Hz)	Filter Higher Pass Edge (Hz)	Filter Higher Attenuation Edge (Hz)
74	120	6	156	13	143	150	163	169
75	110	5,5	143	13	130	137	150	156
76	100	5	130	13	117	124	137	143

2.19 Filter Type Selection Suitable with the Specifications

There are two basic discrete filter types. These types will be investigated and compared in this section and one type of the filter will be chosen. The types of the filter are Finite Impulse Response (FIR) and Infinite Impulse Response (IIR) filters.

According to **[31]**, digital filters can achieve extremely difficult tasks for analog filters. Moreover, they are more suitable for adaptive filtering applications because their characteristic can easily be changed by software. In contrast, digital filters are not suitable for all signal processing applications. In real time operations, all filtering calculations should be completed in one sampling clock period, 1/fs **[31]**. One can calculate the maximum possible bandwidth for an application by using the tap number (number of sensed data points filter uses for identifying the RSH magnitude) of the filter, the calculation time of a tap with the used DSP. For example; ADSP-2189M can be able to calculate a complete filter tap in 13.3ns, and for a 100-tap filter filtering ends in 1.4μs **[31]**. This implies that the maximum sampling frequency is about seven hundred kHz and the upper signal bandwidth could be at most a few hundred kHz for that processor.

2.19.1 FIR Filters

FIR filters delay a number of input samples and average them to create the output sample in various ways **[31]**. The order of the filter is the number of the sample the

filter looks back. Because of this property a buffer called circular buffer is placed before the filter in order to hold the previous samples for the filter. In generalized form the FIR filter performs the following convolution equation in **(32) [31]**;

$$y(n) = h(k) * x(n) = \sum_{k=0}^{N-1} h(k)x(n-k) \quad \textbf{(32)}$$

$h(k)$ represents the filter coefficient array and $x(n-k)$ is the input data array. number N is the filter tap number. The basic FIR filter structure is given in Figure 28.

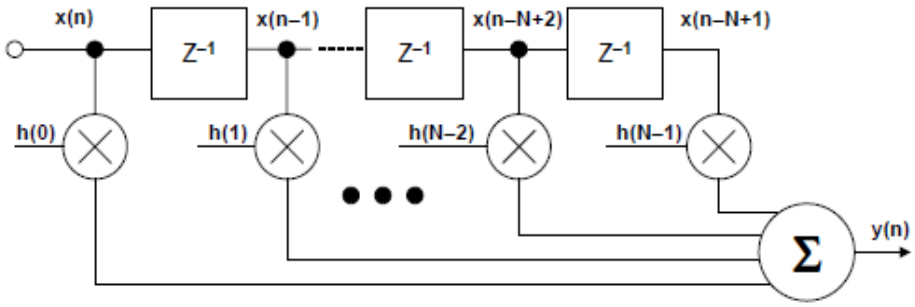

Figure 28 Basic FIR filter structure

The properties of FIR filters can be summarized as follows **[31]**;

- Impulse Response has a finite duration (N Cycles)
- Linear Phase, Constant Group Delay (N Must be Odd)
- No Analog Equivalent
- Unconditionally Stable
- Can be Adaptive
- Easy to Understand and Design

2.19.2 IIR Filters

The second filter type is Infinite Impulse Response filters. As understood from its name, the impulse response of this kind of filter extends for infinite period of time **[31]**. The reason for this is that they are utilizing feedback. IIR filter output can be calculated in less time than FIR filters because they can be realized with fewer computations. However, they are not linear. The other adverse property of IIR filters is that there is a possibility that the filter can be unstable because of feedback.

The properties of IIR filters can be summarized as follows **[31]**;

- Uses Feedback (Recursion)
- Impulse Response has an Infinite Duration
- Potentially Unstable
- Non-Linear Phase
- More Efficient than FIR Filters
- Usually Designed to Duplicate Analog Filter Response

The basic structure of IIR filter is shown in Figure 29.

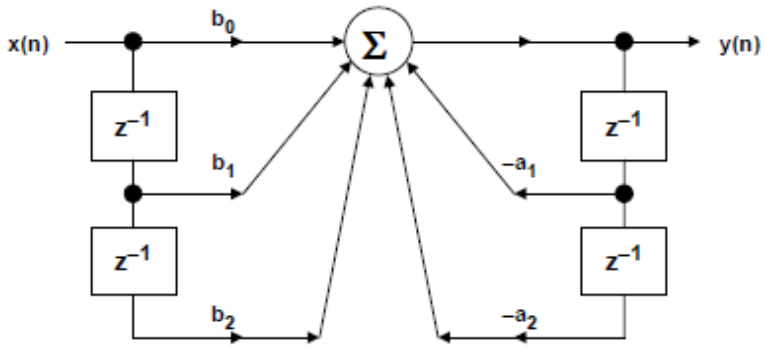

Figure 29 Basic IIR filter structure

The IIR filter performs filtering using the;

$$H(z) = \frac{\sum_{k=0}^{M} b_k z^{-k} \ (Zeros)}{1+\sum_{k=1}^{N} a_k z^{-k} \ (Poles)} \quad \textbf{(33)}$$

2.19.3 Comparison of FIR and IIR Filters

In order to see how the real filter parameters change, two filters (one IIR, one FIR) are designed and their results are compared. Both filters are bandpass filters with a sample rate of 6.67 kHz. Both filters have bandwidth of 52Hz with a center frequency of 1300Hz. Both have a suppression rate of 20dB and 0.4dB/Hz edge slope. Only the filter type will be changed. The filter design tool will be the Matlab 'fdatool'. The designed filter is the filter whose specifications are given in Table 10 in

the first line (will be interpreted as Filter #26) and it is used at 50Hz no-load test when the rotor speed is between 990 and 1010rpm.

Figure 30 and Figure 31 show that for the same suppression rate, same cut-off frequencies and sample rate, the IIR filter has a great advantage on the application as it has less filter order compared to FIR filter. The decreased filter order will decrease time for calculation. As seen from Figure 30, the FIR filter is in 118th order while IIR filter is in 6th order. This implies that the IIR filter calculation is about 20 times faster than FIR filter calculation. Because of this advantage, the filter decided to be used is IIR filter in both offline and online tests.

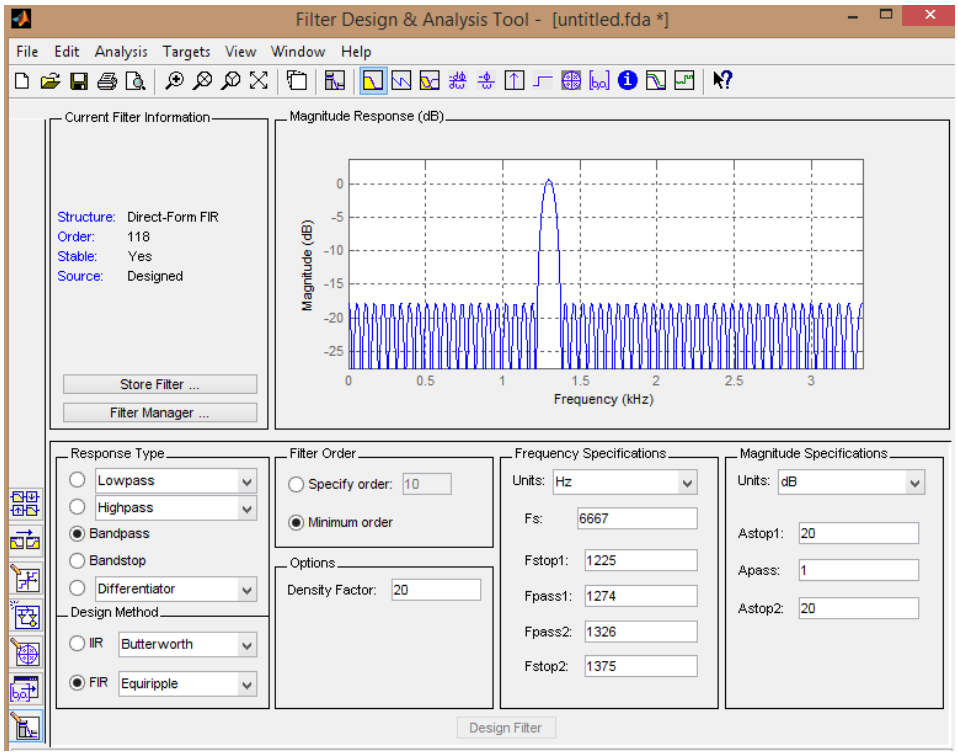

Figure 30 FIR filter design with Matlab fdatool

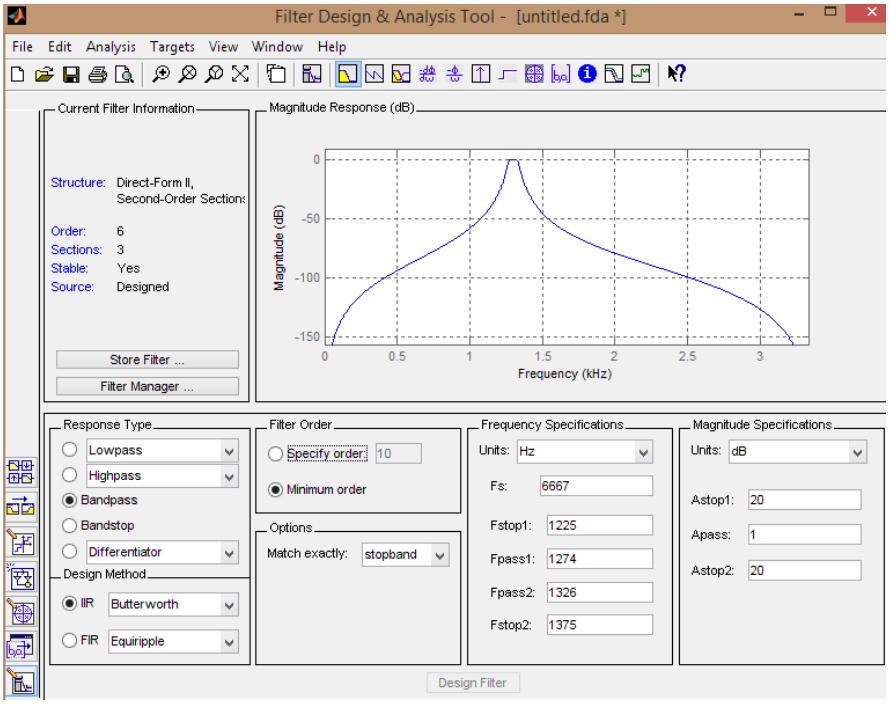

Figure 31 IIR filter design with Matlab fdatool

2.20 Analysis of the Chosen Filter and Comparison with the Proposed Filter in [32]

The chosen filter is IIR filter because of its computational time advantage. The filter #26 given in Table 10 will be analyzed and compared with the proposed filter. The filter will be designed with Filter Design & Analysis Tool of Matlab. The proposed filter by Keysan in **[32]** is a Chebyshev type 1 IIR filter. These type of filters are known from their good dynamic performance and sharp characteristic with low order and computational load compared to other types of filters designed for the same specifications as given in **[32]**. The proposed filter is also designed by Filter Design Toolbox and its details are given in Figure 33.

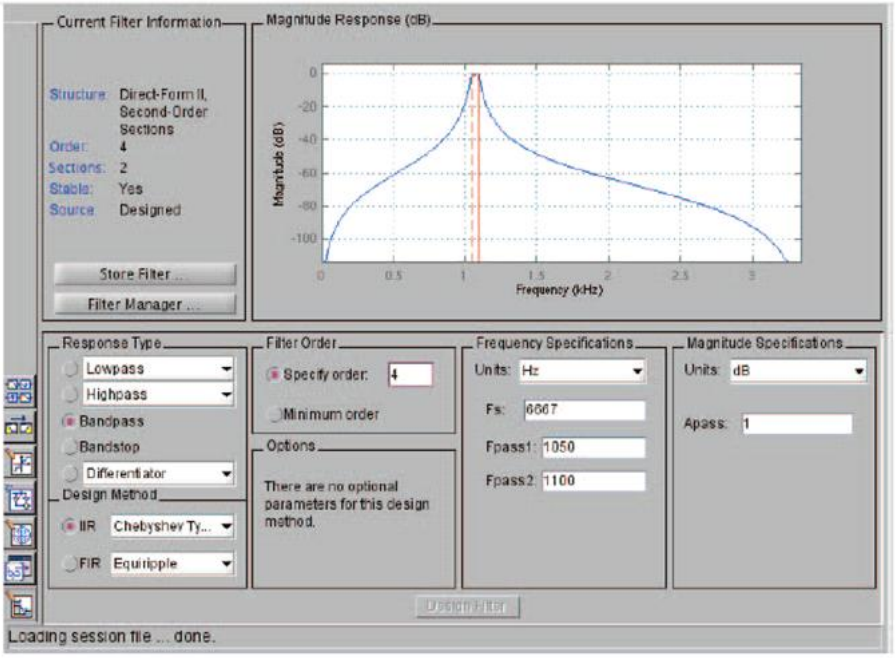

Figure 32 Matlab filter design toolbox screenshot [32]

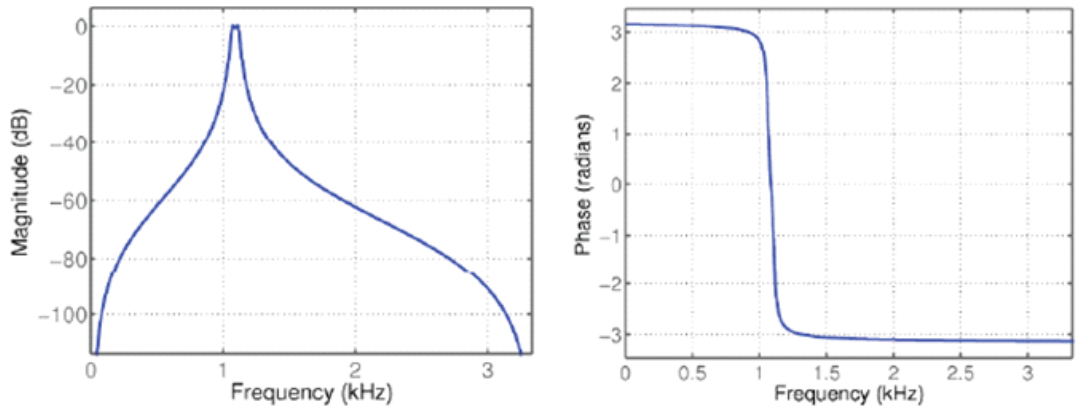

Figure 33 Characteristics of the proposed filter in [32]

The block diagram of the proposed filter is given in Figure 34. The proposed filter is a 4th order 2 section filter, whose bandwidth is 50Hz and center frequency is 1075Hz. It is a 4th order Chebyshev type 1 IIR filter and it contains seven multiplications, six additions and four delay elements and the total computational time is calculated as 3μs in **[32]**.

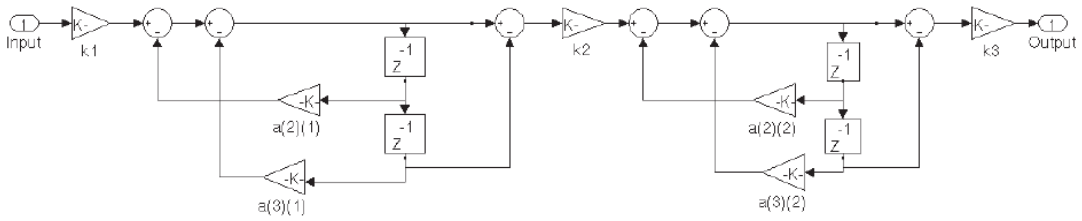

Figure 34 Block diagram of the proposed Fourth-order, two section Chebyshev bandpass filter

The decided filter to be used in this work is also an IIR filter because of its computational time advantage. However, the chosen filter is Butterworth filter instead of Chebyshev filters due to their flat response at the pass-band region **[33]**. This flat response is a desired property because the exact frequency of the RSH is unknown and it is desired that the RSH shall not be attenuated. The flat pass-band response of the filter guarantees that the RSHs will not be attenuated when they are in the pass-band region. The disadvantage of this Butterworth filters compared to the Chebyshev filters is the relatively high order and high computational time. The designed filter given in Figure 35 and Figure 36 is the filter whose characteristic is given as filter number 26 in Table 10 is examined. The details of the designed filter are given in Figure 36.

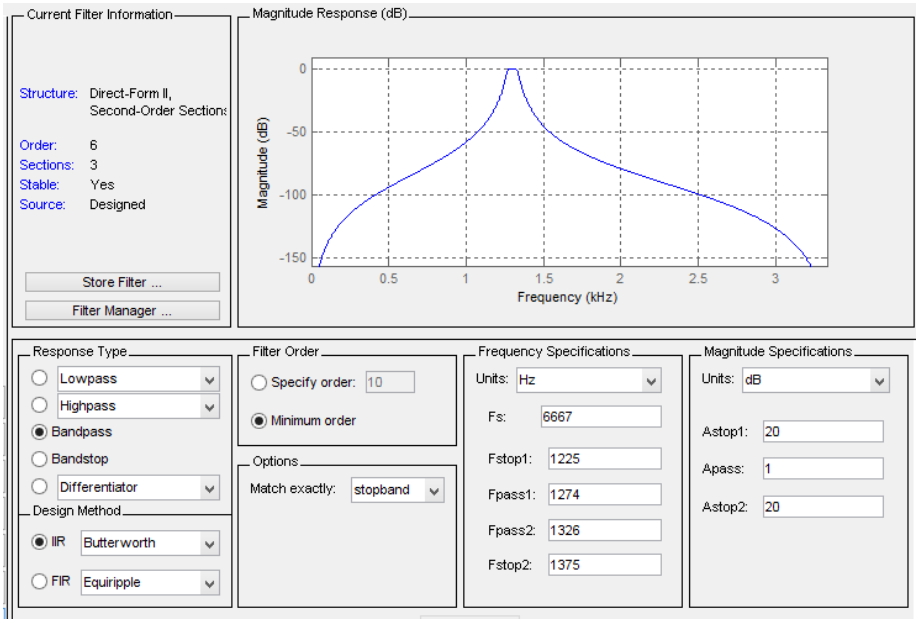

Figure 35 Matlab filter design toolbox screenshot

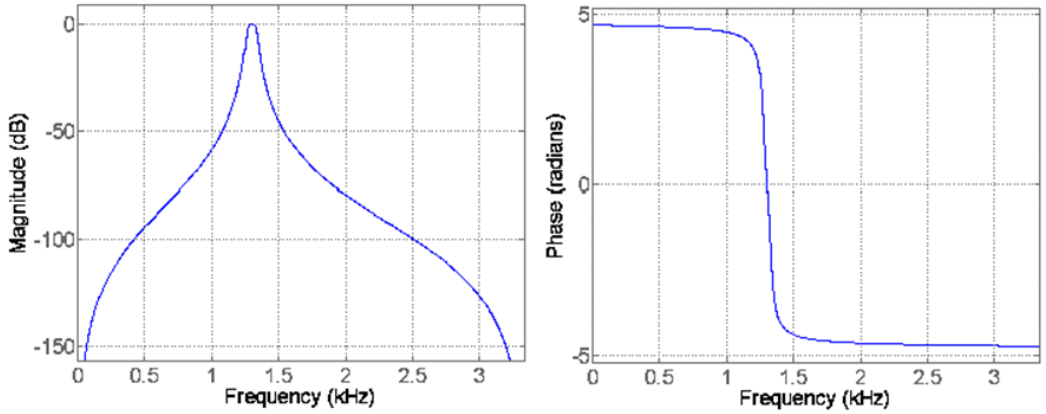

Figure 36 Characteristics of the designed filter

The block diagram of the designed filter is given in Figure 37. As also seen from the block diagram, the Butterworth filter contains more calculation steps, 11 multiplications, 8 additions and 6 delay elements. The calculation time of the filter is then becomes 4.5µs for the same DSP board in **[32].** Even though the calculation time increases, it is much less than the control cycle period, 150µs, and can be implemented online with the advantage of low pass-band ripple.

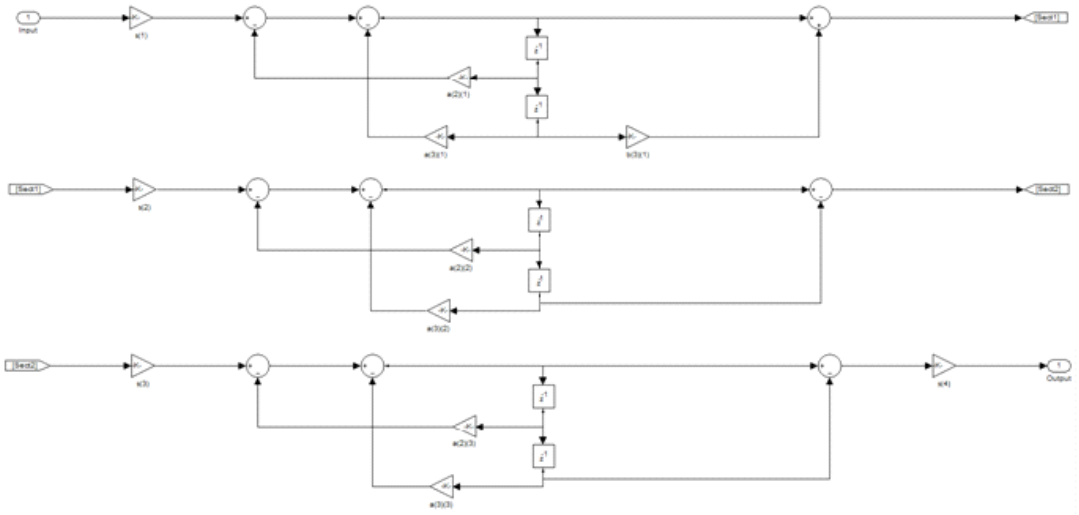

Figure 37 Block diagram of the designed sixth-order, three section Butterworth bandpass filter

2.21 The Results of the Rotor Position Estimation Algorithm with Stator Current Input

The results of the offline algorithm with the chosen filter are given in this section to show that the algorithm and the filter is suitably chosen to be online implementation with stator current input. The results of the offline algorithm are compared with encoder output to see the algorithm works offline properly. In order to see the effect of drivers on offline algorithm, tests are made by using recorded current data of different driver hardware. The hardware contains the variac, the inverter driver given in **[25]** and the commercial driver given in **[24]**. The test results are given for different supply frequencies and as a result different rotor speed. The variac driven case, on the other hand, is driven only at 50 Hz mains frequency. All tests are conducted at no load conditions. The tests are conducted to see whether the 3rd RSH is detectable at different supply frequencies and can be reconstructed with filtering and demodulation.

In this section the results of the rotor speed estimation algorithm is given for 10Hz, 20Hz, 40Hz and 50Hz and 75Hz inverter driven cases. The first figures of Figure 41, Figure 44, Figure 47, Figure 47 and Figure 50 show the frequency content of the raw stator current data. This frequency spectrum, in fact, is not a part of the algorithm, but it is repeated for better understanding of the offline implementation of the method. The second figures of Figure 41, Figure 44, Figure 47, and Figure 50 show the frequency content of modulated and filtered data. It is seen that the 3rd RSH has higher amplitude than other frequencies in the pass-band region

Figure 42, Figure 45, Figure 48, and Figure 51 shows reconstructed time domain 3rd RSH. The figures appear bottom shows the zoomed version. This waveform is used for rotor speed estimation. The frequency of this waveform is linearly related to rotor speed and as a result rotor position.

Figure 43, Figure 46, Figure 49 and Figure 52 show the results of the offline estimation algorithm. The figures appear bottom in these figures show the zoomed version of the corresponding position estimations. The comparison actual position

recorded by a commercial encoder and estimated position calculated by using rotor position algorithm is given in Figure 43, Figure 46, Figure 49 and Figure 52. The position estimation results given in Figure 46, Figure 49 and Figure 52 have some offset error whose solution is described in section 4.7.1. The position estimation is implemented by sensing the zero crossing of the RSH one times in one period and the position estimation result is not updated when a zero crossing is not detected. The stepped estimation of the position is due to this way of implementation of the algorithm and the solution to this case is also given in Section 4.7.2. These position estimation results prove that rotor speed estimation algorithm works as expected with motor stator current information. Even though there seem to be exist some kind of offset error in position estimation which can be solved as explained in section 4.7.1, the slope of the estimated points (actually speed of the rotor shaft) given in Figure 43, Figure 46, Figure 49 and Figure 52 show that the algorithm works and estimates position and speed successfully in offline implementation. The frequency spectrum figures are given just to visualize the RSH once more in this section, FFT analysis is not used as a part of the algorithm.

As the recorded data at 10Hz, 20Hz, 40Hz, 50 Hz and 75Hz are recorded from inverter driven machines, these results also imply that the algorithm can be applied to inverter driven machines by taking stator current as input.

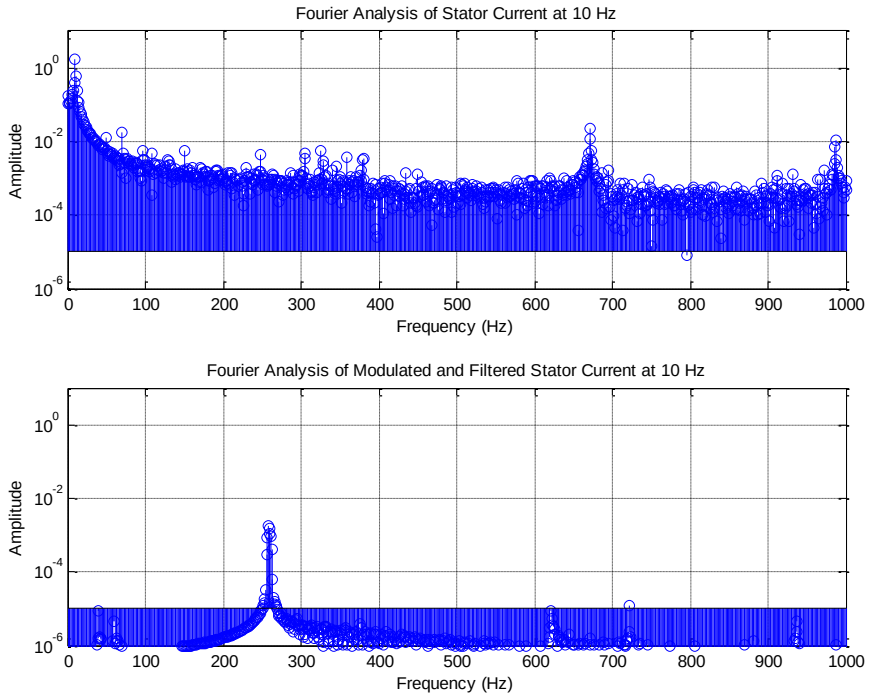

Figure 38 10Hz (199rpm) driven motor current data frequency spectrum before and after demodulation and filtering

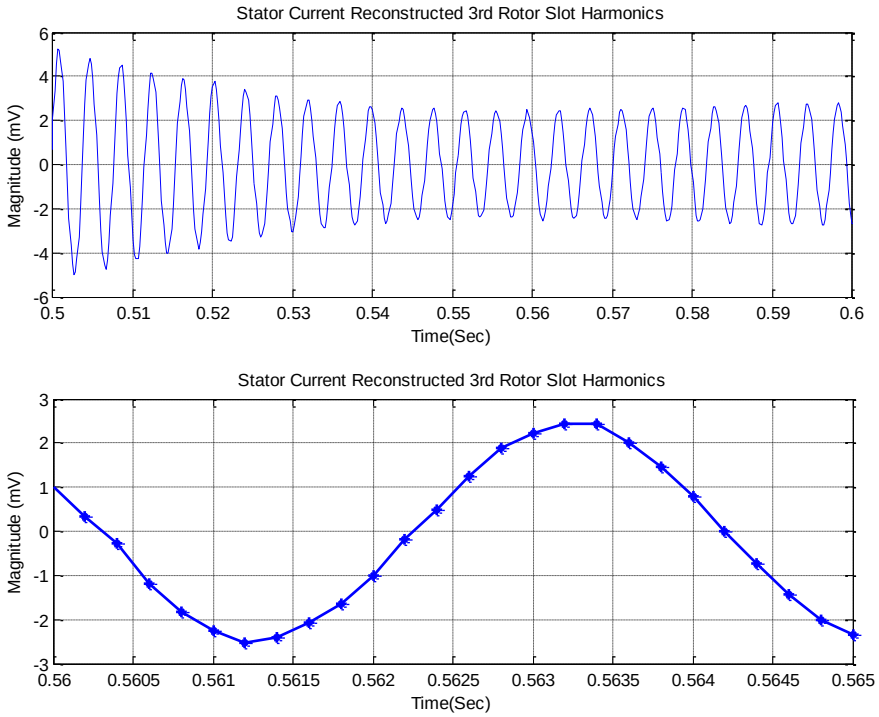

Figure 39 Reconstructed 3rd harmonic of stator current driven at 10Hz (199rpm)

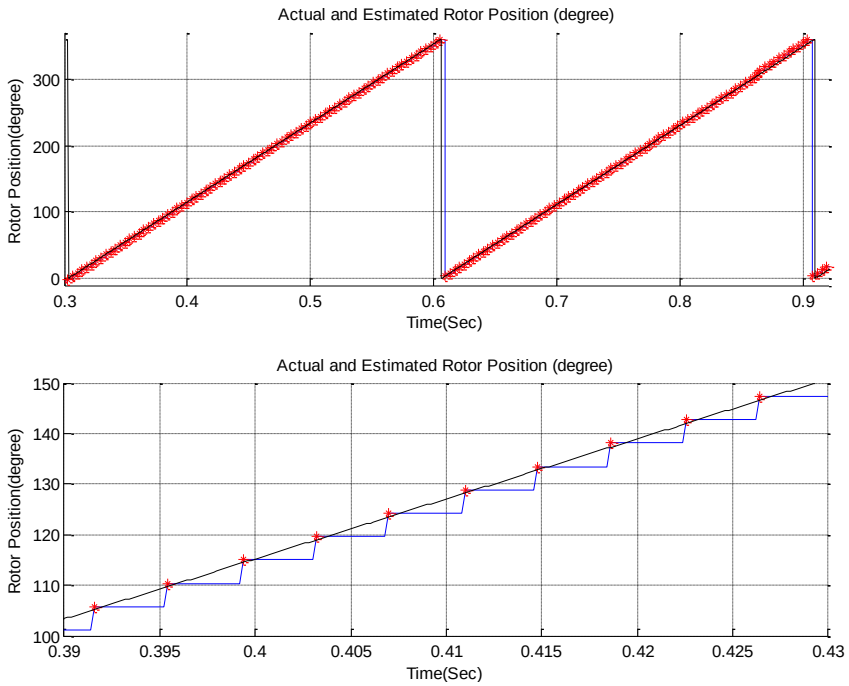

Figure 40 Actual and estimated rotor position driven at 10 Hz (199rpm)

The offline implementation of position estimation algorithm from stator current at 10Hz drive frequency shows that the algorithm can be applied online at 10Hz drive frequency. The offline implementation results of the algorithm and the actual reading results matches as seen from Figure 40.

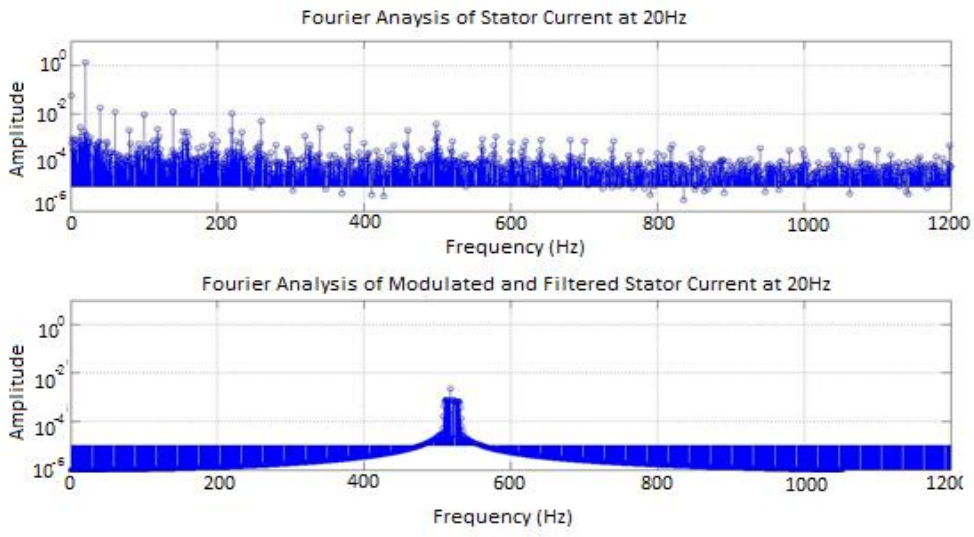

Figure 41 20Hz (398rpm) driven motor current data frequency spectrum before and after demodulation and filtering

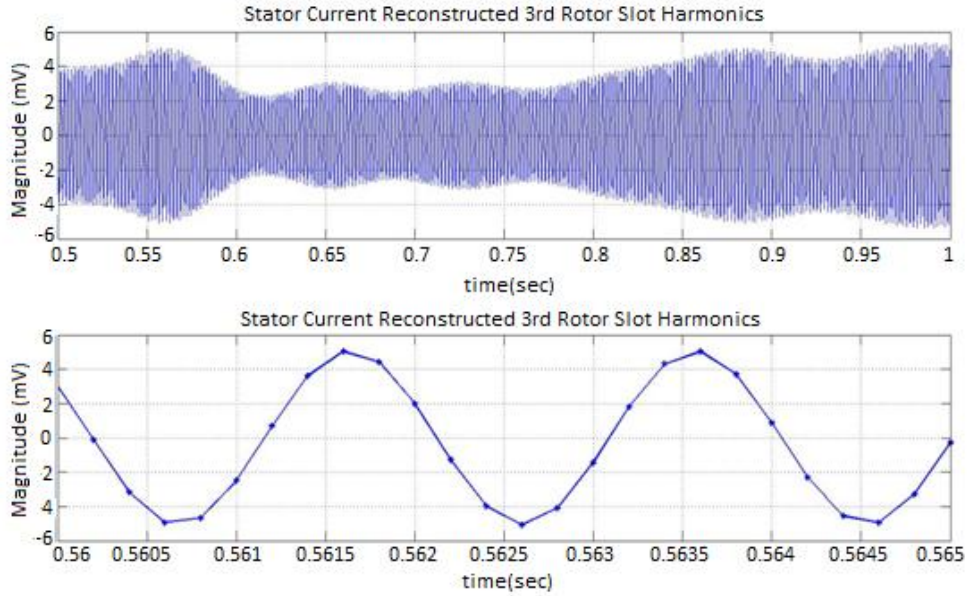

Figure 42 Reconstructed 3rd harmonic of stator current driven at 20Hz (398rpm)

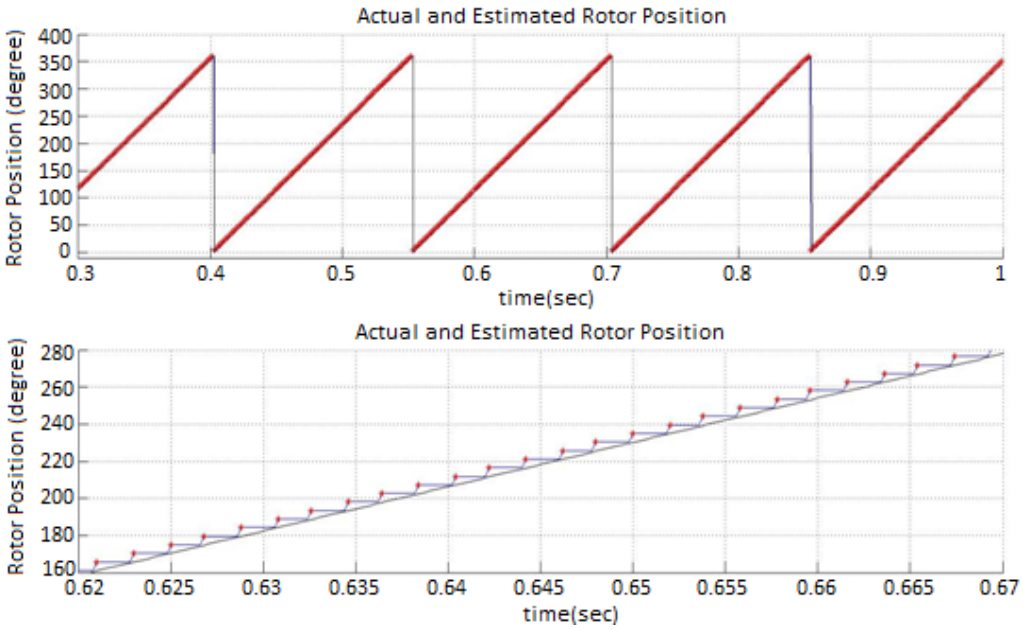

Figure 43 Actual and estimated rotor position driven at 20 Hz (398rpm)

The offline implementation of position estimation algorithm from stator current at 20Hz drive frequency shows that the algorithm can be applied online at 20Hz drive

frequency. The offline implementation results of the algorithm and the actual reading results matches as seen from Figure 43.

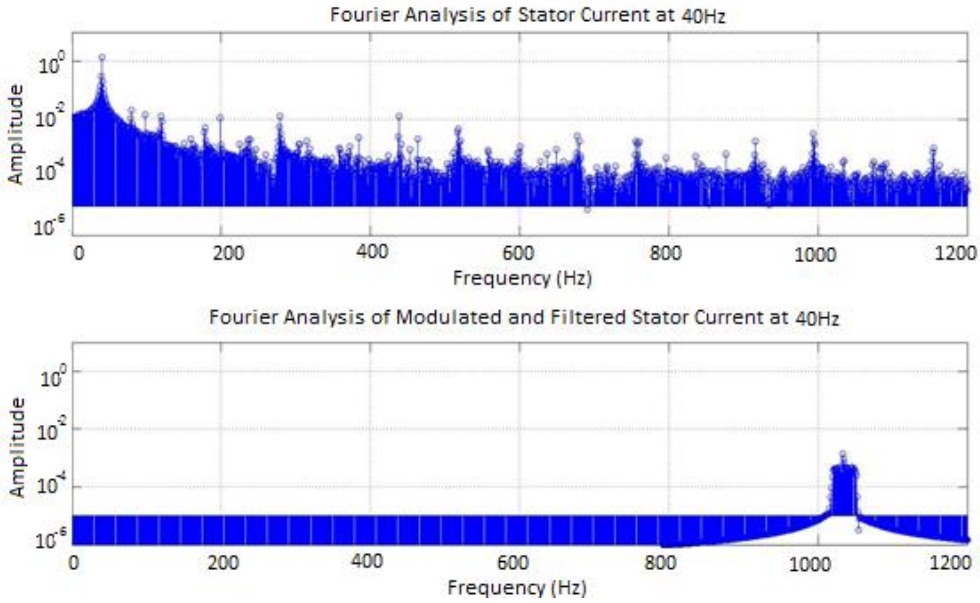

Figure 44 40Hz (798rpm) driven motor current data frequency spectrum before and after demodulation and filtering

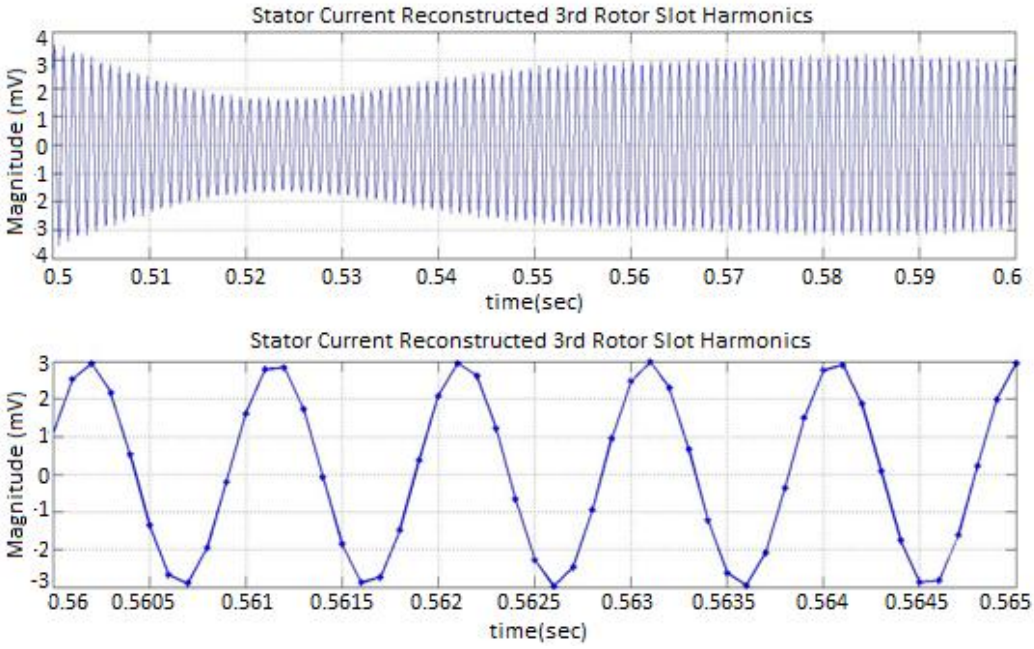

Figure 45 Reconstructed 3rd harmonic of stator current driven at 40Hz (798rpm)

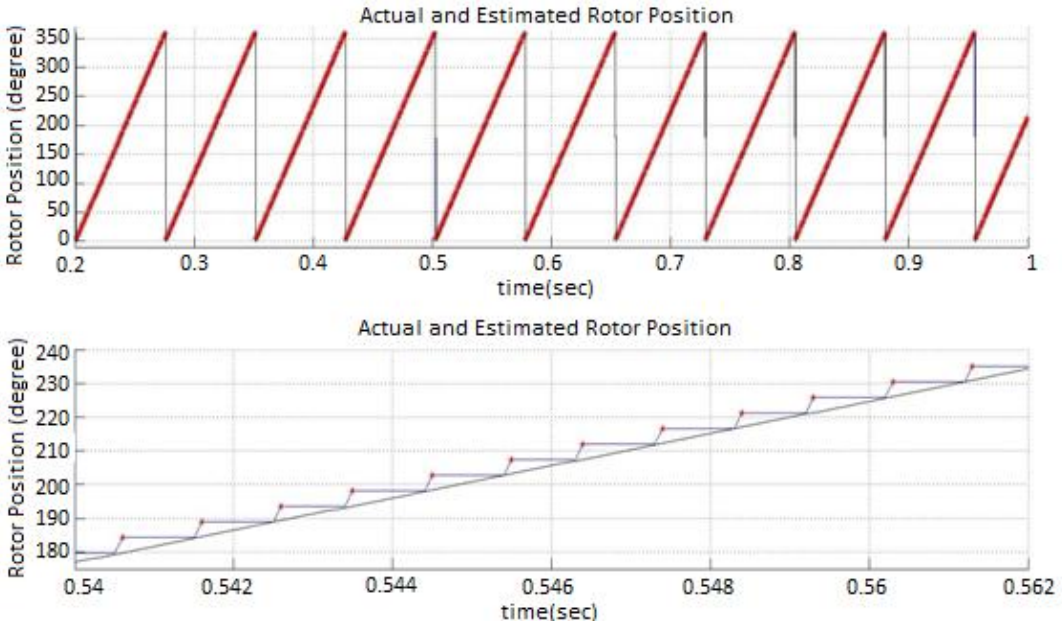

Figure 46 Actual and estimated rotor position driven at 40 Hz (798rpm)

The offline implementation of position estimation algorithm from stator current at 40Hz drive frequency shows that the algorithm can also be applied online at 40Hz drive frequency. The offline implementation results of the algorithm and the actual reading results matches as seen from Figure 46.

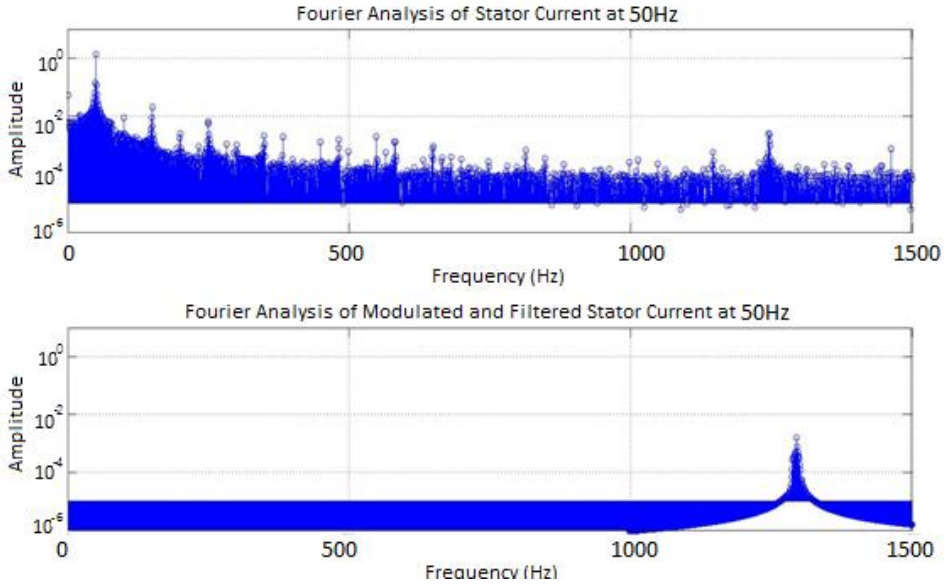

Figure 47 50Hz (996rpm) driven motor current data frequency spectrum before and after demodulation and filtering

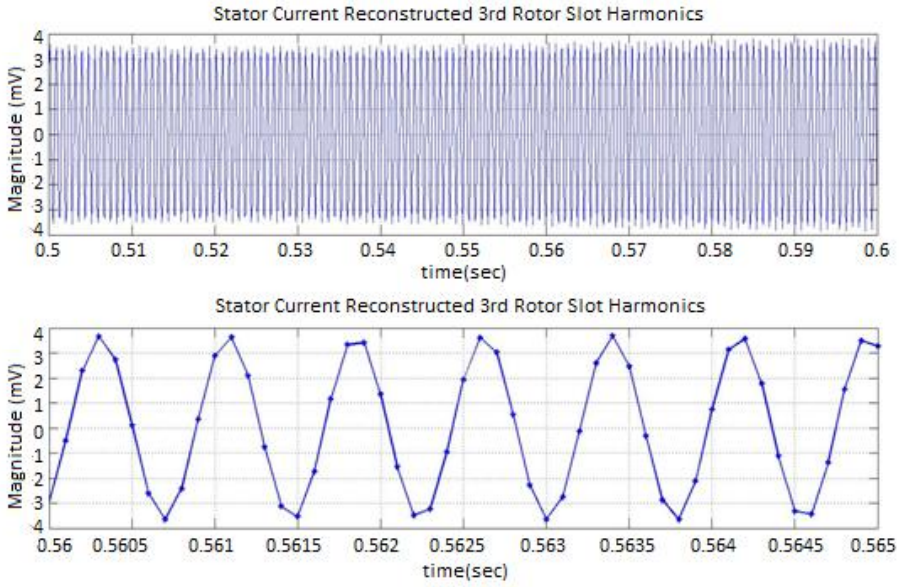

Figure 48 Reconstructed 3rd harmonic of stator current driven at 50Hz (996rpm)

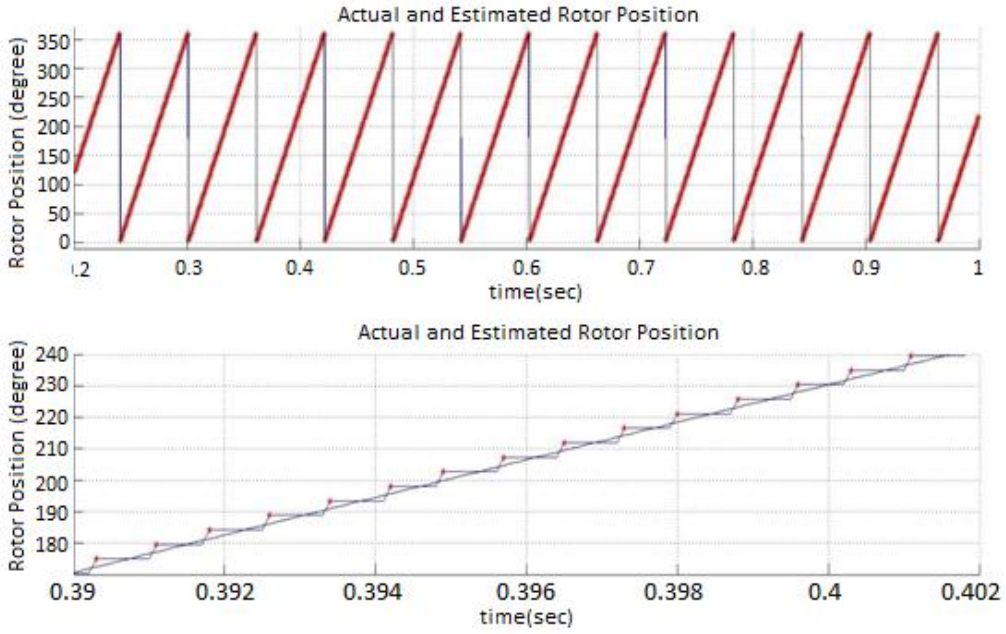

Figure 49 Actual and estimated rotor position driven at 50 Hz (996rpm)

The offline implementation of position estimation algorithm from stator current at 50Hz drive frequency shows that the algorithm can be applied online up to 50Hz rated drive frequency. The offline implementation results of the algorithm and the actual reading results matches as seen from Figure 49.

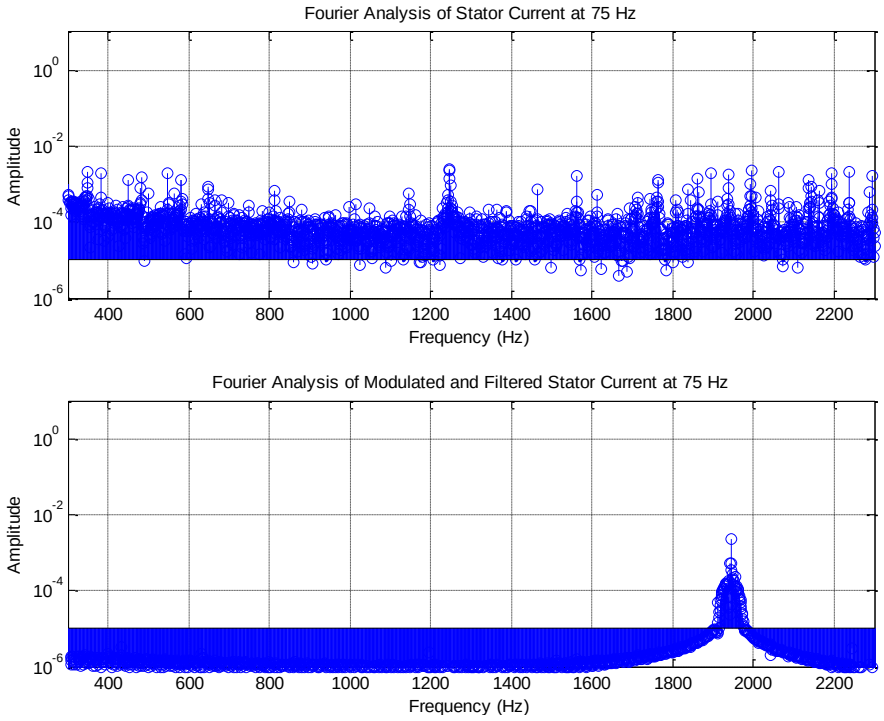

Figure 50 75Hz (1490rpm) driven motor current data frequency spectrum before and after demodulation and filtering

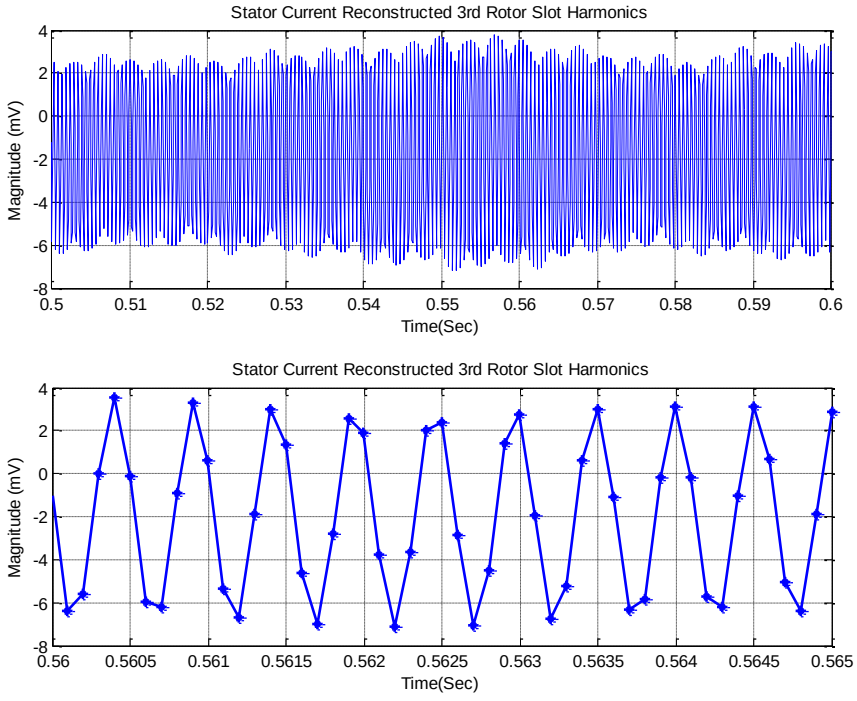

Figure 51 Reconstructed 3rd harmonic of stator current driven at 75Hz (1490rpm)

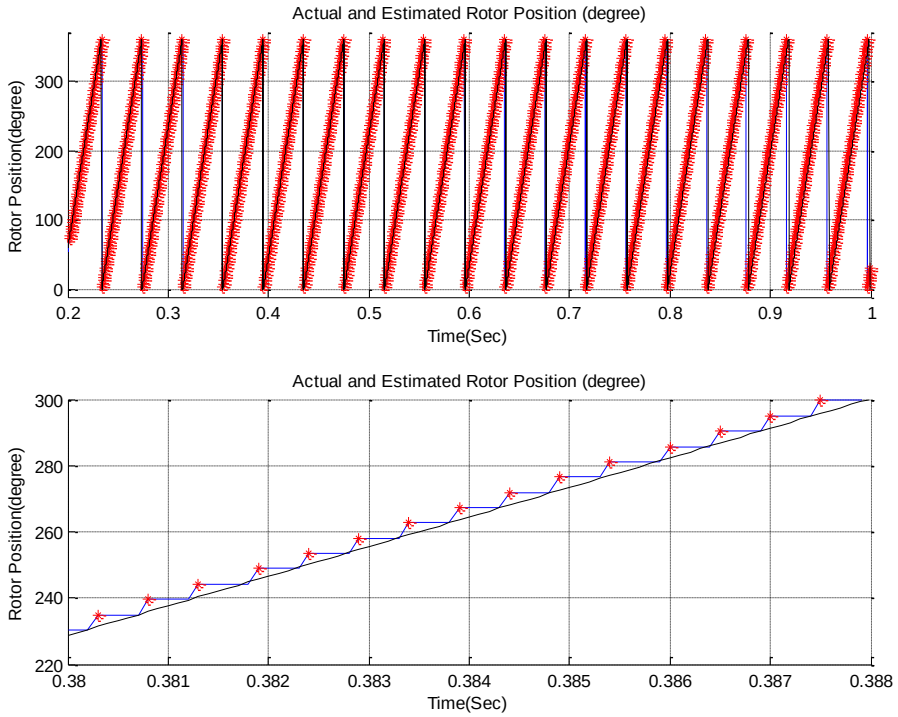

Figure 52 Actual and estimated rotor position driven at 75 Hz (1490rpm)

The offline implementation of position estimation algorithm from stator current at 75Hz drive frequency shows that the algorithm can be applied online at 75Hz drive frequency. The offline implementation results of the algorithm and the actual reading results matches as seen from Figure 52.

In the following chapter, the implementation of the proposed algorithm on the online system with the proposed filter in this section will be described.

CHAPTER 3

IMPLEMENTATION OF ROTOR POSITION ESTIMATION ALGORITHM

It is shown in Chapter 2 that RSHs exist and observable at stator current of the machine. The estimation algorithm is applied with the recorded stator current and it is shown that the algorithm works offline with stator current data input.

In this chapter, the algorithm Chapter 2 is modified to work offline with stator current input. The proposed filter in Chapter 2 will be used as a kind of adaptive filter whose center frequency changes with rotor speed. The adaptive filter implementation will be given in detail in Section 3.9 of this chapter. Another important change in online implementation is the data process type. In the offline implementation a number of (5000 data points recorded over 1 second) data points are processed. However, as online implementation is able to get data points at the instants of they are sensed, a storage of 5000 stator current amplitude data point is not needed. Instantaneous signal processing is done in online algorithm so the speed of the online algorithm becomes much faster (in the order of 1000 times)

While implementing the algorithm, it is aimed to operate the algorithm on online systems and determine the speed limits of the algorithm. This means that the algorithm should be able to predict the rotor position or speed within the free time (about 50 us) available in the 150 us control cycle of the vector controlled drive used for tests.

The most important block of the position and speed detection algorithm, the filtering block will be analyzed in this chapter. The position detection algorithm is intended

to be used in a variable speed drive. Therefore, the motor speed is variable and the filter should be able to adapt itself as the speed of the motor changes. The implementation of adaptive filtering feature to the chosen filter in Chapter 2 is also described here.

The performance of the of the algorithm described in this chapter is tested under various conditions. The result of these tests will be given in Chapter 4.

3.1 Proposed Estimation Algorithm

In this chapter, the proposed position estimation algorithm by Keysan in **[21]** will be summarized. The algorithm consists of five main blocks as given in Figure 53. The online algorithm is constructed basically on the approach given in Keysan's thesis **[21]**. The algorithm proposes to demodulate the stator current and filter out the desired RSH, then calculating the frequency of the RSHs gives the rotor speed. Moreover, each zero crossing or each peak can be directly related to one rotor slot mechanical turn of the rotor shaft. The calculated RSH frequency is also used in the next cycle to decide where to place the center frequency of the filter at the next step. As a zero crossing of the signal does not occur at every 150μs, the position information is not updated at every cycle. However, as RSHs frequency is detected at every cycle, the center frequency of the filter can be fed back at every 150μs on the online algorithm. The aspects of dynamic conditions will be discussed in Section 3.9 of this chapter.

In Section 3.2, Section 3.3 and Section 3.4 the theoretical background of the proposed algorithm will be briefly explained. The online algorithm is also implemented in similar manner with stator current input as described in Section 3.7, 3.8, 3.9 and 3.10. The block diagram of the proposed algorithm in **[21]** is given in Figure 53. The functions of the blocks in the algorithm are described in the following sections.

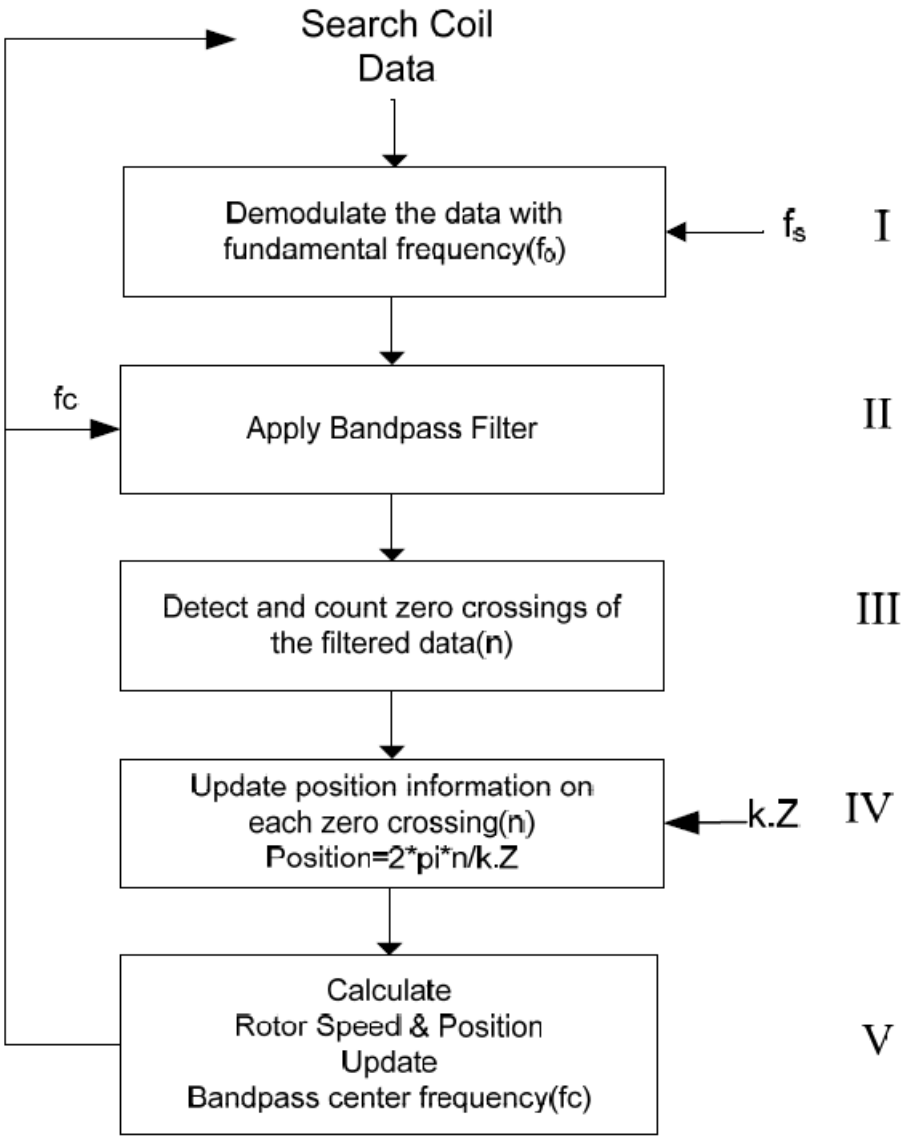

Figure 53 Block diagram for rotor speed and position detection algorithm [21]

3.2 Demodulation Block

The first block of the proposed algorithm is the demodulation block. The RSHs that appear in the stator current are modulated signals with the fundamental supply frequency as in **[21]** given in **(34)**, and shall be demodulated properly in a similar manner to reconstruct the RSHs.

$$f_{rsh} = kf_R \pm fs \quad \textbf{(34)}$$

where f_{rsh} is rotor slot side band harmonics frequency, f_R is rotor slot permeance variation frequency (number of rotor slots per pole multiplied with rotor frequency) and fs is the fundamental stator frequency applied to the motor.

The demodulation is actually multiplication of the demodulated signal with the carrier signal **[27]**, and demodulation of RSHs with the stator supply frequency is given in **[21]** in detail. The result of the demodulation process is given in **[21]** as in **(35)** and **(36)**.

$$f_{demod}(t) = f_{rsh}(t) \times f_s(t) \tag{35}$$

$$f_{demod}(t) = A.\sin(k.2\pi f_R t) + \frac{A}{2}.[\sin\big((k.2\pi f_R - 2.2\pi f_s)t\big) + \sin\left((k.2\pi f_R + 2.2\pi f_s)t\right)] \tag{36}$$

The first part of **(36)**, $A.\sin(k.2\pi f_R t)$, is the desired signal to be obtained, whose frequency is directly related to the rotor speed and the other part is the sideband harmonics of the desired harmonic.

3.3 Filter Block

Filter block, where the RSHs are reconstructed, is the most important block on the algorithm. The first term of **(36)** is separated to identify the magnitude of the RSH frequency The details of filter type selection and specifications are given in Chapter 2, and the adaptive filter implementation will be given in the Section 3.9 of this chapter. Here, the use of the filter in the algorithm will be given.

The filter is used to identify the magnitude of the RSH at a given instant. By successively applying the algorithm the shape of the RSH can be obtained. If the first part of the signal in **(36)** whose frequency is related to the rotor speed can be extracted from its sideband harmonics and other harmonics in the spectrum, the instantaneous RSHs magnitude can be estimated **[21]**. A band-pass filter, whose center frequency is decided with the previous RSHs detection process, is used to filter out the desired signal. The filtering process can be described in frequency domain as in Figure 54.

The desired filter should be chosen properly that it would properly filter out the desired RSH and should complete the filtering process in less than 50 us of the vector control drive cycle.

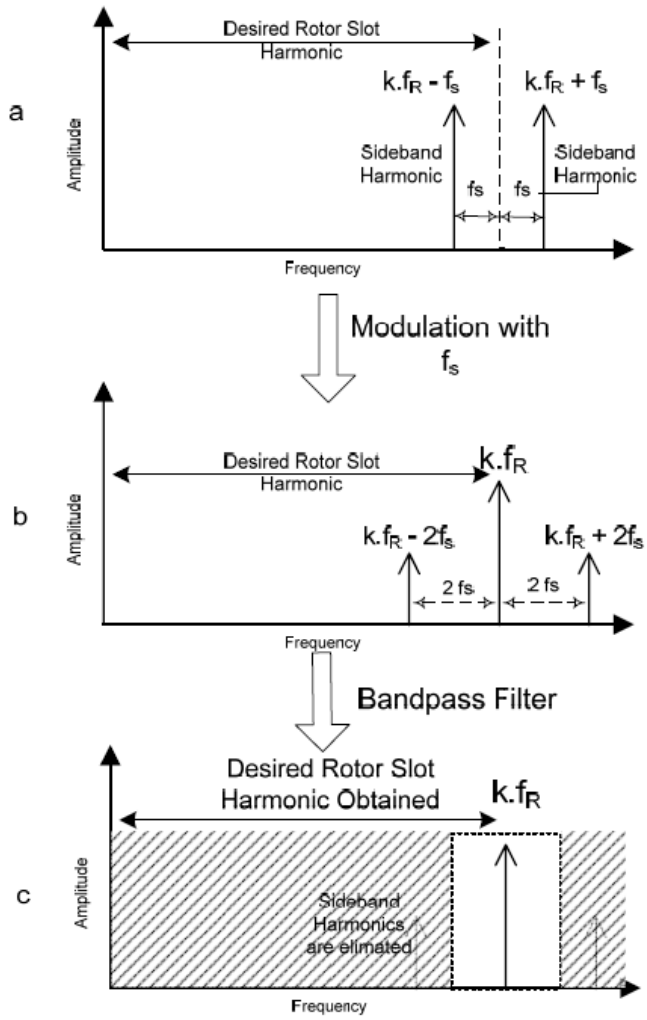

Figure 54 Modulation and filtering process of search coil data [21]

3.4 Zero Crossing Detection

As discussed earlier, the RSHs magnitude is detected at each vector control cycle. The shape of the RSH can thus be constructed as shown in Figure 55 Determination of the frequency of RSH is simple once this shape is determined. Note that in fact the period of this shape corresponds to rotor slot pitch. If the number of rotor slots is

known, The angular distance travelled is known, hence the speed of the shaft can be calculated (the time required for turning the rotor is known) If the starting point of the shaft with respect to a stator reference is known, the position of the rotor at any instant is also known, with respect to the chosen reference on the stator.

The time taken to cross two zero crossings identifies the period of the RSH as well as its frequency. In the algorithm employed in this thesis every other zero crossing is detected. In order to increase the resolution of the estimation, all of the zero crossings may be determined (detection of half a period duration). A further resolution increase can be applied by detecting the peaks of the signal. The detailed discussion about resolution increase with the peak detection is given in the Section 4.7 of this chapter.

In **[21]** it is expressed that one cycle of permeance variation (fundamental RSH) corresponds to one mechanical rotor slot passage. This implies that, every complete RSH cycle can be related to rotation of rotor with one rotor displacement. The displacement angle is given as **(37)** in **[21]**;

$$\theta_r = \frac{2.\pi.n}{k.Z} \qquad \textbf{(37)}$$

In the implementation here, the zero crossing instant is not detected explicitly; instead, the instant where the sign change occurs is detected with small error, marked as x[i] and x[i+n] in Figure 55.. When the sign change occurs at x[i], that instant is assumed as the zero crossing point, however, the zero crossing occurs before that instant as marked as zero crossing in Figure 55. The time difference between the actual zero crossing and the sign change point can cause error and it can become significant in higher speeds where the number of sensed RSHs magnitude in one period is low. This problem can be solved either by increasing the data record rate or alternatively by interpolating the area of sign change and estimating the actual sign change instant. However, this improvement is not implemented in this work.

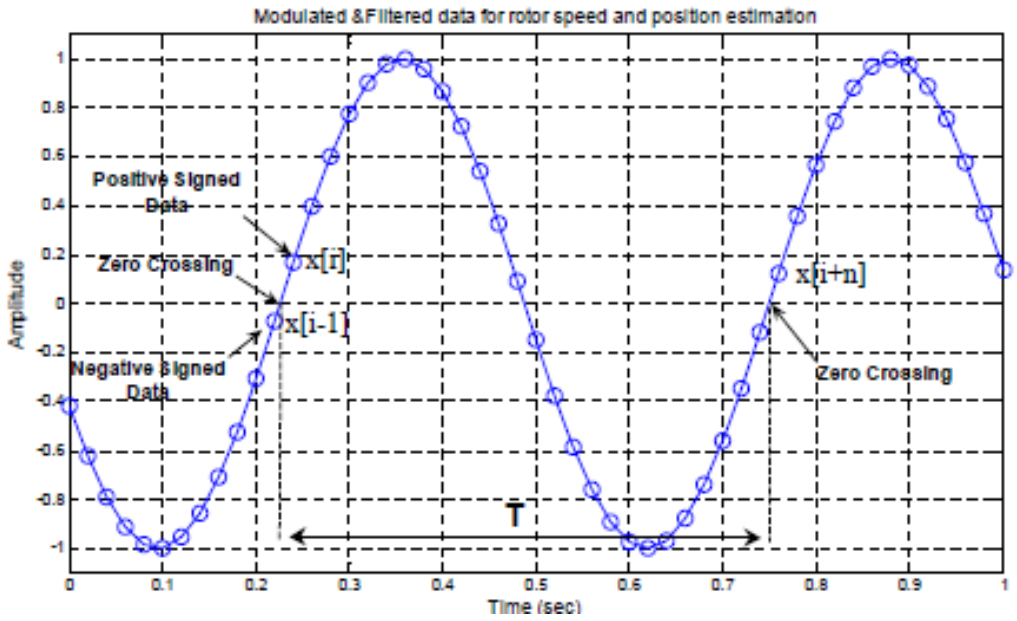

Figure 55 Illustration of zero crossing detection [21]

The rotor speed can also be calculated as in **(38)** given in **[21]** where T is the period of RSH calculated from zero crossings, k is the harmonic order and Z is the number of rotor slots .

$$Rotor\ Speed_{(RPM)} = \frac{60}{T.k.Z} \quad \textbf{(38)}$$

In Section 3.5 the test set-up where online implementation is conducted will be given. The hardware and the software of the test set-up will be explained, then the test procedure will be described briefly. Afterwards, the implementation of the algorithm, especially the adaptive filtering on the online set-up will be given.

3.5 Test Set-up Used for the Tests

3.5.1 Hardware of the Set-up

In order to drive the motor, take measurements and implement the proposed algorithm online, drive hardware capable to do the following requirements is needed. The hardware shall have a processor to implement the algorithm online, moreover, it shall have necessary peripheral interfaces to be able to drive the motor and sense the

needed signals. DS1104 processor board manufactured by dSPACE and the hardware in **[25]** designed by Kayhan are all together constructs a suitable hardware to be used. It is necessary to say that all the features of the system are not used for this work even though they exist in the system. The block diagram of the system is given in Figure 56.

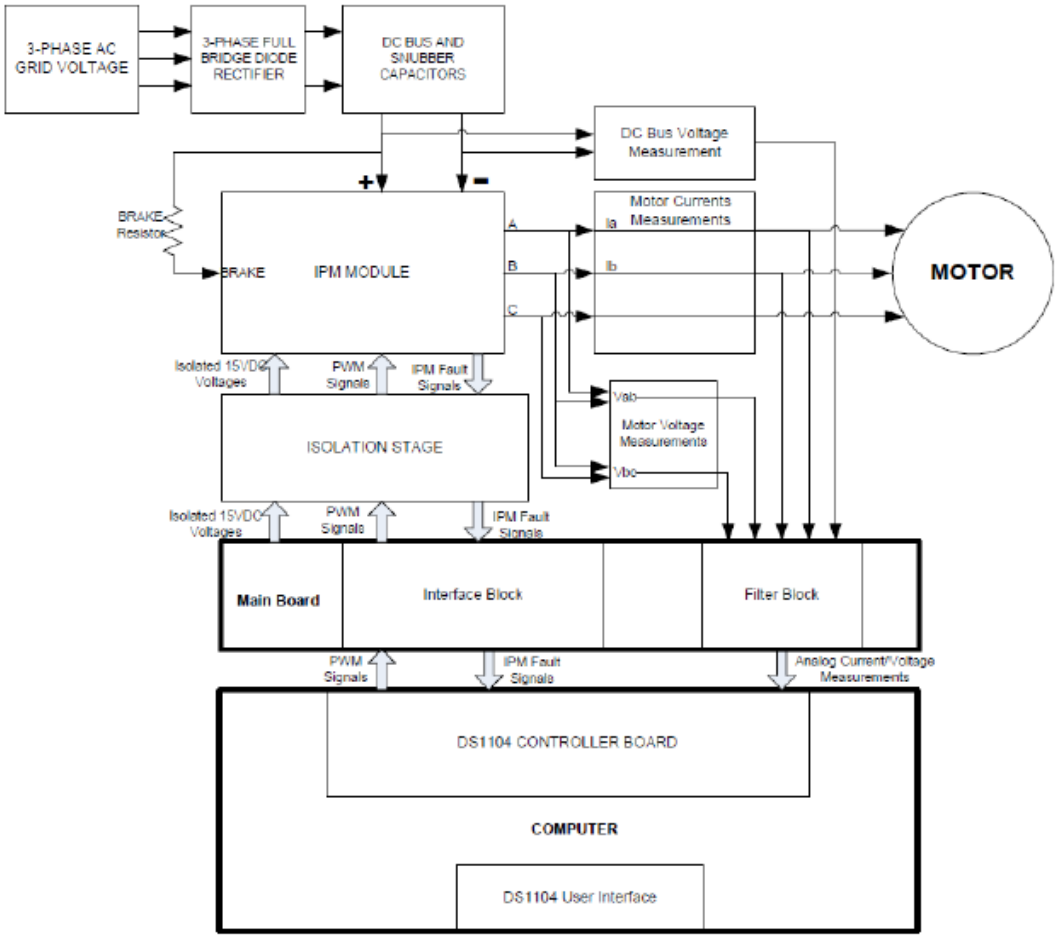

Figure 56 Block diagram of motor driver system [25]

The DS1104 board is used as the processor unit. It is a DSP controller and has the following features **[25]**;

- 8 ADC channels
- 8 DAC channels
- 34 I/O interface
- 2 incremental encoder interface

- 3-phase PWM interface (symmetrical and adjustable dead time PWM pulses)
- 2 serial communication interface

The ADC blocks are used to convert sensed stator line currents to digital to be used in the algorithm. The 3-phase PWM interface is used to generate the IGBT bridge inverter drive signals. The generated PWM signals by the 3-phase PWM blocks are symmetrical and no hardware effort is needed for this **[25]**. Moreover, for speed measurement the incremental encoder interface is used to get the encoder output to be compared to the estimation result.

The hardware designed by Kayhan supplies necessary interfaces for the processor board. One important interface used for the estimation algorithm is the current sense interface. The peak drive current supplied by the IGBT inverter is 22A per phase, and the used sensor is a current transducer rated for 100A peak from LEM Company **[25]**. The LEM sensors sense the current with 1A/20mV conditioning ratio and the current information is digitized by the ADC interface of DS1104.Then, digitized current data is multiplied with 50 in the digital domain (DSP) to get current information 1A/1V in the digital domain. After sensing the phase current, the sensed current is not filtered till it comes to the estimation block not to lose information about the RSHs.

All the signals sensed or created inside the software can be monitored and adjusted by the user interface of DS1104. This feature makes DS1104 more user-friendly and easy to use.

Another important interface of the hardware in **[25]** is the inverter driver. The power circuit of the driver is constructed by an Intelligent Power Module (IPM), PM50RL1A120 from MITSUBISHI Company. IPM has both the IGBT power switches to construct the inverter and the necessary gate driver circuit for each gate. With the help of gate drivers, the needed gate current decreases to 50mA for each gate. The IGBT's existing in the module is capable of carrying 50A peak DC current and can withstand 1200V stress without damage. Opto-isolation is used by Kayhan in **[25]** to provide necessary isolation between the power ground domain and the DSP

board ground. The DSP board PWM outputs are buffered before the isolation, as the DSP outputs are not capable to supply the needed current for the Opto-isolators **[25]**.

The power supply for the power stage of the system is 380V AC grid. The AC grid voltage is rectified and converted to DC, which supplies power for IPM. The IPM is used as an inverter driver and it creates a variable frequency AC **[25]**. By this way, variable frequency drive for the motor is achieved. The total physical drive system is given in Figure 57.

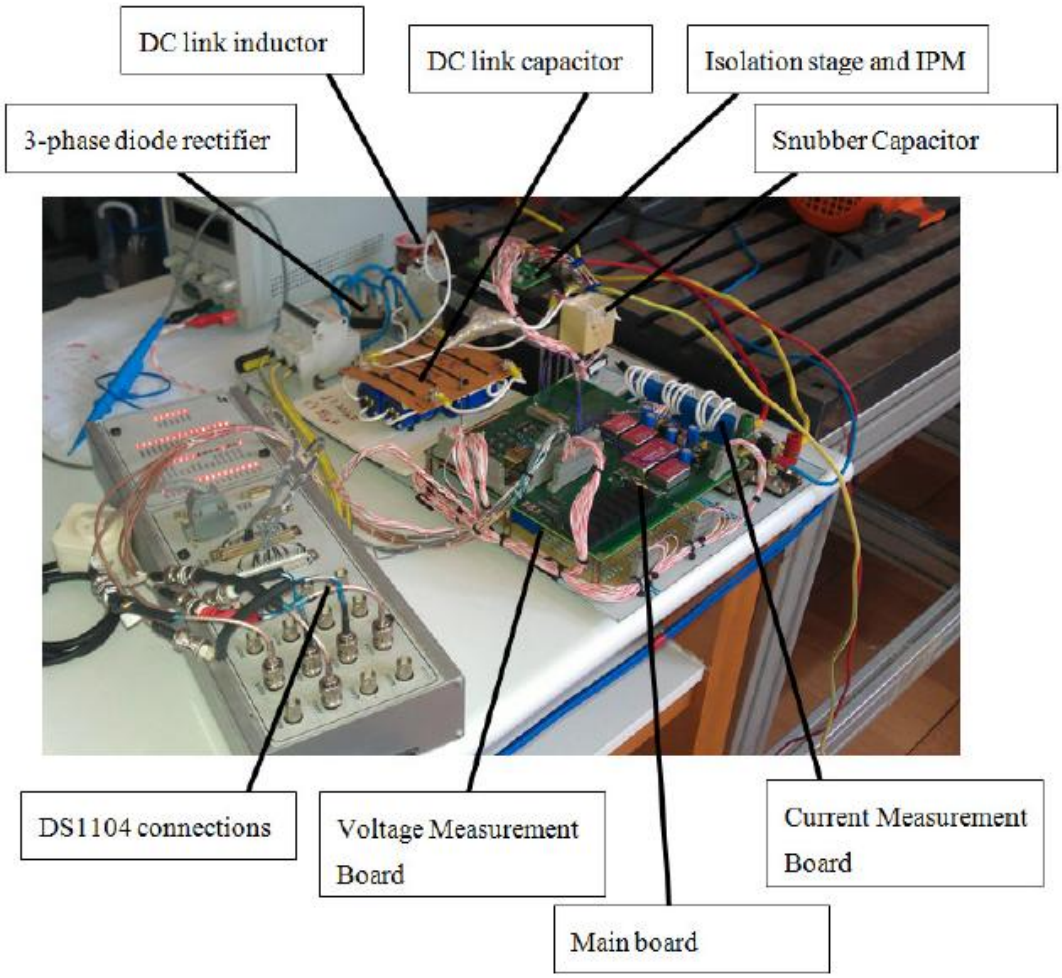

Figure 57 Hardware of the motor driver [25]

The rotor rotation is measured with OMRON E6C2-CWZ6C 1000pulse/revolution incremental encoder. It is mechanically mounted on the motor shaft and its measurement output is evaluated by DS1104 board. The pulses generated by the

encoder are given to the DSP and integrating the pulses gives the position of the encoder over time. Mechanical and electrical oscillations can couple to the encoder and the speed or position output of the encoder can become noisy. This kind of a noise is seen on the comparison figures in Chapter 4. The noise can be filtered in the DSP by digital filtering; however, it is not implemented in this work as the focus is not the encoder. The position and speed output of the encoder in this work is enough to compare with the estimation output. In the following part, the software and the online implementation algorithm generation platform will be explained.

3.5.2 Software Used for Implementation of the Algorithm

In order to implement the proposed estimation algorithm on online systems, some kind of signal processing blocks shall be implemented; which performs the modulation, filtering and zero crossing detection requirements of the algorithm. The DS1104 controller board has the ability to communicate with MATLAB/Simulink. Because of this feature, the algorithm can be implemented on the Simulink and loaded to the DSP by using "Incremental Build" option of MATLAB. Simulink has the ability to implement filtering via self- designed filters. The desired filter can be designed via FDAtool of Matlab, and Simulink block of the filter can be exported via "export Simulink Block" function. The simulink blocks designed can be seen in Figure 61. Moreover, Simulink algorithm development can be achieved by using its integrated blocks like multiplication, addition, hold, delay etc. These features make algorithm development easier and faster. Moreover, while the online implemented estimation algorithm and motor drive algorithm that is running on the DS1104in the system, all signals described in the DSP program can be monitored and the adjustable parameters can be changed via "Control Desk" program. The Matlab, DS1104 and dSPACE Control Desk system is preferred for online implementation of the estimation algorithm development since it is easy to use with Simulink's already existing blocks for mathematical and signal processing and monitoring functions. In the following part of this chapter, the test procedure that is followed while testing the proposed algorithm on online system is described.

3.6 Basic V/f Control

The inverter and motor control hardware is programmed in the same way as in **[25]**. The control method to provide variable speed to the motor is chosen as V/f control as it is easy to implement. V/f control method depends on keeping the motor flux approximately constant to prevent saturation of the rotor and stator cores. The three phase induction motor emf is approximately as in **(39) [26]**.

$$V = 4.44\phi K.T.f \quad \textbf{(39)}$$

Then the flux becomes as in **(40)**,where V is the induced voltage, ϕ is the flux, K is the winding constant and T is the number of turns.

$$\phi = \frac{V}{4.44KTf} \quad \textbf{(40)}$$

Since K, T and 4.44 is constant in **(40)**, ϕ can be kept constant only if V/f is constant. As the rotor speed is dependent on the supply frequency given in **(41)**, the motor speed can be changed by changing the supply frequency and the voltage is changed accordingly to prevent saturation **[26]**.

$$N_s = \frac{120f}{P} \quad \textbf{(41)}$$

3.7 Implemented Algorithm with Stator Current Input

The online algorithm is basically the same as Keysan's algorithm given in **[21]**. The constructed estimation algorithm to implement online with stator current input is given in Figure 58.

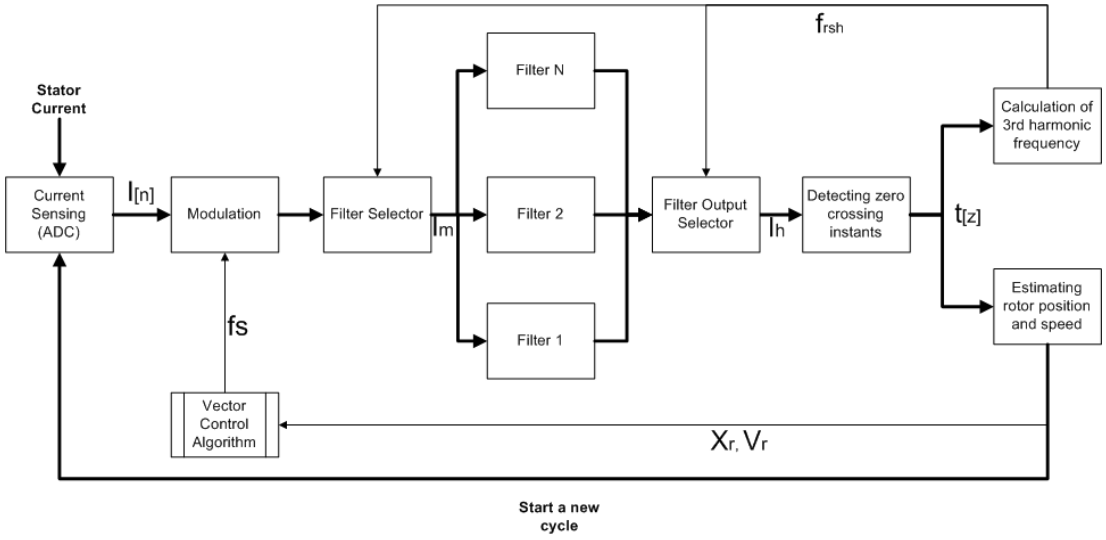

Figure 58 Block diagram of rotor position estimation with stator current input

Before starting the algorithm, the center frequency of the filter shall be determined. It is calculated by the sensed speed of the encoder coupled to the motor shaft. Then the estimation results are used to re-locate the filter with changing rotor speed. After locating the first filter, the stator current is sensed by a sensor. In this case, these sensors are LEM's, a kind of magnetic sensor, which outputs a voltage related to the current passing through its gap. The current sense process is given in detail in Section 3.5.1. This voltage is digitized by the on board ADC of the DS1104 board and it is multiplied with 50 to get the actual stator current amplitude in Amperes. , Therefore, the current data is ready to be manipulated by the processor. The digitized data is then demodulated by the main supply frequency of the inverter. The mains supply frequency is the output of the nearly all control algorithms, so it is an already known value and is 50 Hz. The drive frequency is input to the algorithm from the main motor drive algorithm as a number. After, the demodulation output comes to the filter selector block. This block selects the related filter by taking a feedback of the previous RSH frequency. The assumption here is that the rotor speed remains unchanged in one cycle of the control algorithm, 150µs. As a result of the filter selector block, only one filter takes the demodulated instantaneous input and processes it. Then, the output of the related filter is again selected by the filter output selector block as described in Section 3.9.3 to send it to the zero crossing detector. In

this block, the zero crossing instants are detected and at each zero cross, the output is updated. By this update, the 3rd RSH frequency and the rotor position is updated and the new cycle for the speed estimation process restarts.

3.8 Demodulation Block

This block function is same as the offline algorithm described in the Section 3.2 of this chapter. The input is multiplied by unity amplitude sinusoidal whose frequency is the main drive frequency. A virtual sinusoidal is created for this multiplication by placing a sine wave generation block of Simulink as given in Figure 59, and each sample of the input (sensed stator current amplitude) multiplied by this sinusoidal magnitude point by point at every 150µs over time, resulting in a modulated stator current data point (amplitude) value with the supply frequency.

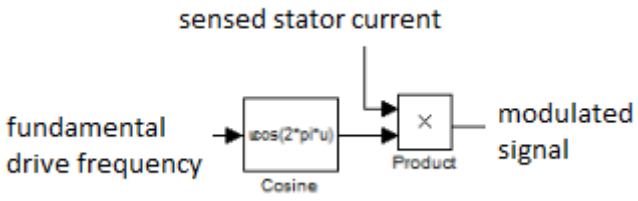

Figure 59 Modulation block implementation at Matlab Simulink

3.9 Filter Block

The filter block is needed to construct the RSH in time domain. The details of filter type selection and filter design is given in Chapter 2. In the online implementation, the adaptive filter implementation is important and the implementation of adaptive filtering will be given in Section3.9.1.The filters are designed by fdatool with the specifications given in Chapter 2. The implementations of the designed filters given in Table 10 are done by creating Simulink blocks of the designed filter by fdaool Export Simulink Model interface. The simulink model is then created and can be used in the Simulink model of the estimation algorithm. An example of the created block is given in Figure 37and it calculates the filter output by processing the input data as shown. The filter generates output, which is the instantaneous amplitude of the RSH, whenever a demodulated stator current data point is given to its input. The

filter holds the previous RSH magnitudes at its delay elements. The feedback existing in the IIR filter model decreases the filter tap number and creates computational advantage as given in Chapter 2.

These features are analyzed in the Chapter 2. In the following section, how adaptive filtering is implemented by selecting already designed filters will be described.

3.9.1 Implementation of Adaptive Filtering

In order to change the center frequency of band-pass filter, different approaches can be implemented. The first alternative that comes to mind is to use an adaptive filter, whose center frequency changes in every control cycle. By this approach, there will be only one filter and its parameters will be changed in every cycle by recalculating them. This approach is suitable; however, its implementation is hard on online systems. The reason for this difficulty is the need for filter design online (ie within the 150 ms control cycle). Filter design is a complicated job and cannot be implemented easily. In addition to that, the design takes a long time and cannot be completed in one cycle of the used control algorithm. However, if the filter parameters are calculated offline and stored to the algorithm loaded in the DSP, instead of changing the filter block, one block can be used and only its parameters can be changed. This method can be applied within 50μs filter calculation time, as only parameter reading is applied instead of filter design.

Another way of center frequency change is to modify one of the already designed filters. By this way, the center frequency will be changed without repeating the filter design procedure **[28]**. In **[28]** and **[29]**, various ways of spectral transformations are offered to meet this need. By using one of these methods, a low-pass filter can be transformed to a low pass filter at different cut off frequency, or a high pass, band-pass or bans stop filters **[28]**. Similarly, a band-pass filter can be transformed into another band-pass filter with different cut-off frequency as in this application. The basic disadvantage of this method is the need of spectral transformation. In Chapter 1, it is stated that spectral transformations take long time for this application and cannot be used for online implementation. Because of the time limitation of online

implementation, spectral frequency shift of a digital filter cannot be used inthe online implementation here.

A different way to implement the center frequency shift is to shift the input signal instead of shifting the filter. A frequency shift of a signal can be implemented by using the properties of Fourier transform. If a signal is multiplied with a complex exponential, its frequency content is shifted **[30]** as stated in **(42)**.

$$e^{j\omega_0 n}x[n] \overset{\mathcal{F}}{\leftrightarrow} X\left(e^{j(\omega-\omega_0)}\right) \quad \textbf{(42)}$$

By filtering the signal and shifting the resultant waveform to its original frequency will give the result. Even though this method seems to be applicable, the phase shift caused by frequency shift results in distortion in the output waveform. This is also visualized by the introduction of complex numbers in the analysis. The output of the implementation contains complex numbers, which does not exist in the original real time data. The introductions of these complex components make the reconstruction the signal and frequency detection harder and they are signs of distortion. Another reason not to use this method is the need of bandwidth change. This method only satisfies the center frequency change requirement. The need of bandwidth change is uncovered as the used filter is fixed.

The last method to be mentioned is to select and use previously designed filters. By using this method the need to re-design the filter or spectral transformation is eliminated. This elimination implies that no additional computational time is needed. Another advantage of the method is it does not cause distortion and phase shift. The sample filter blocks designed for changing speed conditions can be seen on Figure 61. The input of the filter is the demodulated RSH sent by the filter selector block and the output of the filter is the instantaneous value of the RSH which is sent to zero crossing detector by filter output selector block. Although the relatively high memory allocation due to a number of stored filters seems to be a disadvantage, the DSP board used has enough memory to store all the needed code segments and look-up tables. The memory allocation of one filter is about 10KB and the total memory allocation of the estimation algorithm with V/f motor control algorithm is about

1MB. Because of its high computational time efficiency and distortion-free implementation, selecting suitable filter in between from the previously designed ones is the most suitable method for this application.

3.9.2 Filter Selector Block

This block inputs the demodulated data from the demodulation block magnitude output as a single data point and the last RSH frequency estimate. By using the previous rotor speed information, it sends the demodulated data to the related filter. The function of the block is a selectable switch which sends the demodulated current instantaneous information to the appropriate filter. The implementation of the block is achieved by s-function builder function and the selection is achieved programming it. The selection criterion is the last RSHs frequency estimate. For example, if the rotor speed is estimated as 750rpm, the filter output selector outputs the demodulated data point by its out_760 pin. The bandwidth of the filter, Filter_760 in Figure 61 is 40Hz for rotor speed between 780 and 740rpm. So the suitable filter selection is achieved. Two successive filters bandwidth does not intersect; instead one bandwidth starts at the point where the other ends. The illustration of two successive filter intersections is given in Figure 60.

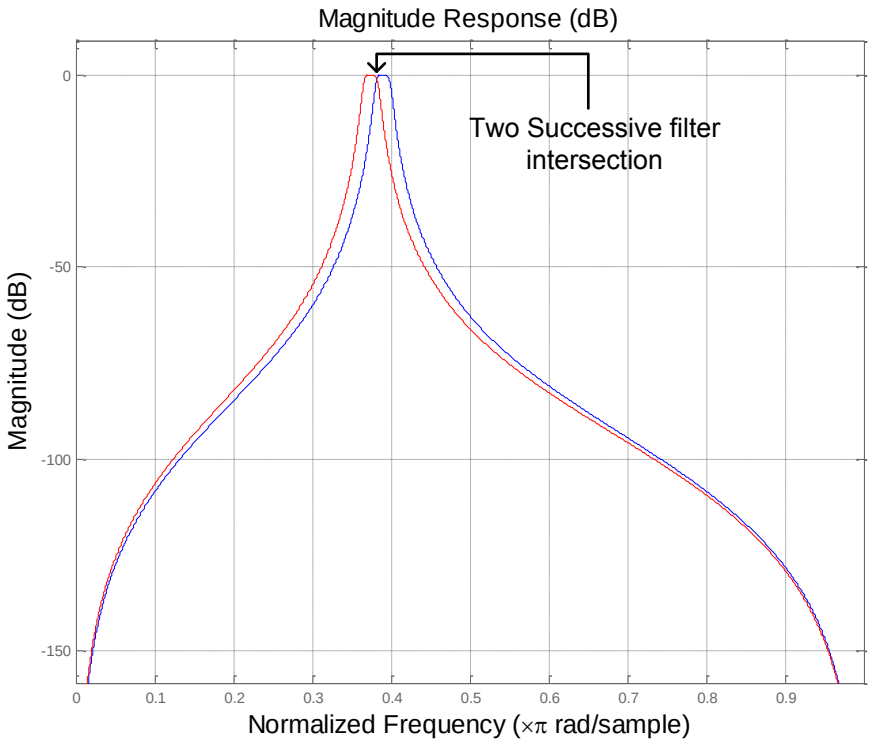

Figure 60 Visualization of two successive filter bandwidths

If the center frequency of the filter is decided at the edge of two filters, the filter with higher center frequency is selected. By this way, although there are many filters on the algorithm, only one of the filters works at one cycle of the algorithm. This keeps the calculation efficiency even though there are many filters on the algorithm. The block is given as "filter_select" block in Figure 61.

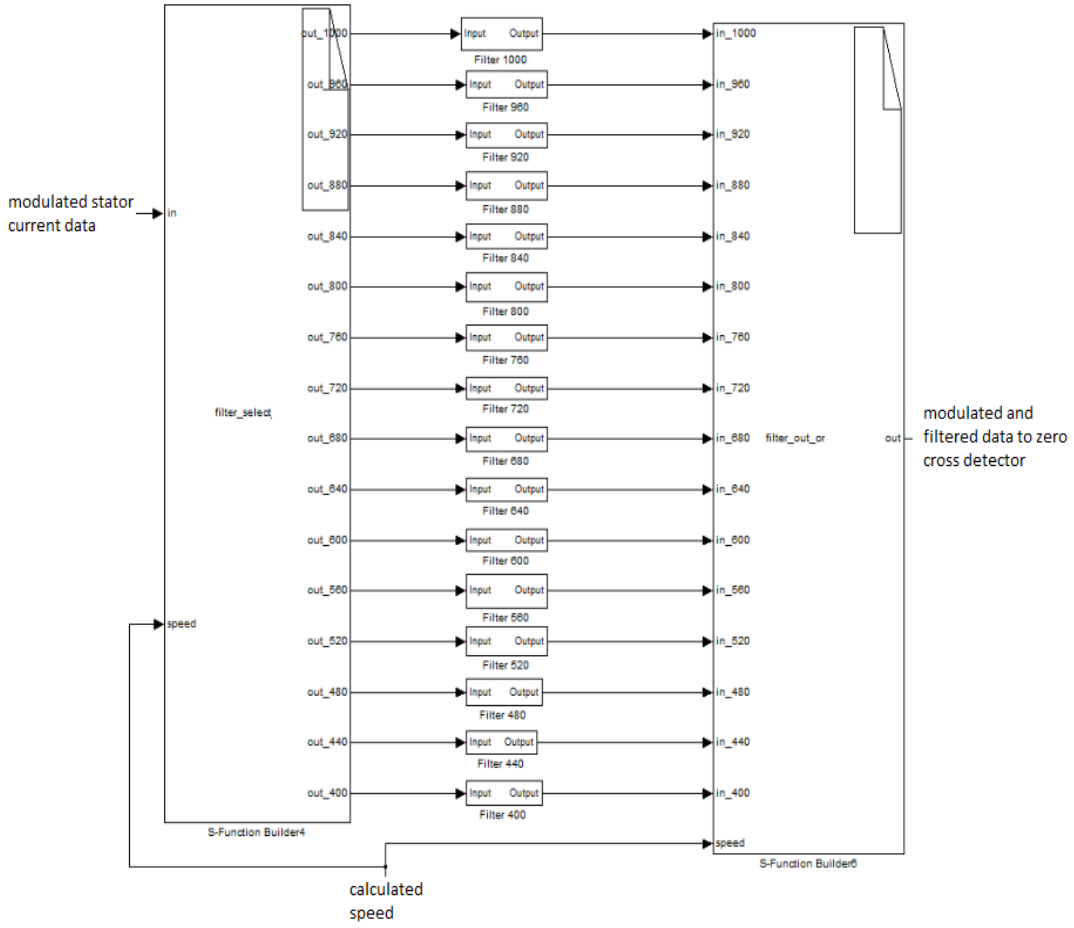

Figure 61 Adaptive filter implementation at Matlab Simulink using multiple filters and selector blocks

3.9.3 Filter Output Selector Block

The filter output selector block inputs the filtered RSH magnitude and the speed information calculated at the previous cycle. As there are about 50 filters, this block has 50 inputs and it selects the filter output which is used at that 150µs by using the speed estimation of the algorithm. The selection range of different inputs is decided by the bandwidths of the filters of each input specified at Table 10.For example, when the speed of the rotor is estimated as 760rpm, the filter output selector gets data from its *in_760* pin, which is the RSH magnitude calculated for that instant, and sends it to the zero crossing detector by its *out* pin. The filter output selector block is

given as "filter_out_or" block in Figure 61. When the used filter is changed, the previous demodulated stator current data held by the previous filter is lost. Due to this, the new filter needs 4-6 cycles to store needed number of data points. In this 4-6 control cycle the filter output is erroneous and this is an error source for the varying speed estimations.

3.10 Zero Crossing Detector and Rotor Position Estimator

The zero crossing detector takes input from the filter output selector and speed estimation calculated at previous cycle. The block holds previous filter output data (which is the magnitude of the harmonic) and previously detected zero crossing update of position information with the unit delay (one control cycle 150 us) elements given in Figure 62. The output of the block is the position estimation. By comparing the previous filter output with the current value, the block detects the change in the sign of RSH. If the change is a zero cross, the estimation output is updated. If the change is not a zero cross, the block uses the speed information and interpolates the position estimation result. The state information exist to remember that the previous estimation is whether a real estimation or an interpolation. This “state remember” function gives us the algorithm to hold the last uninterpolated rotor slot position. When a new zero crossing occurs, the detector updates the the previously determined position at the previous zero crossing. By this way, a possible error caused by the interpolation is cleared. The block is implemented by custom programming an S-Function builder block of Simulink as given in Figure 62.

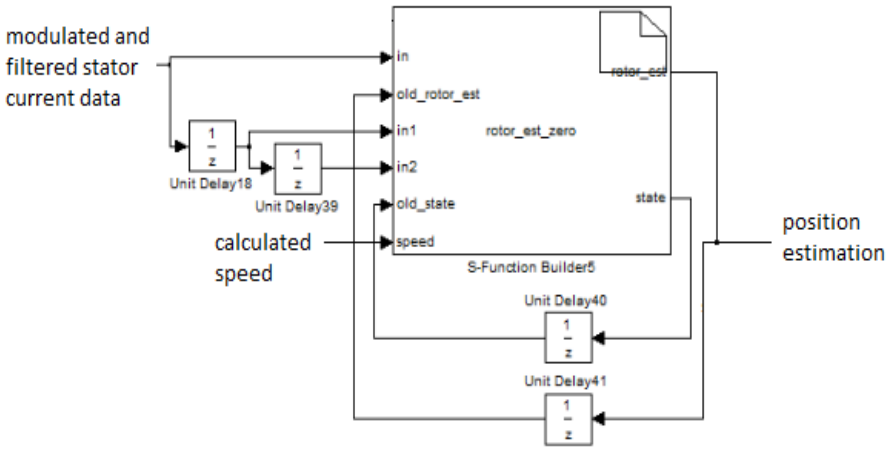

Figure 62 Zero crossing detection and interpolation block

3.11 Rotor Speed Estimation from the Estimation Points

After the position estimation points are calculated; as the derivative of the position gives the speed, the rotor speed can be calculated. In order to implement derivative function to the position points, the time elapsed between two position estimation update is calculated and the slope is calculated by dividing the change in position update to the elapsed time. The speed estimation is calculated over one complete rotation of the rotor shaft, by sensing the position estimation instants where the position changes from 360° to 0°. In order to have more exact speed estimation the slope of the RSHs estimation points can be measured, which is not implemented in this work.

3.12 Conclusions

In this chapter, the online implementation aspects of the proposed rotor position and speed estimation technique from RSHs existing in the stator current are given. The drive hardware, the used software and the implementation of the algorithm is given in detail. The most important part of the algorithm, the adaptive filter implementation is also discussed in detail. In the next chapter, the test results of the implemented algorithm on an online set-up will be given. The limits of the algorithm will be stated and the improvements and the weaknesses of the algorithm will be evaluated.

CHAPTER 4

VERIFICATION OF THE ON-LINE ALGORITHM

The algorithm is built on the online implementation set-up as described in Chapter 3. In this chapter test results are discussed. During the tests, the test motor is run with the hardware designed by Kayhan in **[25]** inV/f control mode. The predicted position of the rotor from the algorithm and the encoder output coupled to the shaft of the motor is recorded via dSPACE Control tool. The results consist of comparing the speed estimation and the position estimation with the encoder output values. The tests are conducted between 10Hz to 75Hz drive frequency. The tests are performed at no-load and full load conditions. At the end of this chapter, the acceleration limit and the improvements of the algorithm implemented by increasing the resolution and by using interpolation methods will be discussed. Moreover, the limitation of the algorithm at will be stated. The no-load and full-load test results will be evaluated with the encoder output and the evaluation includes both constant speed and variable speed conditions. As also discussed in Section 3.10, the zero crossing detection of the RSH is implemented one time in one period. The effect of increasing the resolution of estimation by detecting the sinusoidal at every zero crossing in a period by detecting the zero crossing two times in one period and detecting the peaks will be also be analyzed in this chapter. The results prove that the algorithm can successfully be implemented on a real-time motor control system with stator current as input.

4.1 The Test Procedure

In order to test the online implemented estimation algorithm on an online system the test set-up described in Section 3.5 is used. The motor whose details are given in Section 2.2 is used in the tests. This motor is the same motor which Keysan conducted his tests with search coil data in **[21].** The hardware designed by Kayhan in **[25]** is used to drive the test motor. The encoder whose details are given in Section3.5.1 is coupled mechanically to the test motor shaft to detect the actual position and speed of the rotor. The motor drive algorithm chosen as V/f control due to its easy implementation for variable speed drive as described in Section 3.6. As the algorithm uses the stator current as input to the estimation algorithm, the stator current is sensed as described in Section3.5andthe stator current data is sampled as a single current value at every 150μs. This current data is demodulated and filtered to estimate the rotor position as described in Section 3.7. One of the differences between the offline algorithm and the online algorithm is that there is no need to wait for multiple stator current data sampling as in the offline implementation. As the previously sampled and modulated stator current data needed for proper filter application is held by the filter itself as described in Chapter 2, the filtered RSH magnitude is updated as a new data point at every 150μs after a new stator current magnitude is sampled. So, the zero crossing of the RSH can be detected by comparing two consecutive RSHs magnitude as described in Section 3.4. Finally, the estimation result and the encoder sensor output are compared. When a change in the algorithm is required, it is implemented in the Simulink block of the drive algorithm and re-downloaded on the DSP board DS1104 by using the "Incremental build" function. All the algorithm and the blocks are designed on Simulink program by using additional Matlab features as described in Section 3.5.2, the C code generation for DSP implementation is conducted by "Incremental Build" function of the Matlab.

Lastly, the dSPACE Control Desk Program is used to monitor the internal signal processing signals in the DSP, while it is still operating and controlling the system as well as computing the estimation result. The test results, which are the position and speed estimation results and the encoder output are recorded by image capture of the

dSPACE Control Desk. The tests are first conducted under no-load conditions. The motor is driven to the desired speed by adjusting the motor speed via dSPACE Control Desk interface. In order to locate the filter for start-up of the algorithm, encoder speed information is used to calculate the filter center frequency. Then, the speed change is made by controlling the frequency of the drive, and the estimation results are compared.

Note that position prediction is made over a period of the RSH cycle in the Section 4.3, 4.4 and 4.5. Prediction of half period cycle zero crossing is handled as an improvement of this algorithm and the improvement it introduces is discussed in Section 4.7 and some experimental results are given.

4.2 Speed Limits of the Online Algorithm

In this part, the speed limit limits of the estimation algorithm will be stated. Afterwards, the proposed estimation algorithm and its online implementation will be explained in details.

4.2.1 Upper Speed Limit of the Algorithm

The control cycle of the motor drive system works in every 150µs. This means that that the stator current of the motor is sampled at every 150µs. The sampling rate of the stator current is therefore is 6.67 kHz. As also discussed in Section 2.4, the upper speed limit of the estimation algorithm is limited with the sampling rate. The Nyquist rate proposes that the sampling rate shall be at least two times of the frequency of the signal of interest. If the sampling is done at Nyquist rate, the RSHs can only be sampled for two times at one period. As detecting the zero crossing of the signal in time domain will be erroneous with 2 samples at one period, the sampling rate shall be higher. Moreover, the rated drive frequency of the motor is 50Hz and the rated speed at no load is 1000rpm. Applying the tests at rated speed is a desired condition. The maximum frequency of the 3rd couple of the RSH is 1296Hz. The RSH at 1296Hz will have 5 samples for one period with a sampling rate of 6.67kHz. This sampling rate is enough for zero crossing detection of the harmonic within 150µs, however, if the sampling rate is increased, the zero crossing detection and therefore

the accuracy of the algorithm will be higher. In this work, the sampling rate held constant at 6.67 kHz. The methods to increase the sampling rate will be discussed in Section4.7 of this chapter, and effect of using additional processors and parallel computation will be discussed in Chapter 5.

4.2.2 Lower Speed Limit of the Algorithm

The lower speed limit of the algorithm is determined by the RSHs magnitude. The RSHs magnitude decreases drastically at low rotor speeds as shown in Section 2.9, reconstruction of them becomes difficult. Some tests are applied at low rotor speeds to decide the low rotor speed conditions in Section 2.9, and 5Hz drive frequency is decided as the low speed limit of the implementation.

4.3 Test Results of Constant Speed Operation at No-Load

4.3.1 Position Estimation Test Results

In this section, online implementation results of speed and position estimation is given. The motor is driven with 5Hz, 20Hz, 50Hz and 75Hz fundamental frequency and the speed is held constant. The test is conducted at no load condition. Figure 63 presents the encoder output (green curve) and the predicted position of the rotor (red curve) when the motor is supplied with a 50 Hz PWM supply from the inerter. When this Figure is investigated it appears that at some points the rotor position is well predicted and later the predicted rotor position deviates from what is measured.

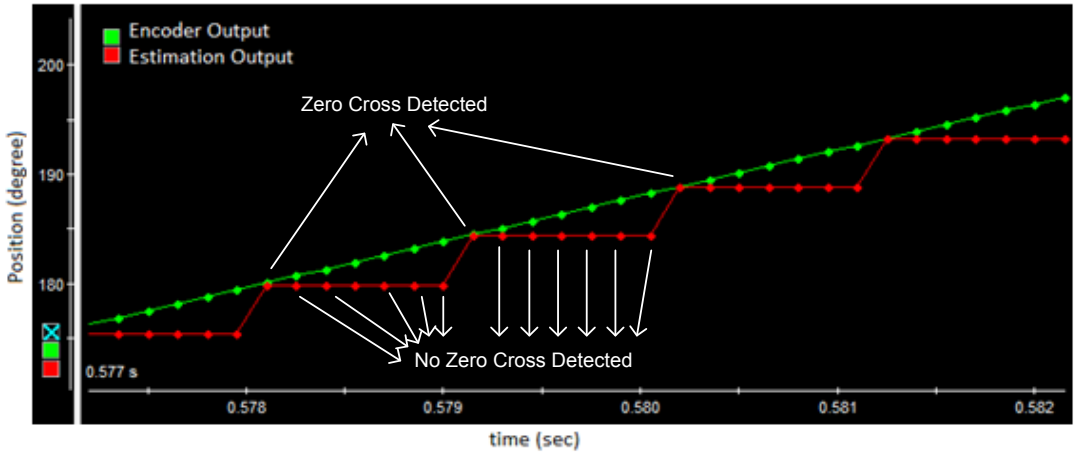

Figure 63 Zoomed view of position estimation at 50Hz drive frequency at no load at constant speed

This is an "artificial" error in position estimation in Figure 63 on the points shown as "No Zero-Cross Detected". The difference between position estimation and encoder output is because of the way which the algorithm is implemented to update the position estimation one time in one period of the RSH and the position is assumed to be constant between two zero crossing detection instants of the RSH. As seen from the "Zero Cross Detected" instants, the estimation algorithm works properly and there exist no measurable error in the position estimation. The artificial error due to assuming the position constant at "No Zero Cross Detected" points will be solved by detecting both zero crosses in one period of the RSH and interpolating the points between zero crossings by using the speed estimation as given in Section 4.7.2.

As also can be inferred from Figure 63, the slope of the "Zero Cross Detected" points are exactly the same as the slope of the encoder output. As the slope of the position is the speed, this proves that the speed of the motor shaft is exactly estimated. The "No Zero Cross Detected" points similarly create artificial speed estimation error and the proposed resolution increase and interpolation methods in Section 4.7 can solve this artificial error.

The position estimation results of 20Hz, 50Hz and 75Hz driven machine at no-load is given in Figure 65, Figure 66 and Figure 67. It can be seen from the figures that there

exist almost no estimation error at high speeds when the RSHs magnitude high and detectable.

In Figure 64, the position estimation of 5Hz driven machine at no load is given when compared to the estimation output. Between 7.25s and 7.3s the position estimation creates an error as marked on Figure 64 because the algorithm misses a zero crossing due to the amplitude decrease at low speeds. Even though the position estimation error remains after that time, the slope of the estimation points, which is the speed, is the same as measured value. So, the position estimation error stays and becomes cumulative in position estimation. However, the same error creates an instantaneous error in speed estimation and the speed information corrects itself when it is updated on the ongoing estimations. The slope of the estimated position and the slope of the encoder output is the same and calculated as 584°/s before and after the error at 7.25s in Figure 64. This property shows that the algorithm is more reliable on speed estimation than position estimation. In this study one complete rotation of the shaft is determined by summing up the corresponding angle for each slot pitch until 360° is reached. The speed is calculated from the time that elapses to complete the cycle. Therefore, if a slot pitch is not identified on time and a pulse is misses for example the 360° appear to be completed in a longer period of time than it actually happens. Naturally this introduced a speed prediction error. For the test in Figure 64, the artificial speed error caused by the missing zero crossing detection on speed would be 5.4rpm/sec while the actual speed of the machine is 97.5rpm/sec. However, if the speed is calculated instantaneously with the slope of the line, which shall give the correct speed estimation, there will be no speed error other than the instantaneous error.

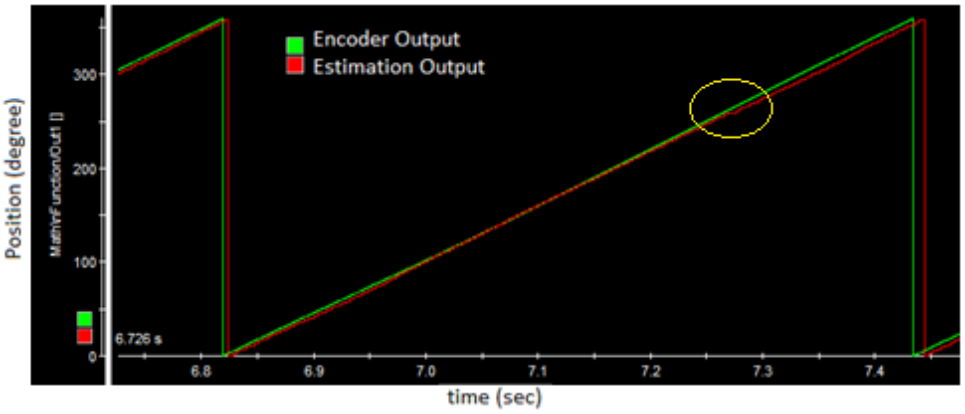

Figure 64 5Hz driven machine at constant speed position estimation comparison with encoder output

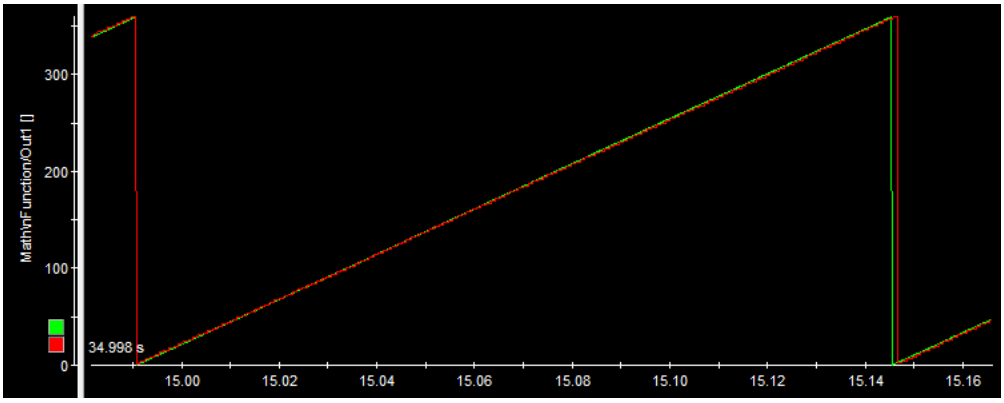

Figure 65 20Hz driven machine at constant speed position estimation comparison with encoder output

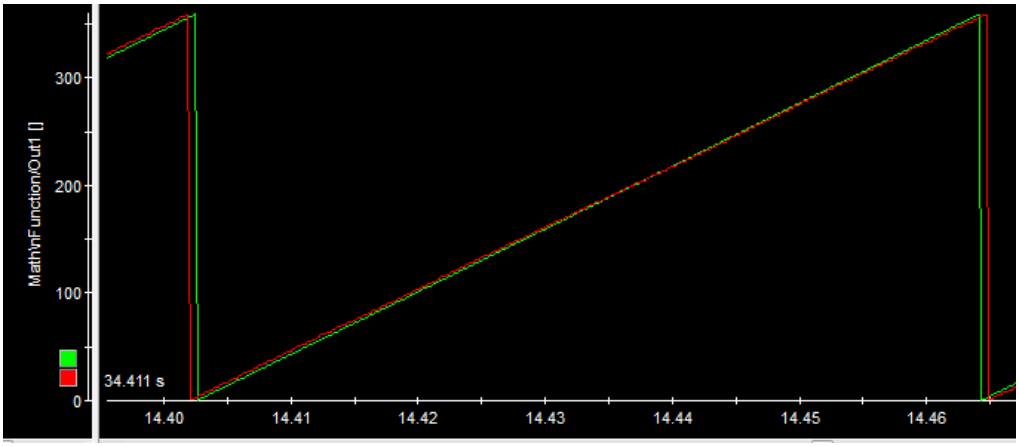

Figure 66 50Hz driven machine at constant speed position estimation comparison with encoder output

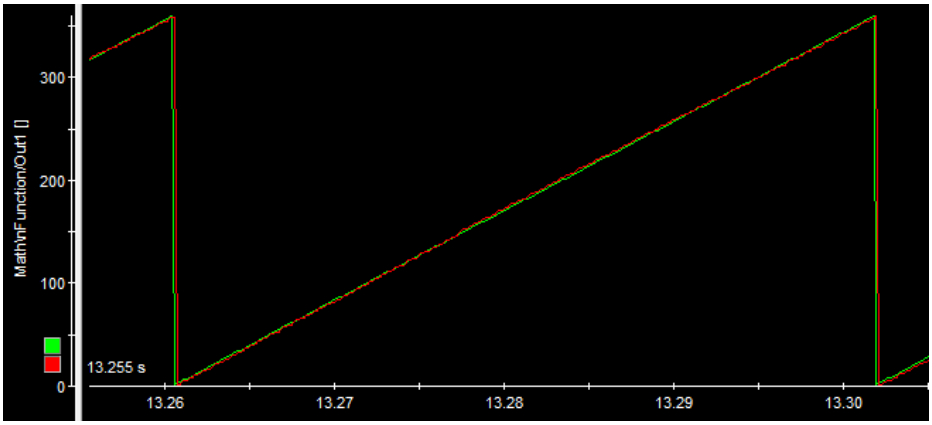

Figure 67 75Hz driven machine at constant speed position estimation comparison with encoder output

4.3.2 Speed Estimation Test Results

Similarly, the speed estimation results at constant speed are given in Figure 68, Figure 69, Figure 70 and Figure 71 at no-load conditions. The speed is calculated by dividing one complete rotation of the rotor shaft to the elapsed time, assuming that the speed is constant in one turn as explained in Section 3.11. If the speed is estimated from the slope of the position, the resolution will increase in speed estimation, and the so called error seen on Figure 71 due to calculating the speed over one 360° turn of the rotor shaft will be eliminated.

It can be observed that in fact the speed can be well predicted. In Figure 69 and Figure 70 the ripples on the encoder speed estimation is expected to exist due to a coupling noise on the encoder speed signal.

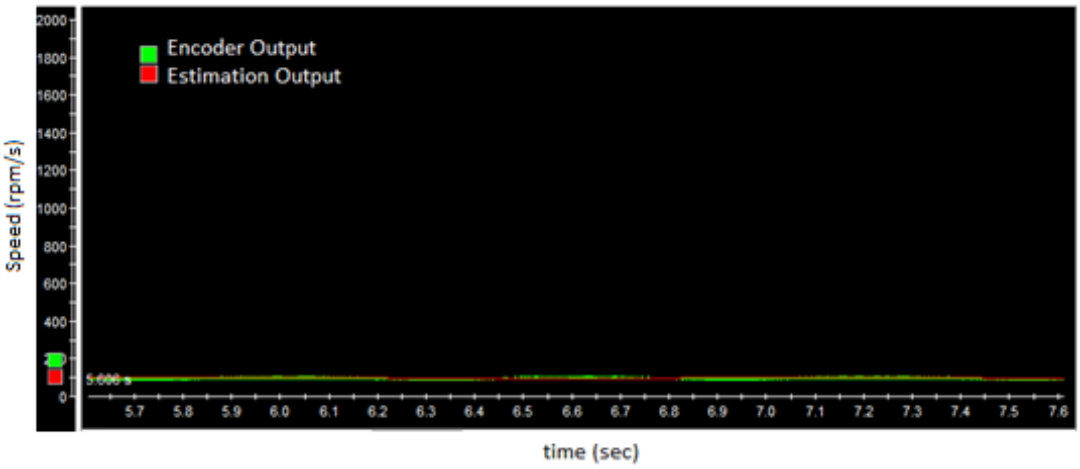

Figure 68 Speed estimation comparison with encoder output of 5Hz driven machine at constant speed at no load

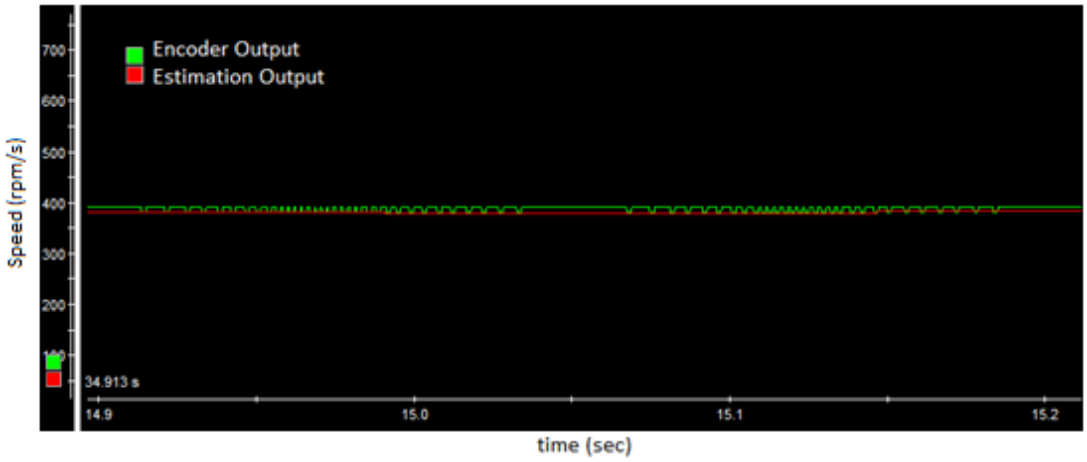

Figure 69 Speed estimation comparison with encoder output of 20Hz driven machine at constant speed at no load

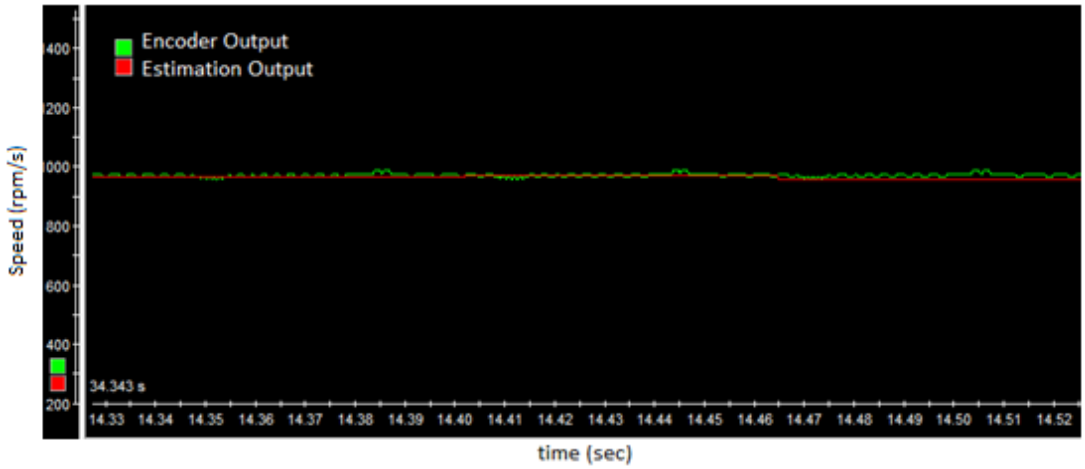

Figure 70 Speed estimation comparison with encoder output of 50Hz driven machine at constant speed at no load

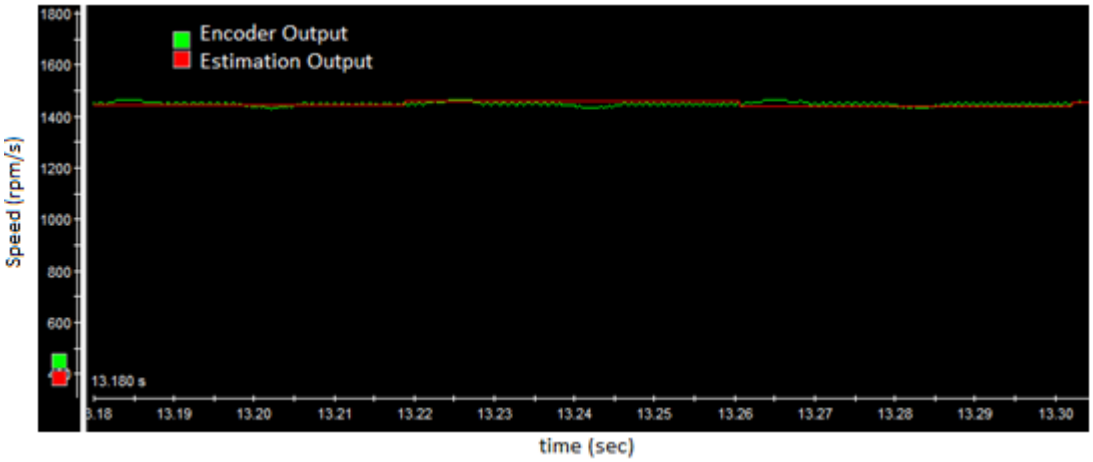

Figure 71 speed estimation comparison with encoder output of 75Hz driven machine at constant speed at no load

The comparisons given in this section verify that the proposed algorithm can be applied on online systems. It is also verified that the needed calculations of the estimation algorithm can be completed within 150µs. There seems to be some error in position estimation as no resolution increase and interpolation is not used in this part of the tests conducted at no-load conditions.

4.4 The Test Results under Full Load Condition

In order to show that the algorithm also works under loaded conditions of the motor, the estimation algorithm is run under full load condition of the motor. The loaded test and the test set up of loaded test is given in section 2.3.The test results are recorded similarly in the no-load tests. The tests are conducted at different rotor speeds and the results show that the algorithm is also applicable under loaded conditions. The tests are conducted while the machine is driven with 10Hz, 20Hz, 50Hz and 75Hz and the results show that the rotor position and rotor speed can be estimated correctly under loaded conditions. As seen from Figure 72, Figure73, Figure74 and Figure75 the estimation accuracy of no-load and full load conditions does not differ significantly. This result is an expected result because the RSHs magnitude does not differ significantly with load conditions as discussed in Section 2.11, Figure 23 and Figure 24.

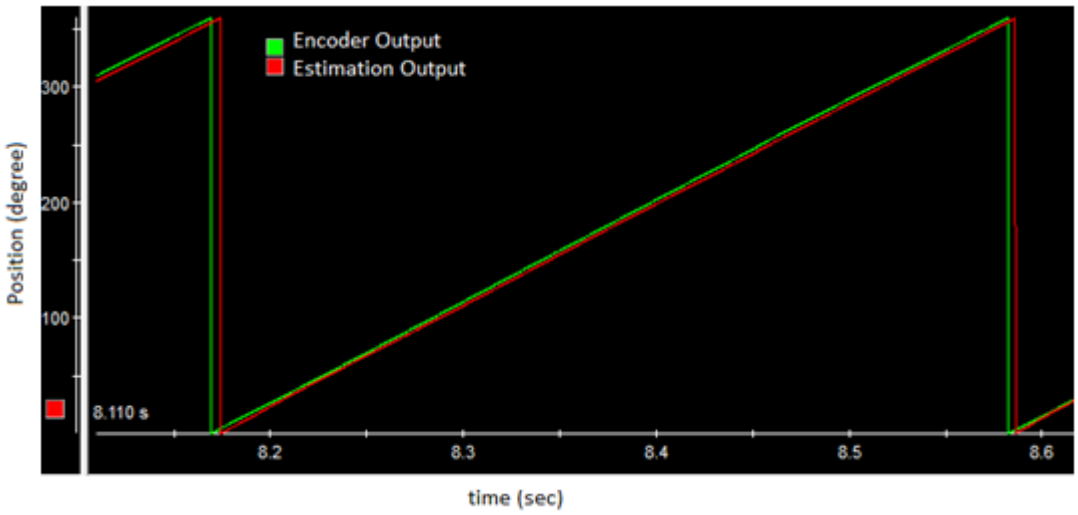

Figure 72 Online rotor position estimation compared with encoder output at full load with 10Hz drive frequency

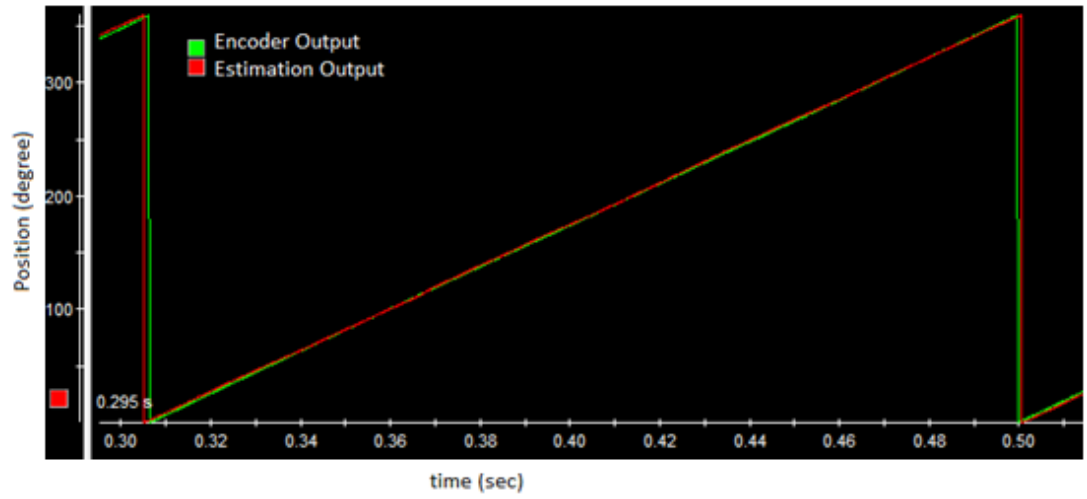

Figure73 Online rotor position estimation compared with encoder output at full load with 20Hz drive frequency

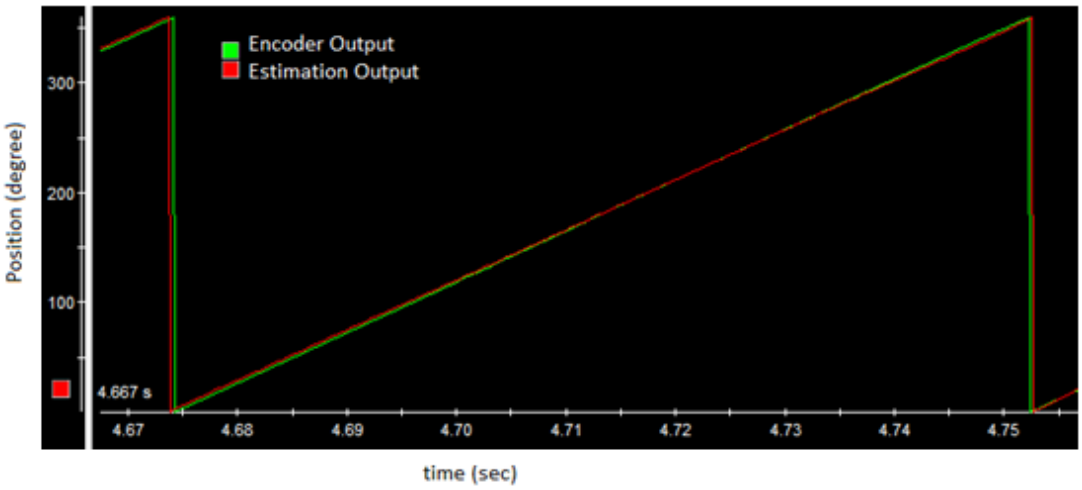

Figure74 Online rotor position estimation compared with encoder output at full load with 50Hz drive frequency

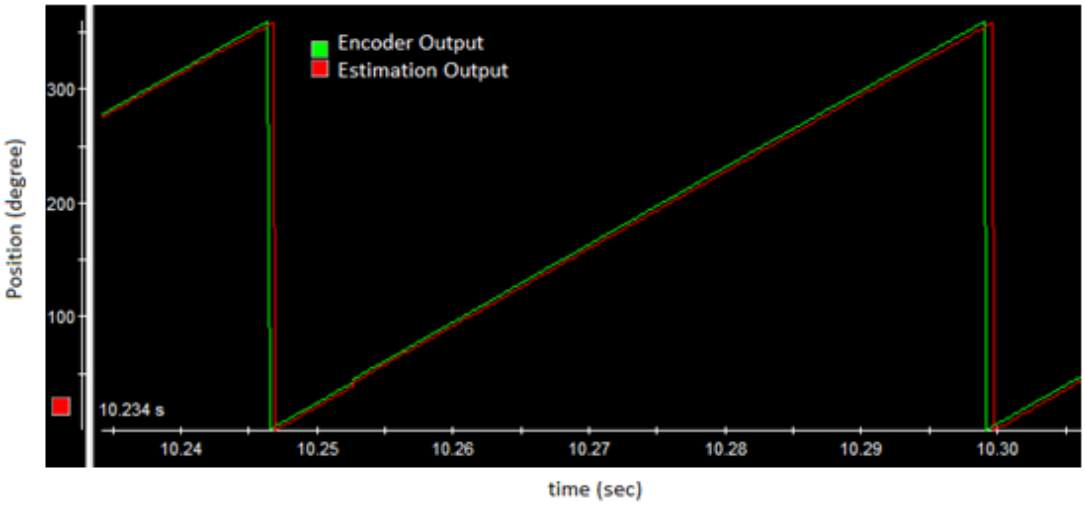

Figure75 Online rotor position estimation compared with encoder output at full load with 75Hz drive frequency

The speed estimation result compared to the encoder output is given in Figure76, Figure77, Figure78 and Figure79. When the speed estimation of loaded and no-load conditions are compared given in this Section and Section 4.3, it is seen that the error does not change significantly. This is the expected result as in the case of position estimation because the RSH characteristic does not differ with changing load conditions as discussed in discussed in Section 2.11, Figure 23 and Figure 24.

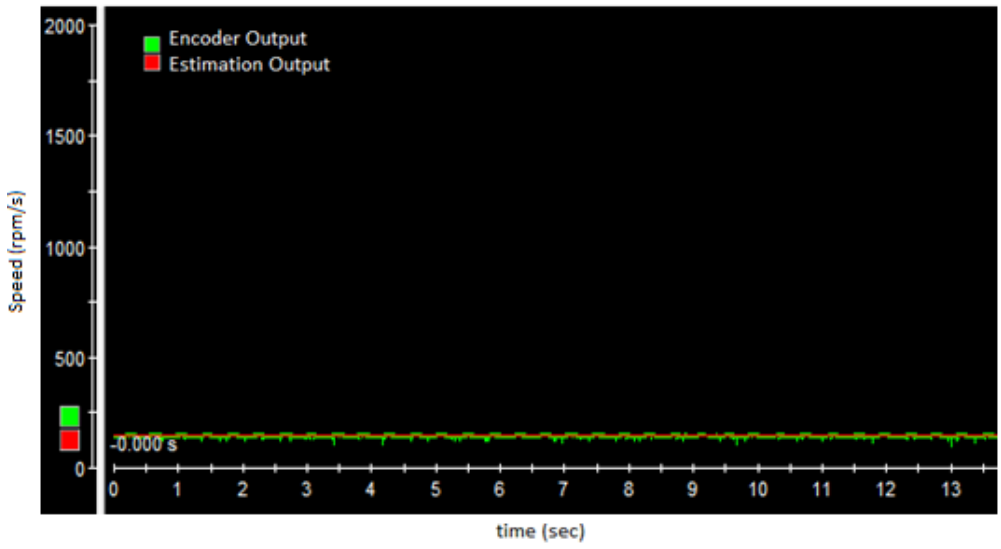

Figure76 Online rotor speed estimation compared with encoder output at full load with 10Hz drive frequency

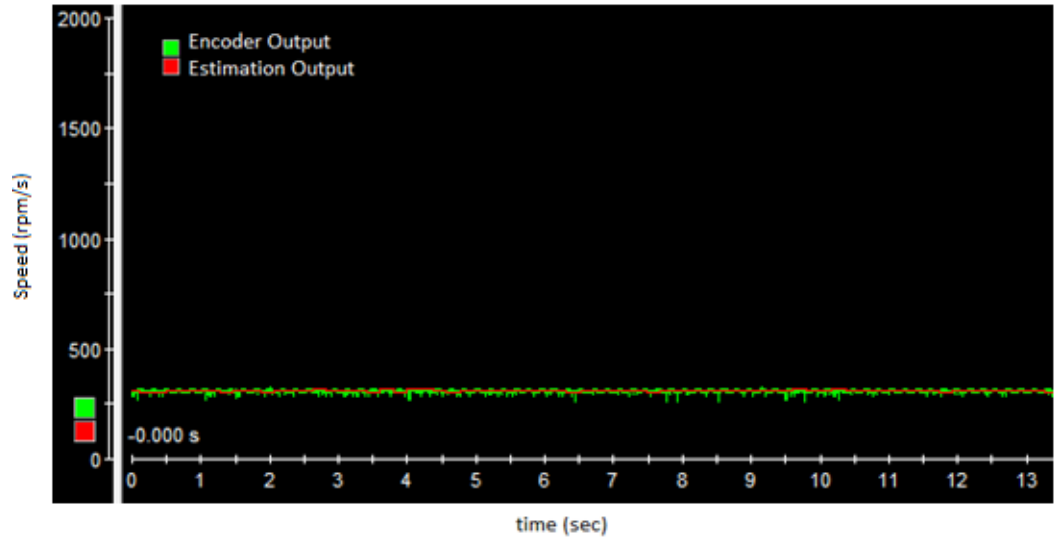

Figure77 Online rotor speed estimation compared with encoder output at full load with 20Hz drive frequency

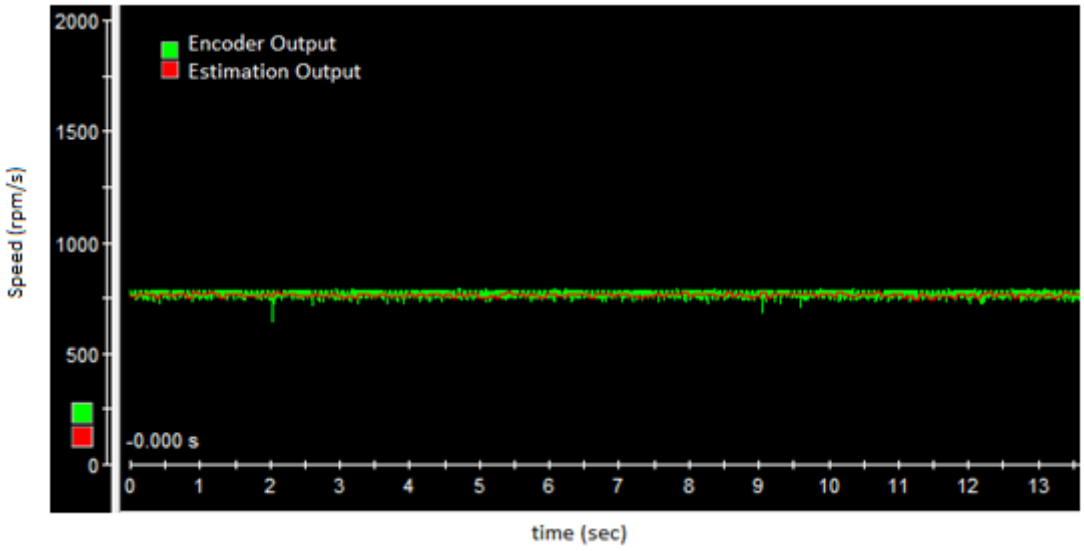

Figure78 Online rotor speed estimation compared with encoder output at full load with 50Hz drive frequency

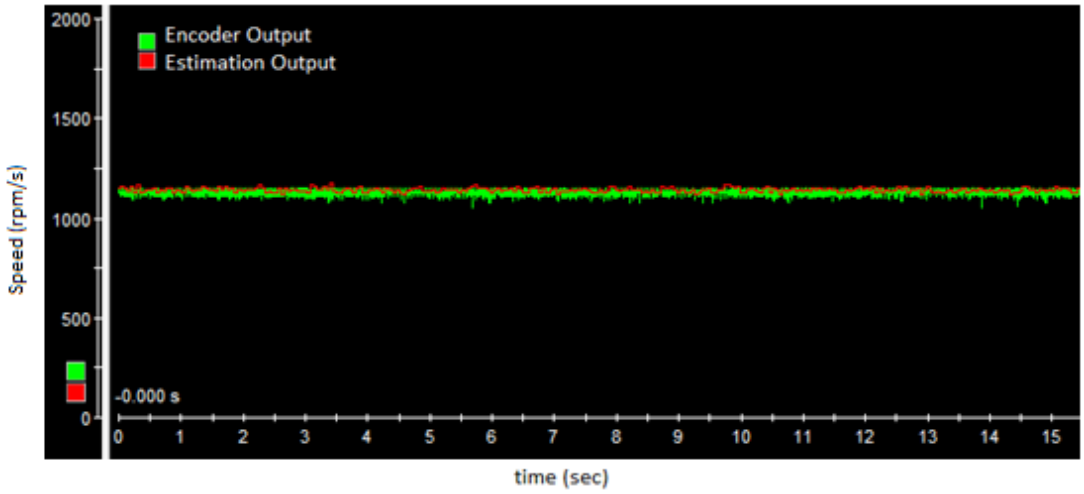

Figure79 Online rotor speed estimation compared with encoder output at full load with 75Hz drive frequency

4.5 Test Results of Variable Speed Operation

In order to see the algorithm works under variable speed conditions some tests are applied when the speed is changed. The test is conducted at no-load conditions and the motor speed changed by changing the V/f control drive frequency. The speed change is adjusted via dSPACE control desk user interface. Even though the algorithm is analyzed to work at higher speed change rates given in Section 4.6, the speed change rate implemented in the test is kept at 125 rpm/second. The speed increase is controlled by changing the drive frequency from 20Hz to 49Hz from dSPACE control desk interface by hand from 1,5s to 5,5s given in Figure 80. Then, the motor is let to run at constant speed at 49Hz drive frequency 960rpm rotor speed for about 3s and speed decrease is again controlled by hand from 960rpm to 400rpm by changing the drive frequency from 49Hz to 20Hz from 9.5s to 13.5sin Figure 80. The estimated speed and the speed output of the encoder corresponds to 125 rpm/second speed change rate, at both acceleration and deceleration regions. It is seen from Figure 80that the speed is estimated with low error at constant speed regions and the error increases at the variable speed regions. This is because of the speed estimation algorithm which estimates the speed after one complete rotation of the motor shaft and assumes constant speed in between two estimations and the filter

change in those regions. The speed estimation accuracy and resolution can be increased by calculating the slope of the position estimation points as discussed in Section 3.11 and 4.3, which is not implemented in this work. Secondly, when the used filter is changed, the previous amplitudes of the demodulated stator current is lost as they are held by the previous filter itself as described in Section 2.20. As the used filter tap numbers are in the range of 4-6, 4-6 new data points are needed to calculate the filter output correctly. Due to this fact, the filter creates the output with slightly higher error in position and speed estimation at the instant of filter change. This error gradually gets smaller as the filter operates 4 to 6 more cycles and completes its data storage with demodulated current amplitudes. This lag caused by the filtering process creates error in the dynamical regions of speed estimation. This problem can be solved by improving the filter change process. If only the filter coefficients can be updated instead of changing the filter as implemented here, the demodulated current data would not be lost and the error in the variable speed conditions given in Figure 80 would decrease. Parallel processing devices can achieve this kind of filter change. While the estimation algorithm continues to work in its normal operation, other part of the processor can update the filter coefficients without the loss of information. As the filter update rate is relatively low due to rotor mechanical time constant (39ms), the new filter coefficients can be calculated in this time interval. Alternatively, the coefficients of the filter could be calculated offline and stored in the DSP. When a filter change is needed, the coefficients can be changed instead of the filter block itself. In this case, the algorithm would operate better in the varying speed regions. The disadvantage of this method is that the tap number of the filter shall be same for all speeds, as the coefficients are calculated for a fixed tap number.

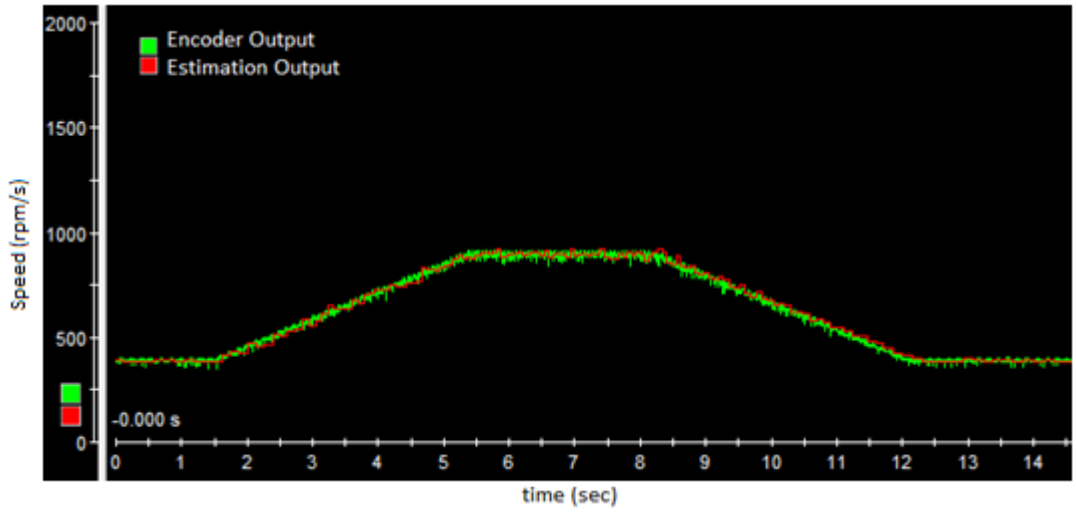

Figure 80 Comparison of rotor speed estimation output of the algorithm and encoder output

In Figure 81, the position estimation results of the algorithm and the encoder output is compared. It can be seen from the comparison that the rotor position can be estimated in an online system from RSHs existing in the stator current when the rotor speed is changing.

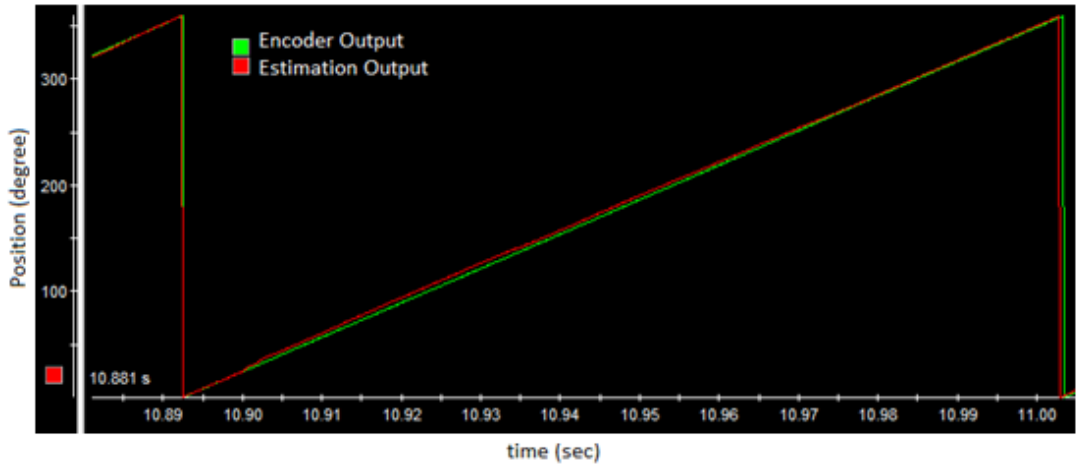

Figure 81 Comparison of rotor position estimation and the encoder output at acceleration condition

The comparison of the output of the algorithm and the encoder output shows that the algorithm is successful in estimating the rotor speed and rotor position estimation in

variable speed conditions. The error in the position estimation in acceleration regions are due to the filter change method implemented.

4.6 Acceleration and Deceleration Speed Limits of the Algorithm with the Used Test Set-up

The acceleration and deceleration rate limit of the algorithm is calculated by the bandwidth of the filter used. At high rotor speed conditions, the filter bandwidth is higher (about 50Hz at 50Hz drive frequency), so the RSH signal frequency can change about ±25Hz. Total 50Hz frequency change in RSH means 38rpm shaft speed change in 150μs at rated 1000rpm rotor shaft speed. This implies that the limit of acceleration in 50Hz drive frequency at no load is 60000rev/s. So the RSH would still be in the bandwidth of the filter even though the speed change rate is high. The limiting point of the speed rate change is the low speed case, where the bandwidth of the filter is narrow. The lower drive frequency limit of the algorithm is described as 5Hz in Chapter 2 and the rotor speed at that frequency is about 100rpm at no load conditions. The 3rd RSH is expected to be about 130Hz and the bandwidth of the filter proposed at that speed is specified as also 10Hz. So, the RSH frequency change within the 150μsprediction period must be at most to ± 5Hz meaning that if the shaft speed of the motor changes more than 3.8rpm, the estimation algorithm will fail. This implies that allowed acceleration or deceleration rate of the motor must be limited to 3.8rev/150μs or6000rev/s. The mechanical time constant of the motor is calculated as 39ms, considering the mechanical speed change occurs at 4τ condition at rated torque, it can be concluded that the motor speed may change at most 3.4rpm in 150μs. So the acceleration limit is applicable down to 5Hz and motor mechanical properties are close to the limits of application at 5Hz.

4.7 Improvements on the Algorithm

In this part of the work, the improvements implemented on the algorithm will be given. In the previous work, the zero crossing of the RSH is detected once in one period of the harmonic and no interpolation is used to update the position information. The zero crossing detection is described in Section 3.4 and the zero

crossing detection is given in Figure 55. Improvements include increasing the resolution of detection by detecting the sinusoidal more than one zero cross. Another important improvement on the algorithm is the interpolation of position estimation by using the estimated speed to decrease error in speed estimation.

4.7.1 Increasing Resolution of Detection

Up to this point, the zero crossing of the RSH is detected one time in one period, so the algorithm with zero crossing detection updates the rotor position at every period of the RSH. However, as the signal makes two zero crosses at one period each zero crossing can be detected and the rotor position can be updated at half of the RSH period. This improvement means that the resolution of the estimation is twice the value used in the previously used algorithm in the tests. Detecting the RSH at two points in a period would results in reduction of so called position error described in Section 4.3.The zoomed view of the implementation of increasing resolution is given in Figure 83. When Figure 83 is compared to Figure 63, it is seen that the estimation accuracy increases as the estimation output updated with at every zero cross. The mismatch between the position estimation points and the actual position readings of the encoder in Figure 83 is due to the reference loss in the previous estimations. The error can be cleared by equating the points at the start of the comparison.

The slope of the estimated points, which is actually the speed of the rotor, is the same as measured encoder position output slope in Figure 83 and if the offset is cleared the estimation result seems to be correct and free of error.

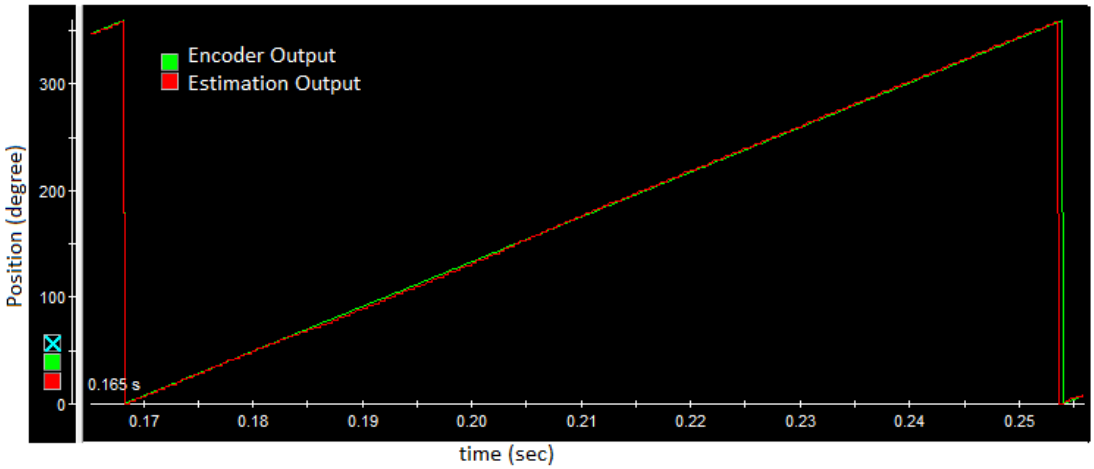

Figure 82 Comparison of encoder output and rotor position estimation with increased resolution

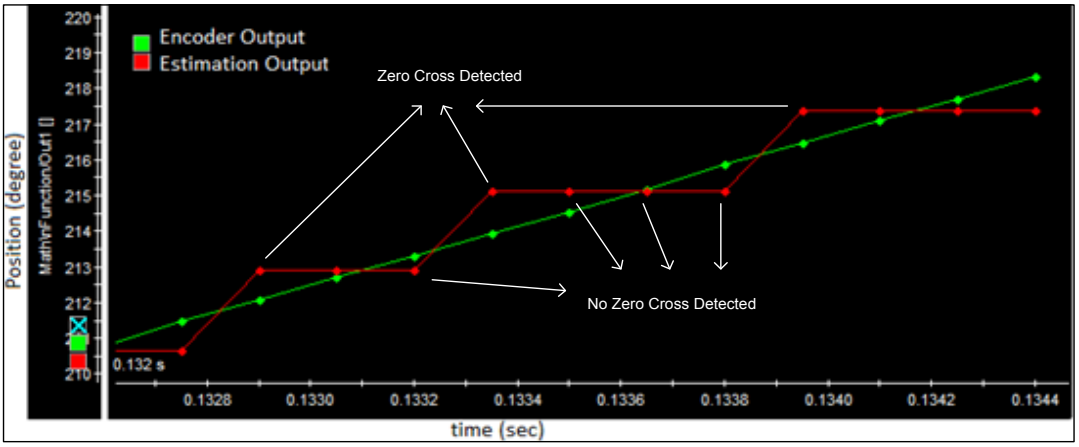

Figure 83 Zoomed view of comparison of encoder output and rotor position estimation with increased resolution at 50Hz drive frequency at no load

The improvement can be made better if the positive peak and the negative peak of the harmonic magnitude are also detected with the zero crosses of the RSH. However, to be able to achieve this improvement, the data record rate of the system should be fast enough, so that the zero crosses and the peaks can be detected properly. As discussed in Section 2.4, in order to achieve zero crossing detection, the sample rate of the system should be higher than at least two times of the RSH because of the Nyquist rate. In order to sense both of the zero crossings of the RSH, the sampling rate shall be 4 times higher than the RSHs frequency. Similarly, to

sense each peak and zero crossing of the RSH, the sample rate shall be at least 8 times of the RSH frequency. As the highest frequency of the interested RSH is calculated as 1300 Hz at 50Hz drive frequency in Section 2.4 and the sample rate is fixed at 6667 Hz, about 5 times of the RSH, the suggested improvement of increasing the resolution of the algorithm 4 times cannot be implemented at rated speed. To implement this resolution increase, the sampling rate shall be increased. However, if the speed of the rotor is decreased, the data record rate of 6.67kHz would be enough for detecting the peak values of the RSH sinusoidal additional to the zero crossing detection. Zero and peak detection can be implemented together to sense a RSH frequency of 1/8 of the sampling rate at Nyquist rate which is 833Hz for the RSH frequency. To give a safety region, half of this frequency, a RSH whose frequency is lower than 416Hz can be detected and reconstructed at time domain. This means that, there will exist 16 data points on one period of the reconstructed RSH, and this number is enough for both peak and zero crossing detection. A RSH existing at 416Hzmeans that resolution increase can be implemented with peak detection at and below 320rpm rotor speed. In Section4.7.2, how further improvement can be implemented with interpolation techniques will be described.

4.7.2 Interpolation Using the Speed Information

The error in estimating speed can be decreased further by using interpolation methods. In the previous improvement, the resolution of the speed estimation algorithm is increased. However, there are still some points where the estimation is not updated. These points are between two consecutive zero crosses and the rotor position is not updated as no zero crossing occurs in the reconstructed RSH. When the position information is not updated by the estimation algorithm, the error between the actual rotor position and estimation result seems to increase as the rotor shaft continues to turn as given in Figure 63. At those instants, the rotor position can be estimated by using the estimated speed with the given formula (**42)**;

$$\mathrm{x(t1)} = x(t0) + w(t1 - t0) \qquad \textbf{(42)}$$

where x(t1) is the interpolated estimation point, $x(t0)$ is the last zero crossing detected position estimation point, w is the shaft speed and (t1-t0) is the elapsed time between two estimation points. As the mechanical time constant is 39ms, assuming that the speed remains constant in 150µs computation period is correct and applicable. When interpolation is used, the maximum position mismatch between position estimation and encoder position speed output decreases. The decrease can be figured out by comparing the Figure 63, Figure 83 and Figure 85. This improvement is implemented on the algorithm and the decrease in the position estimation error show that the resolution increase and interpolation decreases the error in the position estimation.

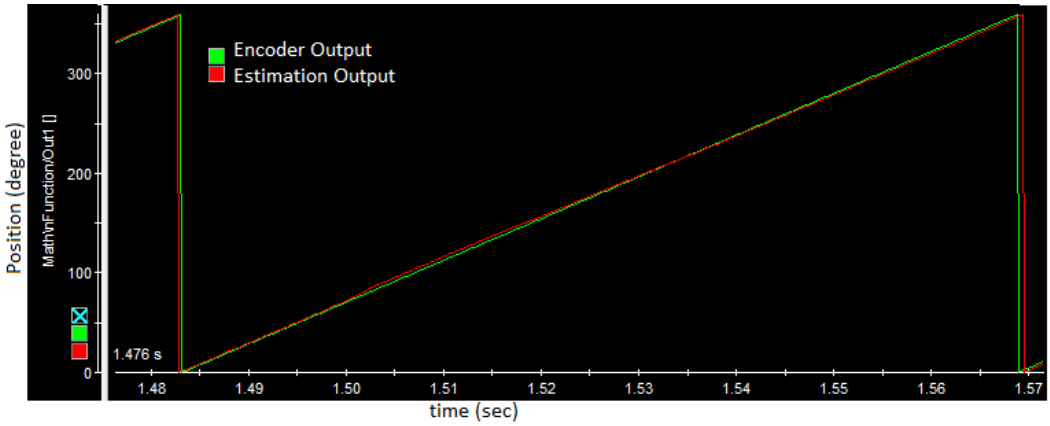

Figure 84 Comparison of encoder output and rotor position estimation with interpolation

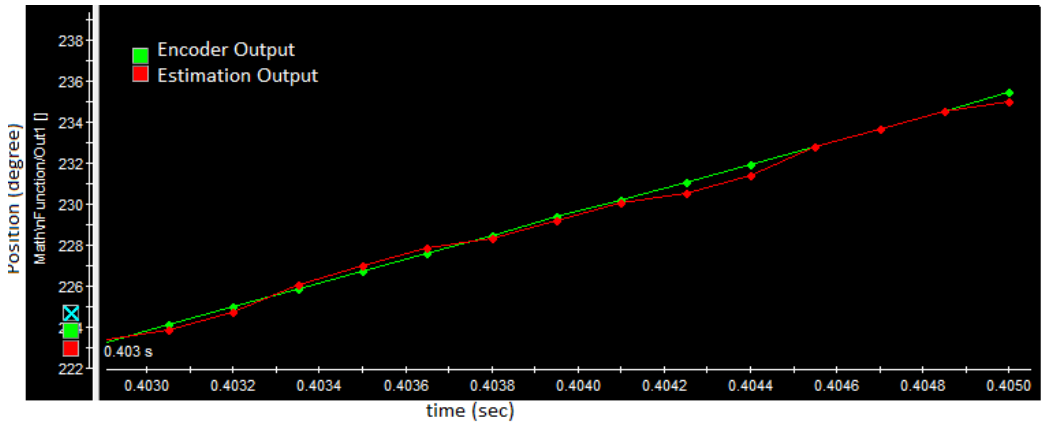

Figure 85 Comparison of encoder output and rotor position estimation with interpolation

The change in estimation output with interpolation and resolution increase in Figure 85 between 0.401s and 0.406s is because there is some mismatch in zero crossing detection time as described in Section3.4. In other words, the error occurs because rather than determining the zero crossing instant exactly, the zero crossing is assumed to occur at the instant the sign change is detected. Naturally, as the speed gets higher, there will be fewer zero crossing detection per RSH and the error in detecting the zero crossing will be greater because of the way the algorithm is implemented. It is possible to avoid this problem simply assuming linear variation between the sign change instant and the detected position just before sign change as discussed in Section 3.4.

4.8 Weaknesses of the Algorithm

Even though the algorithm is able to estimate rotor position and speed, some weaknesses of the algorithm exist. The detected weaknesses and disadvantages of the algorithm will be investigated in this section.

4.8.1 Initial Filter Positioning

One of the weaknesses of the algorithm is the need for knowing the frequency of the RSH in the previous control cycle. This is because the filter center frequency is decided by the frequency of the RSH in previous cycle. The problem in startup is that no RSH and no previous filter center frequency information exists at this condition in the estimation algorithm itself. So, initial filter positioning cannot be achieved by the algorithm itself. However, in all open-loop vector control algorithms, there is a speed estimator which relies on voltage and current measurements on the stator side. Therefore, once the motor starts running, shaft speed estimation with a reasonable accuracy will be available to estimate the filter center frequency for starting the position estimation algorithm. This speed estimator shall estimate the speed, and hence the RSH frequency for proper filters positioning. If the error is high, the RSH cannot be detected as the harmonic stays out of the bandwidth of the filter. Moreover, the speed estimator of the vector control shall be able to supply the speed information at the acceleration ratio of 6000rpm per second which is the acceleration

rate limit of the estimation algorithm. Same problem arises if the tracking the RSH detection algorithm stumbles. The algorithm itself is not capable to redetect the RSH or the speed of the rotor. This kind of a situation would result in total loss of estimation. However, the algorithm used to locate the filter at start-up can also be used here for a corrector of the algorithm and the filter center frequency can be re-located. So, this problem can be solved by using the open-loop speed estimation of vector control algorithms.

4.8.2 Cumulative Error in Position Estimation

Another weakness of the algorithm is the cumulative error which increases in time. If any kind of error occurs in one estimation step of position estimation, the position information will be updated incorrectly. The effect of that mistake on position estimation cannot be corrected by the algorithm and all of the preceding results will contain the same error. Moreover, the errors occurred in time will also be accumulated at position estimation output of the algorithm and total error will increase in time. An example of the situation is given in Figure 86. An error occurs at one of no-load tests and as seen in the Figure 86 second the predicted position jumps above the measured position by the encoder. However, it can also be inferred from the same figure that the shaft speed estimation (slope of the position estimation) contains no cumulative error, and the instantaneous mistake is recovered as can be seen from the slope of the position estimation and encoder position output. This result implies that, using the algorithm as a speed estimator instead of a position estimator is more suitable as no cumulative error problem exist in the estimation.

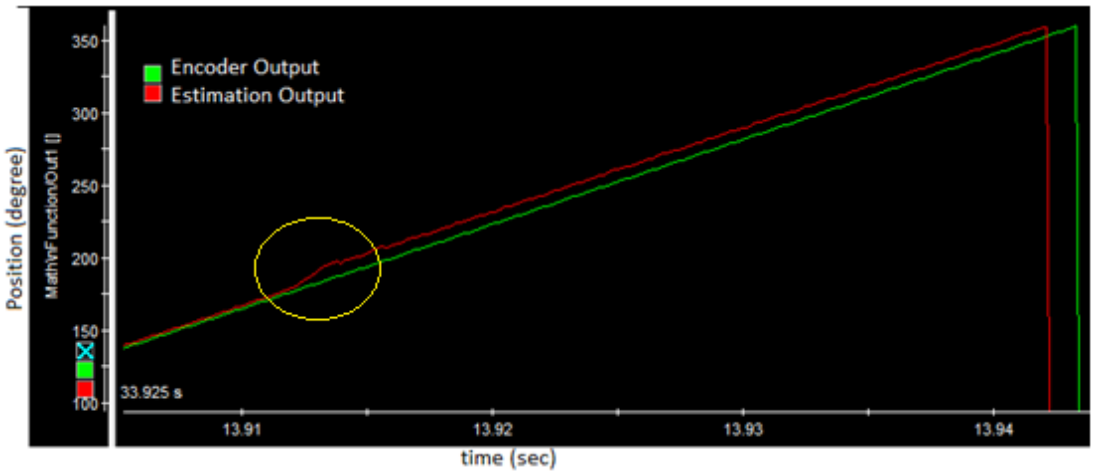

Figure 86 Cumulative error problem in position estimation

4.8.3 Amplitude Decrease in Rotor Slot Harmonic at Low Speed

As stated in Section 2.9, the RSHs' magnitude decreases with decreasing speed. At some speed the harmonics magnitude becomes less than other harmonics in its vicinity; which would most likely result in wrong detection of the RSH. This situation will result in loss of position and speed prediction accuracy of the RSHs detection algorithm. An additional development should be made on the algorithm if the algorithm is to be used at also low speeds. One possible way to estimate the position and the speed of the rotor is using signal injection methods at low rotor speeds as like different methods discussed in Chapter 1. The injected signal magnitude is controlled by the motor drive algorithm, signal injection methods to estimate rotor position and rotor speed does not suffer from the amplitude decrease problems at low speeds.

4.8.4 Direction of Rotation

The speed estimation is done by sensing only one of the phase currents. So, the direction of rotation cannot be understood by the algorithm. The direction of rotation information can be inferred from the phase currents or the phase voltages of the system **[21]**. Even though the algorithm cannot detect the direction of rotation, as the same RSHs are generated while the motor is turning in the reverse direction; same

algorithm can detect the rotor speed and position regardless of the direction of rotation.

4.9 Conclusion

The proposed position estimation algorithm in **[21]** by detecting and sensing the zero crossing instants of the RSHs in search coil voltage is implemented on an online system with stator current input. It is shown that the algorithm can be implemented on an online system. The test results of both constant speed and variable speed conditions at no load and at full load are given in this chapter. The evaluation of the thesis and the results given in this chapter will be given in Chapter 5.

CHAPTER 5

CONCLUSION & FUTURE WORK

In this thesis it is aimed to modify and implement the rotor position estimation algorithm proposed by Keysan in **[21]** on online systems by sensing the stator current instead of sensing the search coil voltage. The proposed algorithm has been implemented offline on a computer by Keysan. It uses a search coil voltage mounted on the motor shaft, extracts the RSH via demodulation and filtering. As the RSH's frequency is related to the rotor speed, rotor speed is estimated. Similarly, each zero crossing of the signal corresponds to one rotor slot pitch motion with respect to the static stator slots. The proposed future work by Keysan in **[21]** was developing the algorithm based on the voltage induced in the search coil and implementing the algorithm on online systems and implementing the algorithm with stator current input.

In this thesis, two of the three of his aims are implemented. The stator current data is analyzed to see that the RSHs are observable. The frequency spectrum of the stator current data is analyzed elaborately at Chapter 2. The frequency spectrum analysis is conducted offline by investigating the FFT result of stator current data. In the analysis, it is shown that the RSHs exist in the stator current like the search coil voltage.

The effect of the data recording rate on the RSH magnitude is also analyzed and it is seen that any record rate higher than Nyquist rate is suitable to implement the algorithm. Moreover, it is illustrated that the RSHs are also observable in the stator current of noisier inverter driven systems. The lower shaft speed limit until which the

algorithm successfully detects the rotor position or speed is decided by investigating the frequency spectrum of the RSHs. The filter needed for online implementation of the algorithm is analyzed, the specifications for the filter is described and the proposed filter is tested by applying the algorithm offline to current data recoded from tests. It is shown that the algorithm works properly with the chosen filter in offline conditions. The analysis in Chapter 2 proved that the search coil can be eliminated and the algorithm can be implemented with stator current input with the proposed filter. The stator current measurement already exists on most of the motor drive systems, so no additional sensor is needed. Because of this, the algorithm can be named as "Sensorless Position and Speed Estimation".

The specifications of the needed filter, the filter types and different implementation techniques are evaluated in Chapter 2. This analysis includes;

- Required Filter Specification
- Adaptive Filter Application
- Filter Selective Block
- Filter Design
- Filter Type Selection

In Chapter 3, it is aimed to implement the algorithm on online system with stator current output. The implementation hardware was the hardware designed by Kayhan in **[25]**. The reason for using that hardware is that it uses DS1104 as processor and necessary peripherals to sense current and drive the motor. DS1104 board is designed for motor drive systems, it has the ability to be programmed and via Matlab Simulink and can be monitored online via dSPACE Control Desk. Moreover it has all necessary peripherals like analog sensing interface (ADC) for stator current sensing, encoder interface to sense rotor position and speed for comparison of the estimation output, PWM outputs to drive the motor drive IGBT inverter etc. The board designed by Murat in **[25]** senses the phase currents, drives the motor with an IGBT inverter, supplies necessary AC/DC conversion to the inverter via rectification, and supplies isolation between the power stage and the processor board.

The estimation algorithm is developed using Simulink tool, and the processor board is programmed via "Incremental Build". The most challenging part, the filter block, is implemented by using IIR filters as they have great computation time advantage over FIR Filters. The need of adaptive filtering is done by selecting a proper filter and using it at every control cycle of the motor drive algorithm, which is selected as 150μs. The initial filter center frequency information is calculated from the encoder output, as it is already mounted on the system for comparison, then the estimated speed is used to locate the filter in the algorithm. The results of the implemented estimation algorithm are compared to the results of the encoder.

Zero crossing detection of the reconstructed RSH gives the rotor position estimation and the update rate of the position gives the speed of the rotor. There seems to be some kind of artificial error in the position and speed estimation results due to the way algorithm is implemented. Zero crossing detection one time in one period of the RSH and keeping the position estimation result until next zero crossing of the RSH creates the artificial error and these artificial errors are corrected by some improvements made in the estimation algorithm. The improvements are achieved by;

- Increasing Resolution of Detection
- Position interpolation Using the Speed Information

It is shown that increasing the resolution of estimation by detecting both zero crosses in one period and detecting the peaks of the sinusoidal waveform decreases the error in the position estimation. Detecting both zero crosses is implemented and the improvement is shown on position estimation. The peak detection is not implemented due to chosen drive period, 150μs (6.67 kHz of control sample rate). Moreover, the position estimation is made far better after using the interpolation techniques this is because the mechanical time constant of the motor is large and assuming that the shaft speed remains constant within the control period is valid. The estimated speed information is used to interpolate the position estimation points where no zero crossing occurs at the RSHs. This decrease in the mismatch can be visualized by comparing the Figure 63 and Figure 85. The real error in position estimation comes from the erroneous detection of the zero crossing of the RSH if it

occurs. If a zero crossing cannot be detected, the position estimation result creates error corresponding to 1 rotor slot. The algorithm cannot recover this kind of position error and this kind of error becomes cumulative in position estimation.

An artificial speed estimation error may also occur, because in the implementation here, the speed of the rotor is calculated after a 360° rotation of the rotor shaft. Any instantaneous error in that 360° rotation affects and creates artificial error in speed estimation. If the speed estimation is calculated with the slope of the position estimation, in each control cycle, the error in the speed estimation would become an instantaneous error in speed estimation and recovered by the algorithm. Because of this property, using this algorithm as a speed estimator instead of position estimator is more suitable and advised to be preferred.

The acceleration rate, low speed and high speed limitations of the position or speed prediction algorithm are also stated. The acceleration and deceleration rate of the rotor speed is limited from the bandwidth of the filter used at low speeds. Moreover, as the RSH signal magnitude decreases at low speeds and it becomes undetectable at low speeds. So, the algorithm is not suitable to work at low speeds. Lastly, it is stated and shown that the high speed limit of the rotor speed to be able to implement the estimation algorithm is decided by the sampling rate of the used online estimation system.

While implementing the algorithm, some disadvantages are also encountered. The detected disadvantages of the algorithm can be listed as;

- Initial Filter Positioning
- Cumulative Error in Position Estimation
- Decrease in RSHs magnitude at Low Speed

The first of these problems can be easily addressed and is not significant. It can be solved by using the estimators of vector control drives depending on stator current and voltage measurements. The second issue, cumulative error in position estimation, indicated that it is best if the algorithm is used to measure speed rather than position. Alternatively some means of position correction algorithm may be developed based

on correctly estimated speed information. The third problem however is an inherent weakness, indicating that the use of the algorithm is possible only for less demanding speed control applications. In short, the reasons and the possible solutions to the weaknesses is analyzed and stated in this work.

The results of online implementation tests prove that the algorithm can be implemented on online systems with a total calculation time of about 50µs. The calculation time includes the V/F control algorithm and the monitoring tasks of dSPACE Control Desk. As the vector control algorithm proposed in **[25]** takes about 75µs and the implemented estimation algorithm is assumed to take about 50 µs, however if filter parameters are calculated offline and stored in the DSP, the estimation time needed for algorithm will be decreased further. The algorithm can be interpreted to be applicable to supply speed and/or position feedback to the vector control drive whose control cycle takes about 150µs.

The weaknesses and the disadvantages of the system and their reasons are also discussed in Chapter 3 and 4. These weaknesses and disadvantages of the system can be solved by the proposed future work listed in Section 5.1.

5.1 Suggestions and Future Work

In this thesis, it is shown that the proposed algorithm can be implemented on online systems within an acceptable computational time and with suitable hardware. As it is shown that the algorithm is suitable for online implementation the given future works can be studied to improve the performance and robustness of the system.

5.1.1 Initial Filter Positioning

In this work, initial filter positioning is done by using the output of the encoder. In order to improve the robustness of the system and eliminate the use of encoder, another speed estimation algorithm, the estimators of vector control drives, can be implemented in parallel to the proposed algorithm as discussed in Chapter 3. The added algorithm can supply the initial filter positioning information. Moreover, the added algorithm can fix a possible malfunction of the algorithm when the RSH

traction is lost by supplying a speed information (even the sensorless vector controllers have position estimation) to re-locate the filter properly on the RSH.

5.1.2 Amplitude Decrease in Rotor Slot Harmonics Magnitude at Low Speed

As shown in Chapter 2, the RSH amplitude decreases with decreasing speed and become unobservable below some speed. In order to estimate the rotor position and speed at low speeds, signal injection methods can be applied with the proposed algorithm and make the algorithm work over all operating conditions.

Further experiments are needed to determine the actual low speed limit at which the RSH can no longer be obtained.

5.1.3 Use of Additional Processor or Parallel Processing for the Estimation:

The algorithm is running on a DSP board with the motor control algorithm. The total execution time of the motor control cycle is chosen as 150μs, so the algorithm updates its estimation in every 150μs. As the DSP is a microcontroller and does not have parallel processing capability, the execution time cannot be faster with this time if the motor control cycle is not changed. However, if an additional processor is used only for position estimation, the position estimation can be updated faster without changing the motor control cycle period. If the adaptive filter implementation of the algorithm is developed with filter coefficient change instead of filter change, the total execution time can also be decreased.

On other hand, if parallel processing devices such as FPGA's are used to drive the motor, its parallel processing capability can increase the position estimation speed without use of additional processor. The FPGA can be programmed such that the motor control algorithm and the position estimation algorithm can run in parallel and the estimation algorithm can produce more position estimation points in 1 motor control cycle which increases reliability and decreases the estimation error.

5.1.4 Application and testing within a vector control algorithm

Finally, the algorithm must be tested within a vector control algorithm. Measurement of drive performance with position information and/or speed feedback, coming from the algorithm would be very enlightening. The position and speed prediction limits of the algorithm must also be tested.

Measurement of this drives' frequency response and comparison of this with the conventional open loop and closed loop type vector control algorithms is also highly desirable.

Besides the issues mentioned above there are many minor issues which could increase the performance of the position and speed prediction algorithm.

However, the study in this thesis clearly illustrates that the approach presented here is applicable and may be used to improve the performance of sensorless vector control drives, at least in quite a wide speed range (roughly between 5 Hz to 75 Hz at least with the method implemented here).

REFERENCES

[1] Vas, P., “Sensorless Vector and Direct Torque Control”, Oxford University Press, 1998.

[2] Gimenez B.R "High Performance Sensorless Control of Induction Motor Drives", University of Nottingham, Doctorate Thesis, 1995

[3] Holtz J., Quan J., Sensorless Vector Control of Induction Motors at Very Low Speed using a Nonlinear Inverter Model and Parameter Identification” IEEE transactions on industry applications, vol. 38, no. 4, 2002, pp. 1087-1095

[4] Bose B. K , "Modern Power Electronics and AC Drives", Prentice Hall, 2001

[5] J. Holtz "Sensorless Speed and Position Control of Induction Motors" IECON, 2001

[6] Jansen P.L, Lorenz R.D. "Transducerless Position and Velocity Estimation in Induction and Salient AC Machines", IEEE transactions on industry applications, vol. 31, no. 2, 1995

[7] Consoli A., Testa A. "A New Zero-Frequency Flux-Position Detection Approach for Direct-Field-Oriented-Control Drives", IEEE, 1999

[8] Degner M. W, Lorenz R. D. "Position Estimation in Induction Machines Utilizing Rotor Bar Slot Harmonics and Carrier Frequency Signal Injection", IEEE, 2000

[9] Negrea M.D "Electromagnetic flux monitoring for detecting faults in electrical machines", Helsinki University of Technology, Doctoral Dissertation 2006

[10] Novotny D.W., T. A. Lipo, "Vector Control and Dynamics of AC Drives", Oxford University Press, 1998

[11] Briz F, Degner M. W., Lorenz R. D. "Comparison of Carrier Signal Voltage and Current Injection for the Estimation of Flux Angle or Rotor Position", IEEE, 1998

[12] Staines C. S., Asher G. M., Sumner M., "Rotor-Position Estimation for Induction Machines at Zero and Low Frequency Utilizing Zero-Sequence Currents", IEEE Transactions On Industry Applications, Vol. 42, No. 1, January/February 2006

[13] Briz F., Degner M. W., Lorenz R.D. "Comparison of saliency-based sensorless control techniques for AC machines", IEEE, 2003

[14] Asher G. M, Sumner M, "Sensorless Position Detection for Symmetric Cage Induction Motor under Loaded Conditions", IEEE, 2000

[15] Degner M.W., Lorenz R.D. "Using Multiple Saliencies for the Estimation of Flux, Position and Velocity in AC Machines", IEEE vol.34, pp.1097-1104, 1999

[16] Holtz J., "Sensorless Position Control of Induction Motors – an Emerging Technology", IEEE transactions on industrial electronics, 1998

[17] Mathew J. Corley, Lorenz R.D., "Rotor Position and Velocity Estimation for a Salient-Pole Permanent Magnet Synchronous Machine at Standstill and High Speeds", IEEE transactions on industry applications, vol. 34, no.4, 1998

[18] M. Ishida, K. Hayashi, Ueda M. "A Speed Detection Method of Squirrel-Cage Induction Motor Utilizing Rotor Slot-Harmonics in the Air Gap and its Application to Slip-Frequency Control" Trans. IEEE Japan, Vol.99B, 1979

[19] Moreria J.C., LipoT.A.,"Modelling of Saturated AC Machines Including Air Gap Flux Harmonic Components", IEEE Trans. Industry Applications, Vol.28, no.2. Mar./April.1992, pp. 343-349

[20] Ishida M., Iwata K. "A New Slip Frequency Detector of an Induction Motor Utilizing Rotor Slot Harmonics", IEEE Transactions on Industry Applications Vol.IA-20, No.3, May-June 1984, pp. 575-582

[21] Keysan O. “A Non-Invasive Speed and Position Sensor For Induction Machines Using External Search Coils”, Middle East Technical University, Master Thesis, 2009

[22] Keysan O., Ertan H. B. “Determination of Rotor Slot Number of an Induction Motor Using an External Search Coil”, Facta Universitatis, Ser.:Elec. Energ. Vol. 22, no.2 August 2009, 227-234.

[23] R. Blasco-Gimenez, G. M. Asher, M. Sumner, K.J. Bradley," Performance of FFT-Rotor Slot Harmonic Speed Detector for Sensorless Induction Motor Drives", IEEE Proc.-Elkctr. Power Appl., Vol. 143/3, May 1996, pp. 258-268

[24] Siemens Micromaster440 User Manuel and Parameter List, Issue 04/02.

[25] Kayhan M. “The Effect of DC Link Filter Design and Compensation on Dynamic Performance of Vector Controlled Drive”, Middle East Technical University, Master Thesis, 2015.

[26] http://www.electrical4u.com/speed-control-of-three-phase-induction-motor/ [Last Accessed: January 2016]

[27] Oppenheim Alan V., Willsky Alan S., Young Ian T. "Signals and Systems", Prentice Hall, 1983, pp. 448-473

[28] Prabhakar S., Sappal A. S, “Characteristic of Tunable Digital Filters”, International Journal of Advanced Research in Computer Science and Software Engineering, Vol. 3, Issue 8, August 2013, pp. 362-369

[29] Stoyanov G., Kawamata M., “Variable Digital Filters”J. Signal Processing 1.4 (1997), pp. 275-289.

[30] Oppenhaim A. V., Wilsky A. S. Nawab S. H., *Signals & Systems*,2nd ed., New Jersey: Prentice-Hall Inc, 1997, pp.374

[31] Analog Devices, “Mixed Signal and DSP Design Techniques-Digital Filters” [online] Available: http://www.analog.com/media/en/training-seminars/design-handbooks/MixedSignal_Sect6.pdf [Last Accessed: January 2016].

[32] Ertan H. B., Keysan O., “Implementation Issues of Real Time Position Estimation for Induction Motors Using Rotor Slot Harmonics” 4th International Conference on Power Engineering, Energy and Electrical Drives, May 2013.

[33] https://en.wikipedia.org/wiki/Butterworth_filter [Last Accessed: January 2016]

[34] Norm ElektrikMotorlarıKataloğu KAT.NMST.02.14, ElsanElektrik San. ve Tic. A.Ş.